Joint Channel Estimation and Detection for Multi-Carrier MIMO Communications

Mohammed B. Kashoob

Doctor of Philosophy

University of York
Electronics

October 2016

Abstract

In MIMO OFDM systems, channel estimation and detection are very important. Pilot-based channel estimation using BEMs is widely used for approximating time-frequency variations of doubly-selective channels. BEMs can provide high estimation performance with low computational load. Data-aided channel estimation outperforms the pilot-based estimation. The data-aided estimation iteratively improves estimates using tentative data symbols and corresponding adaptive weights (reweighted channel estimation). These weights are computed assuming Gaussian data errors, which is inapplicable to OFDM. In this thesis, this assumption is however shown to improve the channel estimation performance. The reweighted channel estimation is shown to significantly outperform the unweighted estimation. Most often used mismatched receivers assume perfect channel estimates when detecting data symbols. However, due to limited pilot symbols and data errors, the channel estimates are imperfect, resulting in a degraded detection performance. The optimal receiver without explicit channel estimation significantly outperform mismatched receivers. However, its complexity is high. To reduce the complexity, a receiver that combines mismatched and optimal detection is proposed. The optimal detection is only applied to data symbols unreliably detected by the mismatched detector, identified using weights computed in the reweighted estimator. The channel estimator and the optimal receiver require the knowledge of channel statistics, which are unavailable and difficult to acquire. To overcome this, an adaptive regularization using the cross-validation criterion is introduced, which finds a regularization matrix providing best channel estimates. The proposed receiver has a reduced complexity than the optimal receiver and provides close-to-optimal detection performance without the knowledge of channel PDP. The adaptive regularization is extended to joint estimation of the Doppler-delay spread and channel. The Doppler and delay spread corresponding to the optimal regularization are selected as their estimates. This approach outperforms other known techniques and provides channel estimation performance close to that obtained with perfect channel statistics.

Contents

List of Figures

List of Tables

Acknowledgments

I would like to express my sincere gratitude to my supervisor Dr. Yuriy Zakharov for his continuous support and guidance. The death of my father in the end of my first year has affected me greatly, but Dr. Zakharov was very understanding and patient. I would not be able to finish this thesis and complete my PhD study without his help and advise. I have learned a lot of valuable information about proper research techniques and technical writing under his supervision.

I would like to thank my friends and fellow PhD students: Yahya Harbi, Benjamin Henson and Jianghui Li for their comments, ideas and support throughout my study. I will always remember the times we spent together and our discussions in many research areas.

I would like to dedicate this thesis to the memory of my late father. He was always my drive for excelling in my studies and encouraged me to spend my time reading books and learning new things. Also, I would like to dedicate it to my mother, wife and little daughter. I would not be able to complete this work without your support.

Declaration

I hereby declare that the work presented in this thesis is composed by myself and contains original work, to the best knowledge of the author. I also declare that the references and acknowledgements to other researchers' work have been given appropriately and that this work has not been submitted for any other degree or qualification except as specified. Parts of this work have been published or submitted as listed below.

Journal papers [23, 24]

1. M. Kashoob, and Y. Zakharov,"Selective detection with adaptively regularized weighted channel estimation for MIMO OFDM", under revision by IEEE Transactions on Wireless Communications, 2016.

2. M. Kashoob, and Y. Zakharov,"Joint Doppler-delay spread and channel estimation in doubly-selective channels", to be submitted to IEEE Transactions on Vehicular Technology, 2016.

Conference papers [25–27]

1. M. Kashoob, and Y. Zakharov,"Data-aided Iterative Reweighted LMMSE Channel Estimation for MIMO OFDM", In the 15th IEEE International Symposium on Signal Processing and Information Technology, ISSPIT 2015, Abu Dhabi, UAE, 2015, pp. 663-667.

2. M. Kashoob, and Y. Zakharov,"Selective Optimal Detection for MIMO OFDM systems", in IEEE Wireless Communications and Networking, WCNC 2016, Doha, Qatar, 2016, pp. 1-6.

3. M. Kashoob, and Y. Zakharov,"Selective Detection with Adaptive Channel Estimation for MIMO OFDM", in IEEE Sensor Array and Multichannel Signal Processing Workshop, SAM 2016, Rio De Janeiro, Brazil, 2016, pp. 1-5.

Chapter 1

Introduction

Contents

1.1 Overview

In MIMO OFDM systems, the acquisition of channel state information with great precision is very challenging. Many receiver schemes in the literature are evaluated assuming the perfect knowledge of the channel state information. However, such information is unavailable in practice. Therefore, channel estimation is crucial in MIMO OFDM receivers. Pilot-based channel estimation is most often used to estimate the channel at pilot locations. Then, channel estimates at data locations are obtained through interpolation [1]. BEMs are widely used in the channel estimation to approximate time and frequency variations of the channel [2–10]. When BEMs are used in pilot-based channel estimation, they provide high accuracy channel estimates jointly at pilot and data locations with low complexity. However, the pilot-based channel estimation can result in a degraded detection performance especially at low Signal-to-Noise Ratio (SNR) and in high Doppler spread and delay spread environments.

A better channel estimation can be achieved by using tentative estimates of data symbols in an iterative manner. The tentative estimates of data symbols can be obtained iteratively

from the output of the turbo decoder [6,11,12]. However, the complexity of iterative receivers with turbo decoding is very high [6] and this limits their practical implementation. Many low-complexity iterative turbo receivers have been proposed to address this issue [13–15]. The tentative estimates of data symbols also can be obtained iteratively from the output of a demodulator without using the turbo decoder [16, 17]. Although this scheme improves the estimation performance, the improvement is limited due to errors in the tentative data estimates [11,18]. In [18] tentative estimates of data symbols with weighting were proposed. The weighting is used to limit the contribution of erroneous tentative estimates of data symbols into channel estimates, and thus improving the estimation performance.

Iterative channel estimation using tentative estimates of data symbols can provide extra improvement in the detection performance over that of the pilot-based channel estimation. However, in the case of a small number of pilot symbols and errors in the tentative data estimates, the detection performance is limited. A better detection performance is obtained by using optimal detection [19] that jointly processes the received data and pilot symbols without explicit channel estimation. In [19], the optimal detection was derived and investigated in MIMO uncorrelated fading channels. The optimal detection with imperfect channel knowledge outperforms mismatched detection (i.e., a minimum distance detector that assumes perfect channel estimates) with Maximum Likelihood (ML) channel estimates. In [20], a general optimal detection with imperfect channel knowledge was proposed and investigated for a MIMO OFDM system in frequency-selective fading channels. The optimal detection was shown to outperform mismatched detectors with ML and Linear Minimum Mean Square Error (LMMSE) channel estimates. Although the optimal detection provides high detection performance, it has a high computational complexity. In this thesis, we investigate the performance of the optimal detection and its complexity reduction in doubly-selective channels. A new receiver is proposed that combines the mismatched detection with iterative channel estimation using weighted tentative estimates of data symbols as in [18] and the optimal detection. This new receiver reduces the complexity of the optimal detection while maintaining its high detection performance. The optimal receiver, the mismatched receiver, and the new proposed receiver are designed using a channel regularization matrix obtained from the full knowledge of the channel PDP. The channel PDP is usually not available and it is difficult to estimate in practice. Therefore, more practical approaches for the channel regularization are proposed such as adaptive model-based uniform regularization [21]. This regularization approach shows a performance close to that with known channel statistics. Therefore, the

performance of the optimal receiver and the proposed receiver are investigated using the adaptive regularization.

The adaptive regularization in [21] does not take into account the Doppler spread which is unknown in practice. Thus, in this thesis, we extend the adaptive regularization approach to joint Doppler spread, delay spread and channel estimation in doubly-selective channels. The Doppler frequency estimates of such a scheme are compared with that of the conventional Doppler frequency estimates [22]. Also, Mean Square Error (MSE) performance of channel estimates using this scheme are presented and compared with that of LMMSE channel estimates.

1.2 Aims

Recently, MIMO OFDM systems have gained a lot of attention and have been deployed in various wireless communication standards. For the last two decades, an extensive amount of research has been conducted to propose practical designs for the MIMO OFDM receivers with improved performance and reduced complexity. In this thesis, we are motivated to design MIMO OFDM receivers that match these criteria.

The aims of this research are the following:

- To improve the channel estimation for MIMO OFDM systems in doubly-selective channels.
- To reduce the computational complexity of detection in MIMO OFDM systems while maintaining close-to-optimal detection performance.
- To investigate the channel estimation in MIMO OFDM receivers without the knowledge of channel statistics.

1.3 Contributions

The contributions of this research include the following:

- The weights derived in [18] assuming Gaussian data errors, although not optimum for OFDM, are proposed for MIMO OFDM systems. The iterative channel estimation with

these weights has been investigated in MIMO OFDM under downlink LTE scenarios. It has been shown that this approach outperforms the iterative unweighted channel estimation in doubly-selective channels.

- A new receiver with BEM channel estimation and selective optimal detection is proposed for MIMO OFDM systems. This receiver combines the mismatched detection with the reweighted LMMSE BEM channel estimation and the optimal detection in order to provide an improved performance with a reduced complexity. Tentative estimates of data symbols and weights are obtained from the reweighted LMMSE BEM channel estimation/detection. The weights are used to identify unreliably demodulated data symbols to which the optimal detection is applied (therefore this is called the selective optimal detection). Simulation results show that a very small percentage of received data are detected by the optimal detection leading to a low complexity. The selective optimal detection has a performance that is very close to that of the optimal detection.

- The new receiver with BEM channel estimation and adaptive model-based regularization, which does not require the knowledge of channel statistics, is investigated. The results show that the receiver provides a performance that is similar or close to that of the regularization with full knowledge of the channel statistics.

- A joint Doppler frequency, delay spread and channel estimator for doubly-selective channels is proposed. The proposed technique has been shown to provide the Doppler frequency estimation performance significantly better than that of the conventional Doppler frequency estimator. The MSE of channel estimates obtained by this scheme is significantly lower than that of channel estimates obtained by the channel estimator using the diagonal loading regularization, and is very close to that of the LMMSE channel estimates.

- A re-adjustable joint Doppler frequency, delay spread and channel estimation in doubly-selective channels is proposed. The re-adjustable estimator provides more improvement in the estimation performance of the Doppler frequency and delay spread to that of the

joint estimator.

1.4 Thesis outline

The thesis chapters are divided into the following:

- Chapter 2: **Fundamentals of MIMO OFDM channel estimation and detection**
  In this chapter, the basics of OFDM, MIMO setup and downlink LTE sub-frame structure and its design parameters are provided. The doubly-selective channel, Clarke's channel model and Jakes' channel model are discussed in details. The basics of channel estimation using BEMs are introduced. BEMs such as : Discrete Prolate Spheroidal Sequences (DPSS) and parabolic B-splines are briefly discussed. Also, a brief description of turbo coding and decoding is provided.

- Chapter 3: **Data-aided reweighted iterative channel estimation for MIMO OFDM**
  In this chapter, the reweighted iterative LMMSE BEM channel estimation for MIMO OFDM systems is considered. The weights optimized for Single Carrier-Frequency Division Multiple Access (SC-FDMA) are proposed to be also used in OFDM systems. These weights are used iteratively in the reweighted channel estimation. Numerical results show that the reweighted iterative LMMSE BEM channel estimation/detection outperforms the unweighted iterative LMMSE BEM channel estimation/detection in single-user downlink LTE scenarios.

- Chapter 4: **Selective detection with adaptive channel estimation for MIMO OFDM systems**
  In this chapter, a multi-stage channel estimation and detection scheme with an symbol-by-symbol selection scheme for a reduced complexity optimal detector (the selective optimal detector) in MIMO OFDM systems is proposed. In this scheme, the optimal detector is only applied to unreliably detected data symbols. The reliably received data symbols are detected by a mismatched detector. The new scheme benefits from the improvement in the detection performance provided by the optimal detector while reducing its high computational load. The selection of received data symbols for the

optimal detector is based on a threshold to weights. The weights are obtained as explained in Chapter 3. We investigate the performance of this new proposed selective detector, the optimal and mismatched detectors with different regularization schemes in single-user downlink LTE scenarios. The regularization schemes are: LMMSE regularization, model-based uniform regularization, adaptive model-based regularization, and diagonal loading. Our results show that the selective optimal detector has a performance similar to that of the traditional optimal detector. Also, the performance of the detector with adaptive regularization is close to that of the detector with the LMMSE regularization.

- Chapter 5: **Joint Doppler-delay spread and channel estimation in doubly-selective channels**

  In this chapter, a new joint Doppler-delay spread and channel estimator is proposed for doubly-selective channels. This estimator precomputes a set of regularization matrices defined by a set of Doppler frequencies and by a set of delay spreads. Then, using the dichotomous search, it selects the optimal regularization, and its corresponding Doppler frequency and delay spread based on the Generalized Cross-Validation (GCV). The reduction of the memory load for the proposed estimator using the properties of the BEM matrix and channel covariance is discussed. This estimator has been shown to provide close-to-optimal channel estimates. However, at low to medium Doppler frequencies, the proposed estimator is affected by the choice of a GCV constant. Therefore, a re-adjustable joint Doppler-delay spread and channel estimation is proposed to take the effect of the adjusted constant into account and to further improve the estimation performance. The performance of the re-adjustable joint estimation is compared with that of the original joint estimation. The proposed joint estimator and re-adjustable estimator provide channel estimates without the knowledge of the channel statistics close to that of the LMMSE channel estimator. The re-adjustable estimation provides an extra improvement in the estimation of the Doppler frequency and delay spread.

- Chapter 6: **Conclusions and future work**

  In this chapter, conclusions and discussion on the possible future work are provided.

1.5 Notation

In this thesis, capital and small bold fonts are used to denote matrices and vectors, respectively; e.g., $\mathbf{W}$ is a matrix and $\mathbf{w}$ is a vector. Elements of the matrix are denoted as $w_{i,j}$. Elements of the vector are denoted as w_i. We also denote: $(\cdot)^T$ the matrix transpose; $(\cdot)^H$ the Hermitian transpose; $\mathrm{tr}(\cdot)$ the trace operator; $||\cdot||$ the vector norm; $(\cdot)^*$ the complex conjugate; $\otimes$ the Kronecker product; $\mathrm{diag}(\cdot)$ a vector of diagonal elements of a square matrix; $|\cdot|$ determinant of a matrix; $\mathbb{E}(\cdot)$ the expectation operator; $\mathbf{I}_M$ an $M \times M$ identity matrix; $\mathbf{0}_M$ is an $M \times M$ zero matrix; $\mathcal{N}_C(\mathbf{a}, \mathbf{C})$ a complex Gaussian Probability Density Function with a mean $\mathbf{a}$ and covariance $\mathbf{C}$.

Chapter 2

Fundamentals of MIMO OFDM channel estimation and detection

Contents

2.1 Introduction

The MIMO technology provides many advantages in wireless communication systems, such as: spatial diversity, high spectral efficiency, high data rates, improved reliability and coverage [28]. These advantages make the MIMO technology very attractive for the deployment in wireless communication systems. The advances in MIMO technology resulted in its implementation in current commercialized wireless communications standards [29–32].

The early research on MIMO focused on basic spatial diversity to reduce the degradation in the performance caused by multipath propagation [33, 34]. In [33] and [34], optimal combining was introduced. In 1994, Paulraj and Kailath [35], pioneered the use of spatial multiplexing with multiple antennas at the transmitter and the receiver. In [36], Telatar derived the channel capacity for MIMO systems for a single user with and without fading. His computations showed that the channel capacity is directly proportional to the number of transmit and receive antennas. In 1996, G. Foschini proposed Bell Laboratories Layered Space-Time (BLAST) [37]. Then, Vertical-Bell Laboratories Layered Space-Time (V-BLAST) was proposed by P. Wolniansky et al. [38]. In 1998, Alamouti [39] proposed a simple transmit diversity scheme that requires less processing at the receiver and provides a good performance. Currently, a lot of research is conducted to improve the MIMO technology.

Future wireless communication systems will require high data rate transmission with high reliability and receivers with low complexity. The combination of MIMO and OFDM technologies can provide most of these requirements. However, the computational complexity of MIMO OFDM receivers can be high. A MIMO receiver with an optimum data detector [19, 20, 40–42] that minimizes the probability of errors in detection decisions and uses an exhaustive search over all possible transmitted data symbols, can provide a high detection performance. However, the optimal MIMO detection is very complicated, especially in large MIMO systems [20]. Another option would be the use of sub-optimal linear detection schemes that have lower complexity, such as: the Zero-Forcing (ZF) detection and Minimum Mean Square Error (MMSE) detection [43]. Although these detection schemes have lower complexity, they can result in a degraded performance [43]. These detectors treat the channel estimates used in the detection as perfect, which is not the case in practice. Therefore, such detectors are called mismatched detectors [19, 20]. In this thesis, we will propose practical approaches to improve channel estimation and detection in MIMO OFDM receivers.

In this chapter, we discuss fundamentals of MIMO and OFDM technologies, the implementation of MIMO OFDM in the LTE downlink, doubly-selective channels, the fading based on Clarke's and Jakes' channel models, the channel estimation based on BEMs, linear mismatched detection and basics of channel coding with LTE turbo coding and decoding.

2.2 OFDM basics

The earlier work on OFDM can be dated back to 1966 in a paper published by Robert W. Chang [44]. Chang proposed a new scheme for the simultaneous transmission of signals in a band-limited channel without taking into account the effects of Inter Carrier Interference (ICI) and Inter Symbol Interference (ISI). In 1971, the Discrete Fourier Transform (DFT) was introduced to the OFDM modulation and demodulation [45], which resulted in a more efficient processing. In [45], a guard interval was used between OFDM symbols to avoid the ICI and ISI. At this point, the benefits of deploying OFDM was reduced due to the loss of sub-carriers orthogonality. In 1980, the Cyclic Prefix (CP) was suggested in [46] as a solution to the orthogonality problem between sub-carriers.

In general, OFDM is a digital transmission technique that transmits information on a number of overlapping and orthogonal narrow-band sub-carriers (frequencies) instead of a single wide-band sub-carrier. The overlapping of the narrow-band sub-carriers results in a high spectral efficiency of OFDM. Every narrow-band sub-carrier can transport information for a different user, e.g., as in the Orthogonal Frequency-Division Multiple Access (OFDMA) [29, 47]. In wide-band communication systems, the modulation bandwidth is typically larger than the channel coherence bandwidth. This causes frequency-selective fading. The frequency-selective fading is very difficult to estimate and equalize. With OFDM, the channel between every two sub-carriers can be made approximately constant (i.e., flat fading channel). This makes OFDM more resistant to the channel frequency-selectivity. As the channel equalization in OFDM is often performed in the frequency domain, it is transformed into a simple multiplication operation [48].

Figure 2.1 shows the structure of one OFDM symbol in the frequency domain with CP. Guard sub-carriers (null sub-carriers) are typically placed in the frequency domain at both sides of an OFDM symbol to reduce ISI between every two consecutive OFDM symbols [49]. The ISI happens due to multipath propagation. Pilot sub-carriers are known at both the transmitter and the receiver; they are used to perform channel estimation and synchronization at the receiver. The Direct Current (DC) sub-carrier is typically a null sub-carrier, which corresponds to a zero frequency.

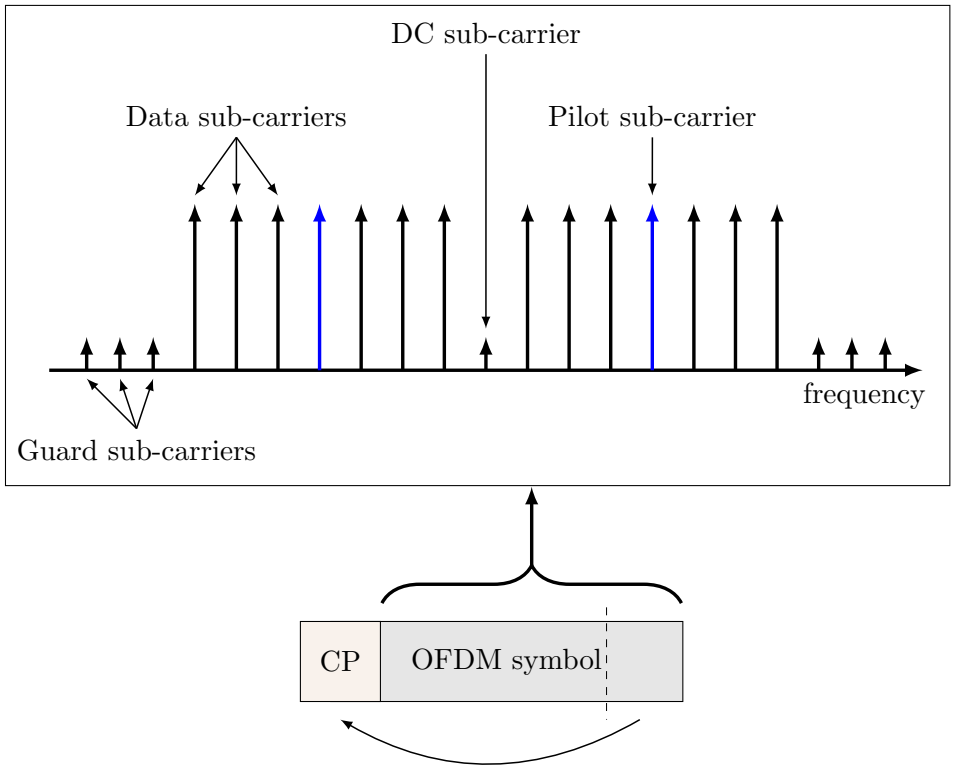

Figure 2.1: OFDM symbol.

In order to avoid the loss of orthogonality due to the ICI, the CP is appended at the beginning of each OFDM symbol [46]. The CP, as shown in Figure 2.1, is a copy of the end part of the OFDM symbol. Although the appended CP causes a loss in the spectral efficiency, its role in maintaining the orthogonality justifies this loss. The CP allows converting the linear convolution between the transmitted OFDM signals and the frequency-selective channel to a circular convolution operation [50]. Thus, the effect of the channel frequency-selectivity is limited to point-wise multiplication of the transmitted signal symbols and the channel frequency response. This way, the CP preserves the orthogonality and eliminates ICI between sub-carriers. The orthogonality between sub-carriers using the CP is maintained as long as the CP is longer than the length of the channel impulse response. Therefore, the length of this CP interval is usually selected to be longer than the expected delay spread in the channel.

The main disadvantage of OFDM is that it has a high Peak-to-Average Power Ratio (PAPR) [51]. The high PAPR results from OFDM having high peak values in time domain as many sub-carriers are added by the IFFT. The efficiency of power amplifiers at the transmitter is degraded due to the high PAPR [52]. Many solutions were proposed to reduce the

PAPR value in OFDM [51, 53]. However, the high PAPR is more critical in the uplink where the battery energy of the User Equipment (UE) is limited. In the downlink, there is more freedom in the power requirement. Thus, OFDM is used in the downlink scenarios of many current technologies [29–31]. Another disadvantage of OFDM is its sensitivity to the carrier frequency offset and Doppler spread [54, 55]. The OFDM frequency offset is caused by the mismatch in the frequency of the local oscillators in both the transmitter and the receiver. Another cause for the carrier frequency offset is the Doppler shift which results from the movement of both the transmitter and receiver or the objects surrounding them. The carrier frequency offset and Doppler spread cause ICI which results in the loss of the sub-carriers orthogonality.

OFDM is adopted in many wireless standards such as: LTE [29], Worldwide Interoperability for Microwave Access (Wi-MAX) [30], digital video broadcasting [32] and IEEE802.11a (Wi-Fi) [31]. In the following section, we discuss the implementation of OFDM into the LTE downlink standard.

2.3 Downlink LTE

The LTE was initiated in 2004 and is currently one of the main technologies commercialized for the 4th generation cellular services [56]. This technology aims to provide a high data rate, low latency and packet optimized radio access technology supporting flexible bandwidth deployments. In this section, an overview of the LTE downlink standard [29] is provided. The LTE downlink scenarios will be used in our simulations throughout this thesis.

2.3.1 LTE frame/subframe structure

In the LTE, various channels are used to transmit different types of data through the radio access network [29]. These channels are divided into the following: physical channels, transport channels and logical channels. The physical channels are used to carry user data and control messages that originate from higher layers. The transport channels are used to transfer information to MAC (Medium Access Control) layer or higher layers while the logical channels provide services to the MAC layer. In the LTE downlink, we are more interested in the physical channels, particularly in the Physical Downlink Shared Channel (PDSCH) [29].

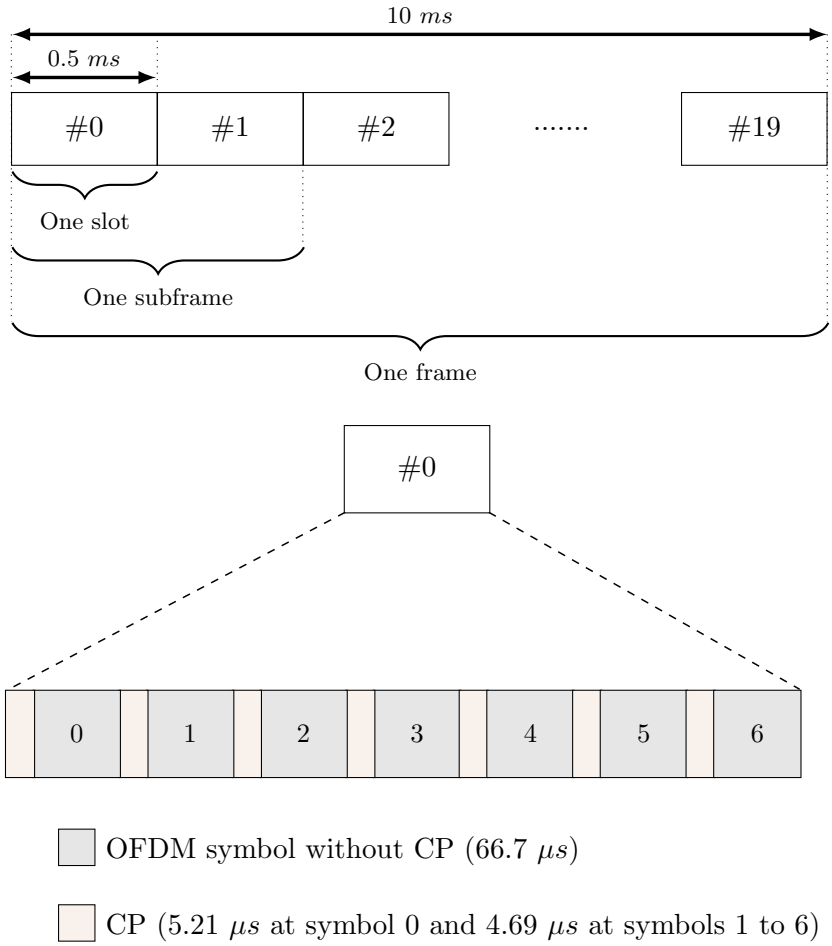

Figure 2.2: LTE frame structure type 1.

The PDSCH is a physical channel that carries data dynamically allocated to users. The user data are carried as transport blocks. In the PDSCH, the turbo coding with recursive convolutional encoders is used to combat errors [29]. The data in the PDSCH are mapped into spatial layers based on the LTE downlink transmission modes (e.g., open/closed loop spatial multiplexing, transmit diversity, or beamforming). After that, the data are mapped to a constellation (e.g., QPSK, 16 QAM or 64 QAM). Then, the physical resources are mapped to a radio frame.

There are two types of the radio frame structure: Radio frame type 1 and type 2 [29]. Radio frame type 1 is applicable to the Frequency Division Duplexing (FDD) [29] in full duplex and half duplex modes. The radio frame type 2 is reserved for the Time Division Duplexing (TDD) [29]. In this thesis, we focus on the LTE radio frame type 1. Figure 2.2 shows the structure of the LTE radio frame of type 1. In this type, every frame contains 10

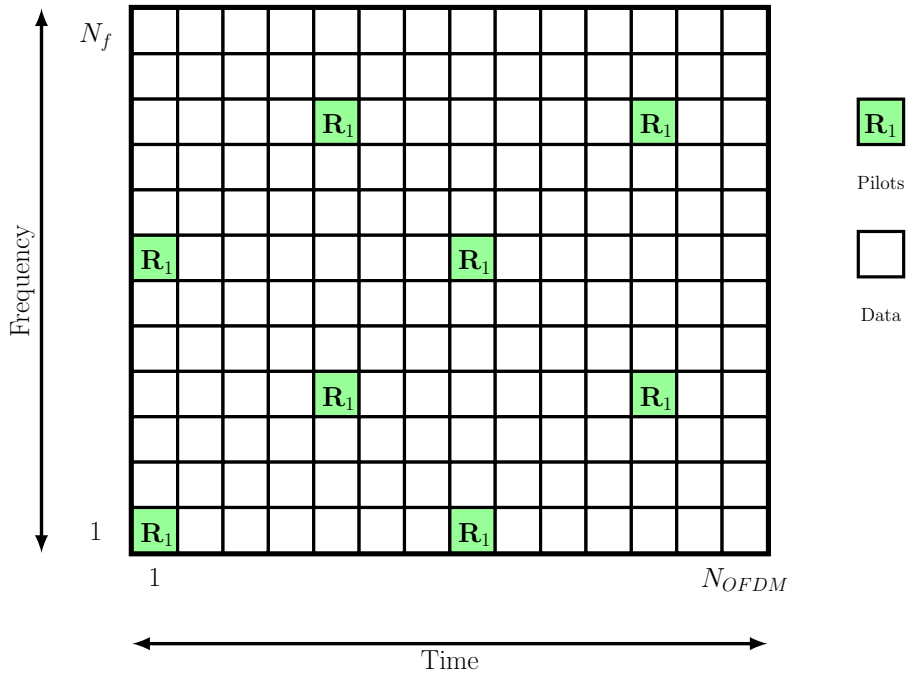

Figure 2.3: LTE downlink resource block with CRS for one transmit antenna.

sub-frames that span over a duration of 10 ms. A sub-frame contains two slots that occupy a duration of 1 ms in time. A slot occupies a duration of 0.5 ms and contains 7 OFDM symbols. A CP is attached at the beginning of every OFDM symbol. In the LTE, there are two types of CP: normal CP (short) and extended CP (long). The objective of the extended CP is to address fading channels with longer delay spread. In this thesis, we consider the case of the normal CP. In OFDM symbol 0, the CP duration is $5.21\mu s$, while at OFDM symbols 1 to 6, it is $4.69\mu s$ [29].

Figure 2.3 shows the time-frequency grid of Resource Elements (REs) in a sub-frame with two slots and one resource block. An RE occupies one OFDM symbol in time and one sub-carrier in frequency. A resource block occupies one slot in time (7 OFDM symbols) and $N_f = 12$ sub-carrier in frequency. In order to perform the channel estimation, known pilot symbols (also called reference signals) are inserted in the time-frequency grid (see Figure 2.2). In the LTE downlink, there are two types of reference signals that support the PDSCH transmission [29]. These two reference signals are: UE-specific Reference Signal (UE-RS) and Cell-specific reference signals (CRS). In the simulations throughout this thesis, the CRS signals are used. Figure 2.3 shows an example of the distribution of the CRS samples (pilots) in a sub-frame for one antenna port.

Zadoff-Chu sequences

Zadoff-Chu sequences [57] are CAZAC sequences (sequences with constant amplitude and zero autocorrelation) that are used in the LTE downlink as a primary synchronization signal for synchronization in the frequency domain [29]. The uth root Zadoff-Chu sequence is given by

$$x_u(n) = e^{\frac{-j\pi un(n+1)}{N_{ZF}}}, \;\; n = 0, ..., N_{ZF} - 1, \tag{2.1}$$

where N_{ZF} is the length of a Zadoff-Chu sequence.

The Zadoff-Chu sequences have a constant amplitude, ideal cyclic auto-correlation and very good cross-correlation properties [56]. The DFT of a Zadoff-Chu sequence $x_u(n)$ is a weighted cyclic-shifted Zadoff-Chu sequence $X_w(k)$ [56]. Thus, Zadoff-Chu sequences can be generated directly in the frequency domain without the need for the DFT. In our simulations throughout this thesis, Zadoff-Chu sequences are used to generate the CRS signals (pilot symbols) in the frequency domain.

2.3.2 Downlink LTE system parameters

OFDM is adopted as the modulation scheme for the LTE downlink [29]. The LTE supports QPSK, 16-QAM and 64-QAM modulation schemes [29]. Table 2.1 shows parameters associated with designing the time-frequency grid of the REs in the LTE downlink. The frequency spacing Δf between every two consecutive sub-carriers is 15 kHz. The sampling rate is $f_s = \Delta f N_{DFT}$. For different bandwidths as shown in Table 2.2, although the duration of the short CP is the same, the number of samples are different. This is because for different bandwidths, the sampling frequency is different as presented in Table 2.1.

2.4 MIMO principles

MIMO refers to the use of multiple antennas at the base station and the UE. Such setup can provide spatial diversity in a dense multipath scattering environment, which improves the reliability of the data link. MIMO also can increase the throughput of the wireless communication system. The MIMO setup can be used with different transmission techniques (e.g.,

Table 2.1: LTE system parameters

Bandwidth	1.4 MHz	3 MHz	5 MHz	10 MHz	15 MHz	20 MHz
sub-carrier spacing	15 kHz	15 kHz	15 kHz	15 kHz	15 kHz	15 kHz
Sampling frequency	1.92 MHz	3.84 MHz	7.68 MHz	15.36 MHz	23.04 MHz	30.72 MHz
FFT size (N_{DFT})	128	256	512	1024	1536	2048
Used sub-carriers	72	180	300	600	900	1200
No. of resource blocks	6	15	25	50	75	110
No. of samples per slot	960	1920	3840	7680	11520	15360
OFDM symbols per slot (short CP)	7	7	7	7	7	7

Table 2.2: CP duration

Bandwidth	Short CP
1.4 MHz	5.21 μs for symbol 0 (10 samples) 4.69 μs for symbols 1-6 (9 samples per symbol)
3 MHz	5.21 μs for symbol 0 (20 samples) 4.69 μs for symbols 1-6 (18 samples per symbol)
5 MHz	5.21 μs for symbol 0 (40 samples) 4.69 μs for symbols 1-6 (36 samples per symbol)
10 MHz	5.21 μs for symbol 0 (80 samples) 4.69 μs for symbols 1-6 (72 samples per symbol)
15 MHz	5.21 μs for symbol 0 (120 samples) 4.69 μs for symbols 1-6 (108 samples per symbol)
20 MHz	5.21 μs for symbol 0 (160 samples) 4.69 μs for symbols 1-6 (140 samples per symbol)

spatial multiplexing, transmit diversity, receive diversity and beamforming). Based on the selected transmission technique, one or more of the following gains can be exploited: multiplexing gain, diversity gain and array gain. Most of the transmission techniques focus on multiplexing gain or diversity gain as it is difficult to obtain all the three gains [58].

Consider a MIMO OFDM system with N_t transmit antennas and N_r receive antennas. In the frequency domain, the received signal at rth receive antenna, as shown in Figure 2.4, can be expressed as:

$$\mathbf{z}_r = \sum_{k=1}^{N_t} \mathbf{S}_k \mathbf{h}_{r,k} + \mathbf{n}_r, \;\; r = 1, ..., N_r, \tag{2.2}$$

where k is the transmit antenna index, $\mathbf{S}_k$ is a diagonal matrix of data and pilot symbols, $\mathbf{h}_{r,k}$

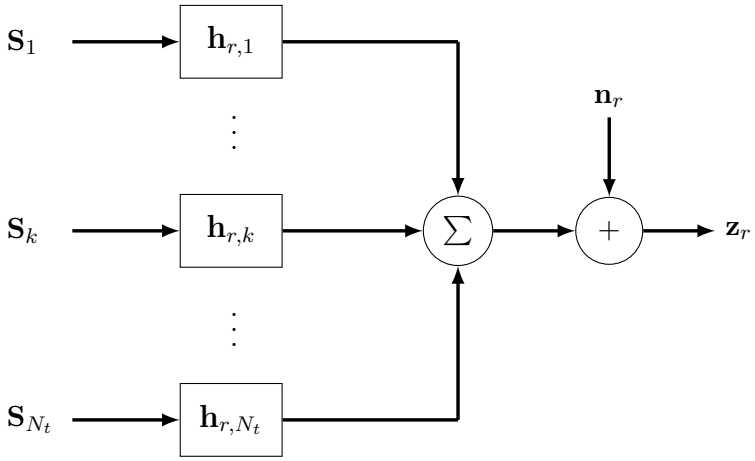

Figure 2.4: Model of received signal.

is a channel fading vector between the kth transmit antenna and the rth receive antenna, $\mathbf{n}_r$ is a complex white Gaussian noise vector with a variance σ_n^2.

2.5 Spatial multiplexing

Spatial multiplexing is a MIMO technique that can provide higher data rates by transmitting independent encoded and modulated data streams [28]. In spatial multiplexing, for equal number of antennas at the transmitter and receiver, the spatial multiplexing gain is directly proportional to the number of antennas. This can be represented in terms of data streams as the following [28]:

$$N_s = \min(N_t, N_r), \tag{2.3}$$

where N_s is the number of data streams. Equation (2.3) shows that a higher throughput can be achieved with no requirement for more bandwidth. Thus, the spectral efficiency of the MIMO system increases with increase in the number of transmit and receive antennas. Although this technique increases the transmission data rate, its performance is affected by the lack of redundancy in the transmitted data.

Open/closed loop spatial multiplexing transmission modes were introduced in the LTE downlink [29] in Release 8. In these modes, the base station uses more than one transmit antenna (i.e., 2, 4 or 8). In the open loop spatial multiplexing transmission mode, the transmitter has no feedback on the channel state information from the receiver. This mode is

used when the channel is rapidly changing due to the fast movement of the UE. In the closed loop spatial multiplexing transmission mode, the UE sends a feedback on the channel state information to the base station. However, this mode is only applicable for channels with low mobility (i.e., fading channels with low Doppler frequency). In Chapters 3 to 5, the open loop spatial multiplexing transmission mode is selected for our investigation.

2.6 Doubly-selective channels

The wireless mobile radio channel is frequency-selective and time-selective. The time and frequency selectivity of the fading channel is commonly called the doubly-selective channel [59, 60]. The frequency-selectivity is caused by the multipath propagation and can be characterized by a delay spread. The channel time-selectivity is caused by the moving transmitter and/or receiver and/or objects within the transmission environment and it can be characterized by a Doppler spread. In OFDM systems, the accurate estimation of doubly-selective channels in time and frequency is crucial for achieving a high detection performance.

The Wide Sense Stationary Uncorrelated Scattering (WSSUS) channel model [61] can be used to model the typical mobile radio wireless channel [62, 63]. In the WSSUS channel model, the fading coefficients from different paths are statistically independent. The WSSUS channel impulse response can be modelled as [63],

$$h(t,\tau) = \sum_{l=0}^{L-1} \gamma_l(t)\delta(\tau - \tau_l), \tag{2.4}$$

where t is time and $\gamma_l(t)$ represent Wide Sense Stationary (WSS) complex Gaussian processes. For WSSUS, $\gamma_l(t)$ are uncorrelated for different paths, τ_l is the delay for the lth path and L is the number of paths. The frequency response of the WSSUS channel can be obtained applying the Fourier transform to (2.4) over the delay τ,

$$H(t,f) = \sum_{l=0}^{L-1} \gamma_l(t)e^{-2\pi j f \tau_l}, \tag{2.5}$$

where f is frequency. In the following subsections, we discuss the classical fading simulator based on Clarke's and Jakes' models.

2.6.1 Clarke's channel model

One of the first proposed mathematical models of the fading channel is Clarke's model [64]. A special case of Clarke's reference model is Jakes' model [65]. However, Jakes' model is not WSS and does not meet most of the statistical properties of Clarke's reference model [66]. Many modifications to Jakes' model were proposed [66–71] to improve some of it statistical properties.

In [64], Clarke developed an isotropic scattering model for narrowband cellular channels assuming a fixed transmission with a vertically polarized antenna. In his model, Clarke assumed that the field incident on the mobile antenna to be comprised of a number of azimuthal plane waves that have arbitrary carrier phases and arbitrary azimuthal angles of arrival. When there is no line of sight path, every wave has equal average amplitude. Thus, the arrived scattered components at the receive antenna are expected to experience similar attenuation in transmissions over small distances.

Let a low-pass fading process describes a frequency-flat fading channel with N_{pc} propagation channels. Then, in complex form, it can be given by

$$h(t) = h_{\Re}(t) + jh_{\Im}(t), \tag{2.6}$$

where

$$h_{\Re}(t) = E_0 \sum_{n=1}^{N_{pc}} C_n \cos(\omega_d t \cos(\alpha_n) + \phi_n), \tag{2.7}$$

$$h_{\Im}(t) = E_0 \sum_{n=1}^{N_{pc}} C_n \sin(\omega_d t \cos(\alpha_n) + \phi_n), \tag{2.8}$$

where E_0 is a scaling factor; ω_d is the angular Doppler frequency with $\omega_d = 2\pi f_d$, f_d is the Doppler frequency; C_n is a random gain of the nth path and α_n and ϕ_n are phases uniformly distributed over $[-\pi, \pi)$.

The auto-correlation and cross-correlation functions associated with Clarke's model are given by the following [65]:

$$R_{h_{\Re}h_{\Re}}(\tau) = \mathbb{E}(g_r(t)g_r(t+\tau)) = J_0(\omega_d \tau), \tag{2.9}$$

$$R_{h_{\Im}h_{\Im}}(\tau) = J_0(\omega_d \tau), \tag{2.10}$$

$$R_{h_{\Re}h_{\Im}}(\tau) = 0, \tag{2.11}$$

$$R_{h_{\Im}h_{\Re}}(\tau) = 0, \tag{2.12}$$

$$R_{hh}(\tau) = 2J_0(\omega_d \tau), \tag{2.13}$$

where $J_0(\cdot)$ is the zero-order Bessel function of the first kind [65].

2.6.2 Jakes' channel model

Jakes' channel model [65] is a simplified version of the Clarke's reference model. Jakes' model makes the following assumptions to Clarke's model:

$$C_n = \frac{1}{\sqrt{N}}, \tag{2.14}$$

$$\alpha_n = \frac{2\pi n}{N}, \quad n = 1, ..., N, \tag{2.15}$$

$$\phi_n = 0, \quad n = 1, ..., N, \tag{2.16}$$

When the assumptions in (2.14) to (2.16) are applied to Clarke's model, we arrive at the complex form of Jakes' channel model (2.6) with the real and imaginary parts given by

$$h_{\Re}(t) = \frac{2}{\sqrt{N}} \sum_{n=1}^{M_{os}} a_n \cos(\omega_n t), \tag{2.17}$$

$$h_{\Im}(t) = \frac{2}{\sqrt{N}} \sum_{n=1}^{M_{os}} b_n \sin(\omega_n t), \tag{2.18}$$

where $N = 4M_{os} + 2$ and M_{os} represents the number of oscillators. The variables a_n and b_n are obtained as the following [65]

$$a_n = \begin{cases} \sqrt{2}\cos(\beta_0) & n = 0 \\ 2\cos(\beta_n) & n = 0, 1, ..., M_{os} \end{cases} \tag{2.19}$$

$$b_n = \begin{cases} \sqrt{2}\sin(\beta_0) & n = 0 \\ 2\sin(\beta_n) & n = 0, 1, ..., M_{os} \end{cases} \tag{2.20}$$

Table 2.3: LTE channel power delay profiles

	EPA		EVA		ETU	
Tap	Delay (ns)	Power (dB)	Delay (ns)	Power (dB)	Delay (ns)	Power (dB)
1	0	0.0	0	0.0	0	-1.0
2	30	-1.0	30	-1.5	50	-1.0
3	70	-2.0	150	-1.4	120	-1.0
4	90	-3.0	310	-3.6	200	0.0
5	110	-8.0	370	-0.6	230	0.0
6	190	-17.2	710	-9.1	500	0.0
7	410	-20.8	1090	-7.0	1600	-3.0
8	-	-	1730	-12.0	2300	-5.0
9	-	-	2510	-16.9	5000	-7.0

$$\beta_n = \begin{cases} \pi/4 & n = 0 \\ (\pi n)/M_{os} & n = 0, 1, ..., M_{os} \end{cases} \tag{2.21}$$

$$\omega_n = \begin{cases} \omega_d & n = 0 \\ \omega_d \cos(\frac{2\pi n}{N}) & n = 0, 1, ..., M_{os} \end{cases}. \tag{2.22}$$

The assumptions in (2.14) to (2.16) result in Jakes' channel model being a deterministic model [67]. Jakes' channel model (or its modifications) is often used for fading channel simulation.

2.7 LTE propagation channel models

The LTE standard defines three PDP models for multipath propagation [72]: Extended Typical Urban (ETU), Extended Vehicular A (EVA) and Extended Pedestrian A (EPA) models. As shown in Table 2.3, the ETU PDP represents a high delay spread, while the EVA and EPA PDPs represent medium and low delay spreads, respectively, in comparison to the short CP duration. The multipath fading channel in the LTE standard is often described by one of the PDPs and a maximum Doppler frequency. The Doppler frequency can be computed as

$$f_d = \frac{v f_c}{c} \cos(\alpha_n), \tag{2.23}$$

where v is the velocity of the moving object measured in meters per seconds (m/s), f_c is the carrier frequency in Hertz, c is the speed of light ($c \approx 3 \times 10^8$ m/s) and α_n is the angle of arrival for the nth path. To obtain the maximum Doppler frequency in (2.23), we set $\cos(\alpha_n) = 1$. For example, for a carrier frequency of 2 GHz, a velocity of the user mobile of

52.5 m/s (about 189 km/h), the maximum Doppler frequency can be calculated as

$$f_d = \frac{(52.5) \times (2 \times 10^9)}{3 \times 10^8} \approx 350\text{Hz}. \tag{2.24}$$

2.8 Channel estimation

The channel state information can be obtained through blind channel estimation [73–76], semi-blind channel estimation [73, 77–79] or pilot-based channel estimation [1, 80–83]. In the blind channel estimation, the input of the channel is unavailable at the receiver and pilot symbols are not used [73–76]. In the literature, many blind channel estimation techniques were proposed. Most of these techniques rely on the evaluation of second or higher order channel statistics to perform channel estimation [75]. The blind channel estimation avoids the large overhead in the spectral efficiency caused by the addition of pilot signals. However, it requires an accurate knowledge of the channel length and the channel correlation matrix as well as a high computational complexity [83]. Also, it requires a large time interval (number of symbols) for the estimation. This can be unavailable in fast varying channels. On the other hand, semi-blind channel estimation employs techniques that are proposed for blind channel estimation with partial knowledge of the channel [79]. In the semi-blind channel estimation, the partial knowledge of the channel can be obtained by using the known pilot symbols [79]. In this thesis, the channel estimation is mostly semi-blind, as the estimation is relying on unknown data with partial knowledge of the channel through pilot-based channel estimation.

In the LTE downlink, the pilot-based channel estimation is a two dimensional problem. As the channel is varying in time and frequency (doubly-selective channel), pilots are distributed over the time-frequency grid (see Figure 2.3). Then, these pilots are used to estimate the doubly-selective channel. This can be achieved by using separable one-dimensional channel estimators [84] or a joint time-frequency channel estimator (i.e., a two-dimensional estimator). Two-dimensional channel estimators are more accurate, but they can require a high computational load. In the following section, the pilot-based channel estimation using BEMs is introduced, which can reduce the channel estimation complexity.

2.9 BEM channel estimation

BEMs can be used to estimate doubly-selective channels in time and frequency [2–4]. The time varying channel response $\mathbf{h}$ can be represented in terms of BEMs as:

$$\mathbf{h} = \mathbf{B}\mathbf{a}, \tag{2.25}$$

where $\mathbf{B}$ is an $N \times M$ matrix of basis functions, N is the length of data package, M is the number of basis functions, and $\mathbf{a}$ is an $M \times 1$ vector of expansion coefficients. This may reduce the complexity of channel estimation as M is usually much smaller than N.

The two dimensional BEM matrix $\mathbf{B}$ in time and frequency can be computed by [23]

$$\mathbf{B} = \mathbf{B}_t \otimes \mathbf{B}_f, \tag{2.26}$$

where $\mathbf{B}_t$ is an $N_{OFDM} \times M_t$ matrix of basis functions in time, M_t is the number of basis functions in time, $\otimes$ denotes the Kronecker product, $\mathbf{B}_f$ is an $N_f \times M_f$ matrix of basis functions in frequency and M_f is the number of basis functions in frequency. The time-frequency basis functions can be found by selecting the highest M_t and M_f, $M = M_t M_f$, that provides a low approximation error in the case of the worst channel (e.g., in this thesis, the ETU channel).

Different BEMs have been considered in the literature for the estimation of doubly-selective channels. Karhunen-Loeve (KL) [5, 85] and Discrete Prolate Spheroidal Sequences (DPSS) [6, 7] basis functions can provide high accuracy when approximating the fading channel. However, KL and DPSS BEMs require the knowledge of the statistical information of the channel. Complex Exponentials (CE) [4], B-splines [8–10] and Legandre polynomials [86] basis functions do not require the knowledge of the channel information, but they can provide a lower channel approximation performance in comparison to that of the KL and the DPSS basis functions [87]. On the other hand, the complexity of estimation with the CE and cubic B-splines can be lower than that with the KL and the DPSS [87]. In this thesis, we consider DPSS as the basis functions used to estimate the frequency variations of the fading channel and parabolic B-splines for the time variations. However, these basis functions are only used for demonstration purpose, and other basis functions can be equally used. Below,

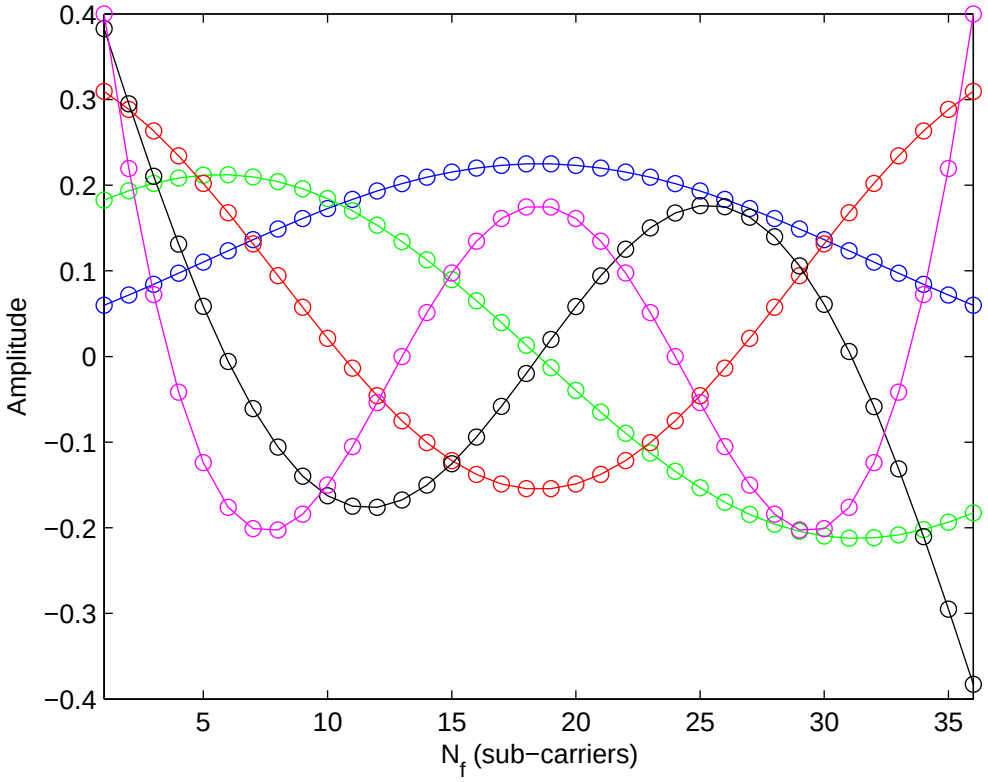

Figure 2.5: DPSS basis functions $\mathbf{B}_f$ for $N_f = 36$ and $M_f = 5$.

we introduce the DPSS and the parabolic B-spline basis functions.

2.9.1 Discrete Prolate Spheroidal Sequences (DPSS)

The DPSS (also called Slepian sequences [88]) are widely used for the approximation of frequency-selective and time-selective fading channels [7, 12, 59]. These functions are orthogonal [59] and optimal (i.e., they are KL basis functions) in multipath channels with a uniform PDP within the channel delay spread. In frequency-selective channels, the BEM matrix $\mathbf{B}_f$ of DPSS is given by:

$$[\mathbf{B}_f]_{u,l} = \beta_l(u), \quad u = 1, ..., N_f, \tag{2.27}$$

where l refers to the lth basis function, $l = 1, ..., M_f$, and $\beta_l(u)$ represent the first M_f eigenvectors with the highest eigenvalues of a matrix $\mathbf{M}$ given by

$$[\mathbf{M}]_{i,j} = \frac{\sin[\Omega(i-j)]}{\Omega(i-j)}, \quad i, j = 1, ..., N_f, \tag{2.28}$$

Ω is a value in the range $(0, \frac{1}{2})$, $\Omega = \frac{\tau_{max}\Delta f}{2}$, τ_{max} is the channel delay spread, and Δf

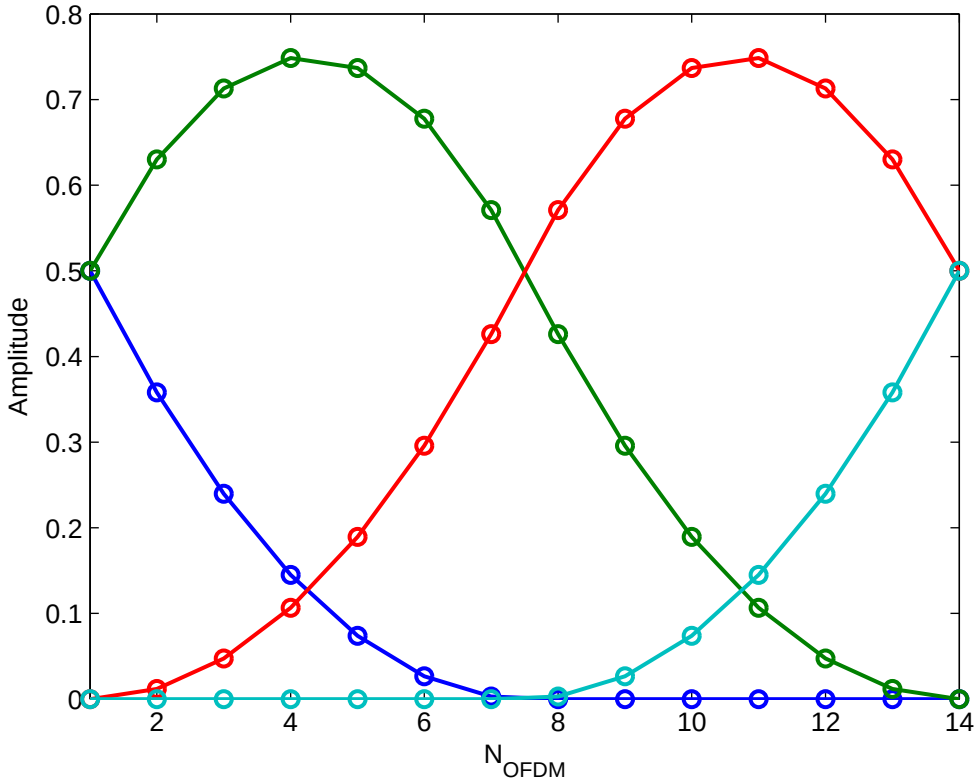

Figure 2.6: Parabolic B-splines basis functions $\mathbf{B}_t$ for $N_{OFDM} = 14$ and $M_t = 4$.

is the frequency spacing between two consecutive sub-carriers (e.g., $\Delta f = 15$ kHz for the LTE [29]). Figure 2.5 shows an example of the DPSS for $M_f = 5$ basis functions and $N_f = 36$ sub-carriers.

2.9.2 Parabolic B-splines

B-splines are popular and widely used for the approximation of continues functions. B-splines can provide a high estimation accuracy with a low computational load [8–10]. B-spline of order q is given by [10]:

$$B_q(t_n) = \frac{1}{q!}\sum_{i=0}^{q+1}(-1)^i \binom{q+1}{i} \left(\frac{t_n}{T_b} + \frac{q+1}{2} - i\right)_+^q, \tag{2.29}$$

where $(x)_+ = \max\{0, x\}$, t_n is a time instant given by $t_n = (n-1) - (m - ((q+1)/2))T_b$, $n = 1, ..., N_{OFDM}$, $m = 1, ..., M_t$, and T_b is the spacing between two basis functions, $T_b =$

$(N_{OFDM}-1)/(M_t-q)$. For the parabolic B-spline ($q=2$), the matrix $\mathbf{B}_t$ is generated by

$$[\mathbf{B}_t]_{n,m} = B_2(t_n) = \begin{cases} \frac{3}{4} - \frac{t_n^2}{T_b^2}, & |t_n| < \frac{T_b}{2}; \\ \frac{1}{2}(\frac{t_n}{T_b})^2 - \frac{3|t_n|}{2T_b} + \frac{9}{8}, & |t_n| \geq \frac{T_b}{2}; \\ 0, & \text{otherwise.} \end{cases} \tag{2.30}$$

In Figure 2.6, an example of basis functions generated using (2.30) for $N_{OFDM} = 14$ OFDM symbols and $M_t = 4$ is shown.

2.10 Pilot-based channel estimation using BEMs

2.10.1 Least Squares (LS) pilot-based channel estimation

For the case of a SISO OFDM system, the received signal model can be given by

$$\mathbf{z} = \mathbf{S}\mathbf{h} + \mathbf{n}, \tag{2.31}$$

where $\mathbf{z}$ is an $N \times 1$ received signal vector, $\mathbf{S}$ is an $N \times N$ diagonal matrix of data and pilot symbols, $\mathbf{h}$ is an $N \times 1$ vector of channel frequency response and $\mathbf{n}$ is an $N \times 1$ vector of white Gaussian noise. From (2.31), the received pilot signal can be described as

$$\mathbf{z}_p = \mathbf{S}_p\mathbf{h}_p + \mathbf{n}_p, \tag{2.32}$$

where $\mathbf{z}_p$ is an $N_p \times 1$ vector of received pilots, $p = 1, ..., N_p$, N_p is the total number of pilot symbols, $\mathbf{S}_p$ is an $N_p \times N_p$ diagonal matrix of pilot symbols, $\mathbf{h}_p$ is an $N_p \times 1$ vector of channel frequency response at pilot locations and $\mathbf{n}_p$ is an $N_p \times 1$ vector of white Gaussian noise at pilot locations. The pilot symbol matrix $\mathbf{S}_p$ can be obtained from $\mathbf{S}$ by selecting the pilot locations, and thus we have

$$\mathbf{S}_p = \begin{bmatrix} s(0) & 0 & \cdots & 0 \\ 0 & s(1) & \cdots & 0 \\ \vdots & \vdots & \ddots & \vdots \\ 0 & 0 & 0 & s(N_p-1) \end{bmatrix}. \tag{2.33}$$

Representing the channel vector $\mathbf{h}$ in terms of BEMs, we have $\mathbf{h} = \mathbf{B}\mathbf{a}$. The LS estimate

$\hat{\mathbf{a}}_{LS}$ of the expansion coefficients $\mathbf{a}$ can be obtained by the following:

$$\hat{\mathbf{a}}_{LS} = (\mathbf{B}_p^H \mathbf{S}_p^H \mathbf{S}_p \mathbf{B}_p)^{-1} \mathbf{B}_p^H \mathbf{S}_p^H \mathbf{z}_p, \tag{2.34}$$

where $\mathbf{B}_p$ is an $N_p \times M$ matrix of basis functions obtained from $\mathbf{B}$ at pilot location.

Now, we consider the case of a time varying MIMO OFDM system. The received signal model can be described by

$$\mathbf{z} = \mathbf{\Psi}\mathbf{a} + \mathbf{n}, \tag{2.35}$$

where $\mathbf{z}$ is an $NN_r \times 1$ vector of received signals, $\mathbf{z} = [\mathbf{z}_1^T, ..., \mathbf{z}_r^T, ..., \mathbf{z}_{N_r}^T]^T$, $\mathbf{z}_r$ is an $N \times 1$ received vector at the rth receive antenna, N_r is the number of receive antennas, $\mathbf{\Psi}$ is an $NN_r \times MN_tN_r$ matrix, $\mathbf{\Psi} = \mathbf{I}_{N_r} \otimes [\mathbf{S}_1\mathbf{B}, ..., \mathbf{S}_k\mathbf{B}, ..., \mathbf{S}_{N_t}\mathbf{B}]$, $\mathbf{S}_k$ is an $N \times N$ diagonal matrix of data and pilot symbols transmitted by the kth transmit antenna, N_t is the number of transmit antennas, $\mathbf{a} = [\mathbf{a}_1^T, ..., \mathbf{a}_r^T, ..., \mathbf{a}_{N_r}^T]^T$, $\mathbf{a}_r = [\mathbf{a}_{r,1}^T, ..., \mathbf{a}_{r,k}^T, ..., \mathbf{a}_{r,N_t}^T]^T$, $\mathbf{a}_{r,k}$ is an $M \times 1$ vector of BEM expansion coefficients for the channel between the kth transmit antenna and the rth receive antenna, $\mathbf{n} \sim \mathcal{N}_C(0, \sigma_n^2 \mathbf{I}_{NN_r})$ is an $NN_r \times 1$ vector of complex-valued Gaussian noise with variance σ_n^2, $\mathbf{n} = [\mathbf{n}_1^T, ..., \mathbf{n}_r^T, ..., \mathbf{n}_{N_r}^T]^T$, and $\mathbf{n}_r$ is an $N \times 1$ noise vector on the rth receive antenna.

The received data and pilot signals can be obtained from (2.35) as

$$\mathbf{z}_d = \mathbf{\Psi}_d\mathbf{a} + \mathbf{n}_d, \tag{2.36}$$

$$\mathbf{z}_p = \mathbf{\Psi}_p\mathbf{a} + \mathbf{n}_p, \tag{2.37}$$

where $\mathbf{z}_d$ is an $N_dN_r \times 1$ vector of received data, $\mathbf{z}_d = [\mathbf{z}_{d,1}^T, ..., \mathbf{z}_{d,r}^T, ..., \mathbf{z}_{d,N_r}^T]^T$, $\mathbf{z}_{d,r}$ is an $N_d \times 1$ vector of received data at the rth receive antenna, N_d is the number of data symbols, $\mathbf{\Psi}_d = \mathbf{I}_{N_r} \otimes [\mathbf{S}_{d,1}\mathbf{B}_d, ..., \mathbf{S}_{d,k}\mathbf{B}_d, ..., \mathbf{S}_{d,N_t}\mathbf{B}_d]$ is $N_dN_r \times MN_rN_t$ matrix, $\mathbf{S}_{d,k}$ is an $N_d \times N_d$ diagonal matrix obtained from $\mathbf{S}_k$ at data locations, $\mathbf{B}_d$ is an $N_d \times M$ matrix of basis functions ($\mathbf{B}$ at data locations), $\mathbf{n}_d$ is an $N_dN_r \times 1$ vector of complex-valued Gaussian noise, $\mathbf{z}_p$ is an $N_pN_r \times 1$ vector of received pilot symbols, N_p is the number of pilot symbols, $\mathbf{\Psi}_p = \mathbf{I}_{N_r} \otimes [\mathbf{S}_{p,1}\mathbf{B}_p, ..., \mathbf{S}_{p,k}\mathbf{B}_p, ..., \mathbf{S}_{p,N_t}\mathbf{B}_p]$ is $N_pN_r \times MN_rN_t$ matrix, $\mathbf{S}_{p,k}$ is an $N_p \times N_p$ diagonal matrix obtained from $\mathbf{S}_k$ at pilot locations, $\mathbf{B}_p$ is an $N_p \times M$ matrix of basis functions ($\mathbf{B}$ at pilot locations), $\mathbf{n}_p$ is an $N_pN_r \times 1$ vector of complex-valued Gaussian noise.

The LS estimate $\hat{\mathbf{a}}_{LS}$ of $\mathbf{a}$ is given by

$$\hat{\mathbf{a}}_{LS} = (\mathbf{\Psi}_p^H \mathbf{\Psi}_p)^{-1} \mathbf{\Psi}_p^H \mathbf{z}_p. \tag{2.38}$$

The implementation of the LS channel estimator is straightforward. However, the LS channel estimation does not take into account the effect of the additive noise and the channel time-frequency correlation. It enhances the noise power and results in a degraded performance.

2.10.2 Pilot-based LMMSE BEM channel estimation

Pilot-based LMMSE BEM channel estimation extends the LS channel estimation by taking into account the noise power and channel time-frequency correlation. For the SISO case, the BEM-based LMMSE channel estimate $\hat{\mathbf{a}}_{LMMSE}$ of $\mathbf{a}$ can be obtained by the following:

$$\hat{\mathbf{a}}_{LMMSE} = (\mathbf{B}_p^H \mathbf{S}_p^H \mathbf{S}_p \mathbf{B}_p + \mathbf{\Gamma})^{-1} \mathbf{B}_p^H \mathbf{S}_p^H \mathbf{z}_p, \tag{2.39}$$

where $\mathbf{\Gamma}$ is an $M \times M$ regularization matrix, $\mathbf{\Gamma} = \sigma_n^2 \mathbf{R}_a^{-1}$ and $\mathbf{R}_a$ is an $M \times M$ covariance matrix of the expansion coefficients. The covariance matrix $\mathbf{R}_a$ is given by

$$\mathbf{R}_a = \mathbb{E}[\mathbf{a}\mathbf{a}^H]. \tag{2.40}$$

An explicit expression for the covariance matrix of the expansion coefficients $\mathbf{R}_a$ can be obtained using the channel covariance matrix $\mathbf{\Upsilon}$ as the following

$$\begin{aligned} \mathbf{\Upsilon} &= \mathbb{E}[\mathbf{h}\mathbf{h}^H] \\ &= \mathbb{E}[\mathbf{B}\mathbf{a}\mathbf{a}^H\mathbf{B}^H] \\ &= \mathbf{B}\mathbb{E}[\mathbf{a}\mathbf{a}^H]\mathbf{B}^H \\ &= \mathbf{B}\mathbf{R}_a\mathbf{B}^H. \end{aligned} \tag{2.41}$$

Rearranging (2.41) to obtain an expression for $\mathbf{R}_a$, we multiply the left side of $\mathbf{\Upsilon}$ by $(\mathbf{B}^H\mathbf{B})^{-1}\mathbf{B}^H$ and the right side of $\mathbf{\Upsilon}$ by $\mathbf{B}(\mathbf{B}^H\mathbf{B})^{-1}$. From this, $\mathbf{R}_a$ can be found as

$$\mathbf{R}_a = \mathbb{E}[\mathbf{a}_{r,k}\mathbf{a}_{r,k}^H] = (\mathbf{B}^H\mathbf{B})^{-1}\mathbf{B}^H\mathbf{\Upsilon}\mathbf{B}(\mathbf{B}^H\mathbf{B})^{-1}. \tag{2.42}$$

For the case of MIMO OFDM, using the linear models for data and pilots in (2.36) and (2.37), the LMMSE estimate $\hat{\mathbf{a}}_{LMMSE}$ is given by

$$\hat{\mathbf{a}}_{LMMSE} = (\mathbf{\Psi}_p^H \mathbf{\Psi}_p + \mathbf{\Gamma}_{MIMO})^{-1} \mathbf{\Psi}_p^H \mathbf{z}_p, \tag{2.43}$$

where $\mathbf{\Gamma}_{MIMO} = \sigma_n^2 (\mathbf{I}_{N_r} \otimes \mathbf{I}_{N_t} \otimes \mathbf{R}_a)^{-1}$. In the following section, we show how the channel estimates are used in MIMO detection.

2.11 Linear MIMO mismatched detection

In this section we introduce two popular linear detectors: Zero Forcing (ZF) detector and Minimum Mean Square Error (MMSE) detector. These detectors assume that the channel estimates used in the detection process are prefect. However, in practice, the obtained channel estimates are imperfect and thus when used in these detectors they are called mismatched detectors. The ZF and MMSE detectors are Symbol-by-Symbol (SbS) detectors. This means that the detection is performed on a symbol basis. Therefore, we simplify the signal model in (2.35) which describes all data and pilot symbols. For the SbS case, $\mathbf{z}$ is simplified to $\mathbf{z} = [z_1^{(i)}, ..., z_r^{(i)}, ..., z_{N_r}^{(i)}]^T$, $i = 1, ..., N$, $z_r^{(i)}$ is the ith element of the received vector $\mathbf{z}_r$, $\mathbf{\Psi}$ is simplified to $\mathbf{\Psi} = \mathbf{I}_{N_r} \otimes [s_1^{(i)} \mathbf{b}^{(i)}, ..., s_k^{(i)} \mathbf{b}^{(i)}, ..., s_{N_t}^{(i)} \mathbf{b}^{(i)}]$, $s_k^{(i)}$ is the ith element of the transmitted vector $\mathbf{s}_k$, $\mathbf{S}_k = \text{diag}(\mathbf{s}_k)$, $\mathbf{b}^{(i)}$ is an $1 \times M$ vector obtained as the ith row of the matrix $\mathbf{B}$.

2.11.1 ZF MIMO mismatched detection

ZF MIMO detection is a linear MIMO detection technique that provides sub-optimal performance with a relatively low complexity. In this detection, the ZF filter is simply an inverse filter which eliminates the ISI while the effect of noise is ignored. Therefore, the performance of this detector is degraded due to the enhancement of the noise. The ZF filter is given by [43]

$$\mathbf{F}_{ZF} = (\mathbf{H}_i^H \mathbf{H}_i)^{-1} \mathbf{H}_i^H, \tag{2.44}$$

where $\mathbf{H}_i$ is an ith $N_r \times N_t$ MIMO channel matrix given by

$$\mathbf{H}_i = \begin{bmatrix} h_{1,1}^{(i)} & \cdots & h_{1,k}^{(i)} & \cdots & h_{1,N_t}^{(i)} \\ \vdots & \ddots & \vdots & & \vdots \\ h_{r,1}^{(i)} & \cdots & h_{r,k}^{(i)} & \cdots & h_{r,N_t}^{(i)} \\ \vdots & & \vdots & \ddots & \vdots \\ h_{N_r,1}^{(i)} & \cdots & h_{N_r,k}^{(i)} & \cdots & h_{N_r,N_t}^{(i)} \end{bmatrix}, \tag{2.45}$$

where $h_{r,k}^{(i)}$ is the ith element of a channel vector $\mathbf{h}_{r,k}$ that describes the channel frequency response between the rth receive and kth transmit antennas. Using (2.44), the ith symbol estimate in the linear ZF detector is given by [43]

$$\begin{aligned} \hat{\mathbf{s}}_{ZF}^{(i)} &= \mathbf{F}_{ZF}\mathbf{z}^{(i)} \\ &= (\mathbf{H}_i^H\mathbf{H}_i)^{-1}\mathbf{H}_i^H\mathbf{z}^{(i)} \\ &= \mathbf{s}^{(i)} + (\mathbf{H}_i^H\mathbf{H}_i)^{-1}\mathbf{H}_i^H\mathbf{n}^{(i)}, \end{aligned} \tag{2.46}$$

where $\hat{\mathbf{s}}_{ZF}^{(i)}$ is an $N_t \times 1$ vector of estimates of the transmitted data symbols, $\hat{\mathbf{s}}_{ZF}^{(i)} = [\hat{s}_1^{(i)}, ..., \hat{s}_k^{(i)}, ..., \hat{s}_{N_t}^{(i)}]^T$, $\mathbf{z}^{(i)}$ is an ith $N_r \times 1$ vector of received signals, $\mathbf{z}^{(i)} = [z_1^{(i)}, ..., z_r^{(i)}, ..., z_{N_r}^{(i)}]^T$, $\mathbf{s}^{(i)}$ is an $N_t \times 1$ vector of transmitted data symbols, $\mathbf{s}^{(i)} = [s_1^{(i)}, ..., s_k^{(i)}, ..., s_{N_t}^{(i)}]^T$, and $\mathbf{n}^{(i)}$ is an an $N_r \times 1$ vector of complex noise, $\mathbf{n} = [n_1^{(i)}, ..., n_r^{(i)}, ..., n_{N_r}^{(i)}]^T$. The term $\mathbf{s}^{(i)}$ in (2.46) is free of ISI, thus it is called zero forcing detection (i.e., forces the ISI to zero). The term $[(\mathbf{H}_i^H\mathbf{H}_i)^{-1}\mathbf{H}_i^H\mathbf{n}^{(i)}]$ in (2.46) causes an enhancement of the noise, and subsequently degrades the performance of the ZF detector.

2.11.2 MMSE MIMO mismatched detection

The ZF detector removes the ISI, but does not give the best detection performance as it does not take the noise enhancement into account. A better linear detector is the MMSE detector which reduces the effect of the ISI while taking into account the effect of noise. The MMSE filter is given by [43]

$$\mathbf{F}_{MMSE} = (\mathbf{H}_i^H\mathbf{H}_i + \sigma_n^2\mathbf{I}_{N_t})^{-1}\mathbf{H}_i^H. \tag{2.47}$$

Using (2.47), the ith symbol estimate in the linear MMSE detector is given by [43]

$$\begin{aligned} \hat{\mathbf{s}}_{MMSE}^{(i)} &= \mathbf{F}_{MMSE}\mathbf{z}^{(i)} \\ &= \check{\mathbf{s}}^{(i)} + (\mathbf{H}_i^H\mathbf{H}_i + \sigma_n^2\mathbf{I}_{N_t})^{-1}\mathbf{H}_i^H\mathbf{n}^{(i)}, \end{aligned} \tag{2.48}$$

where $\hat{\mathbf{s}}^{(i)}_{MMSE}$ is an ith $N_t \times 1$ vector of estimates of the transmitted data symbols, $\hat{\mathbf{s}}^{(i)}_{MMSE} = [\hat{s}^{(i)}_1, ..., \hat{s}^{(i)}_k, ..., \hat{s}^{(i)}_{N_t}]^T$. The regularization term $\sigma_n^2 \mathbf{I}_{N_t}$ causes the effect of the noise power on the symbol estimate to be reduced [89].

2.12 Optimal detection

In the previous section, mismatched detectors that have relatively low complexity were discussed. However, these detectors can result in a degraded performance [43]. A better detection can be achieved by the use of the optimal detector [19,20,40–42]. This detector processes the received data and pilot symbols jointly to detect the transmitted data symbols without explicit channel estimation. The optimal detector exploits the same *a priori* information as that of the mismatched detector with LMMSE channel estimates. However, the LMMSE channel estimator minimizes errors in the channel estimates while the optimal detector minimizes the probability of detection errors [87]. Therefore, the optimal detection outperforms the mismatched detection with LMMSE channel estimation [20]. Although the optimal detector provides the best performance, it is impractical due to its high complexity. A detailed discussion on the optimal detector, its detection performance and complexity reduction is presented in Chapter 4.

2.13 Turbo coding

The noisy channel introduces data errors to the received data. These errors can be corrected by the use of Forward Error Correction (FEC), i.e., channel coding. The FEC encodes the transmitted data bits by adding redundant information bits which allow the receiver to correct the errors. One of popular FEC techniques that is widely used is the turbo coding [90]. The turbo coding was first proposed by Berrou, Glavieux and Thitimajshima in [91,92]. This coding was shown through numerical simulation to provide a performance close to that of the Shannon channel capacity limit with the Binary Phase Shift Keying (BPSK) modulation scheme. A turbo encoder usually consists of two parallel identical encoders as shown in Figure 2.7. The parallel encoders can be convolutional or block encoders. The first encoder encodes the input bits directly. The second encoder encodes an interleaved version of the input bits using an internal interleaver. This guarantees a low probability of both encoders having input bits that result in low weight outputs [90]. For LTE uplink/downlink scenarios [29], the two encoders are 8-state constituent encoders with an interleaver forming a

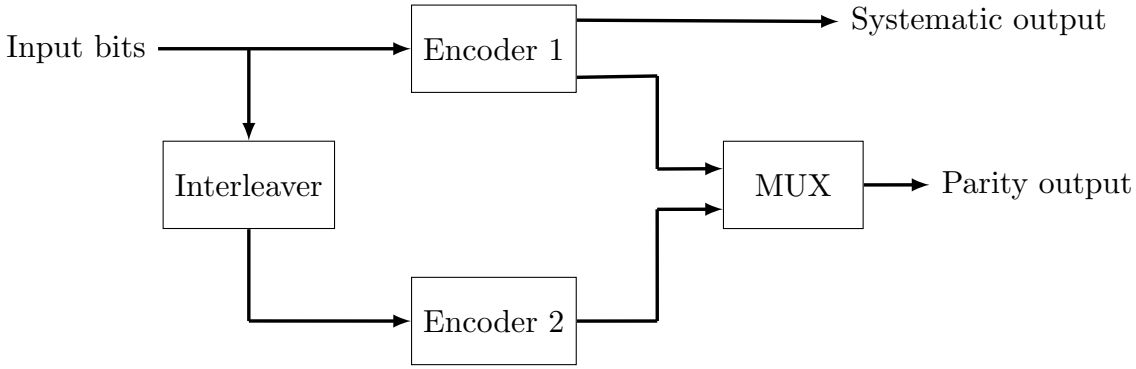

Figure 2.7: Turbo encoder.

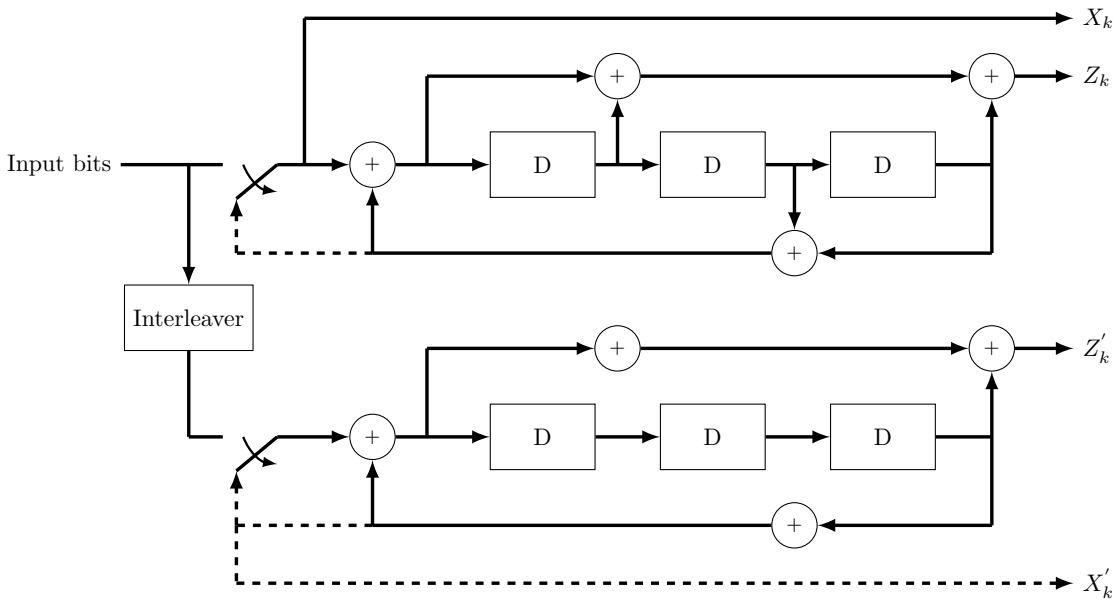

Figure 2.8: Rate $\frac{1}{3}$ turbo encoder.

recursive parallel concatenated convolutional coding. LTE supports trubo codes with a $\frac{1}{3}$-code rate only [29]. In order to achieve different code rates for turbo coding, rate matching is used.

Figure 2.8 shows the detailed structure of the encoders used in turbo codes [29, 90]. The turbo encoder has a systematic output X_k and two parity outputs Z_k and Z'_k. D refers to a delay. The systematic output X_k is passed without change from the input bits while the two parity outputs Z_k and Z'_k are encoded by convolutional encoders 1 and 2, respectively. The dotted lines in Figure 2.8 refer to trellis termination. The turbo encoder multiplexes the three streams: the systematic output X_k and two parity outputs Z_k and Z'_k (as shown in Figures 2.7 and 2.8).

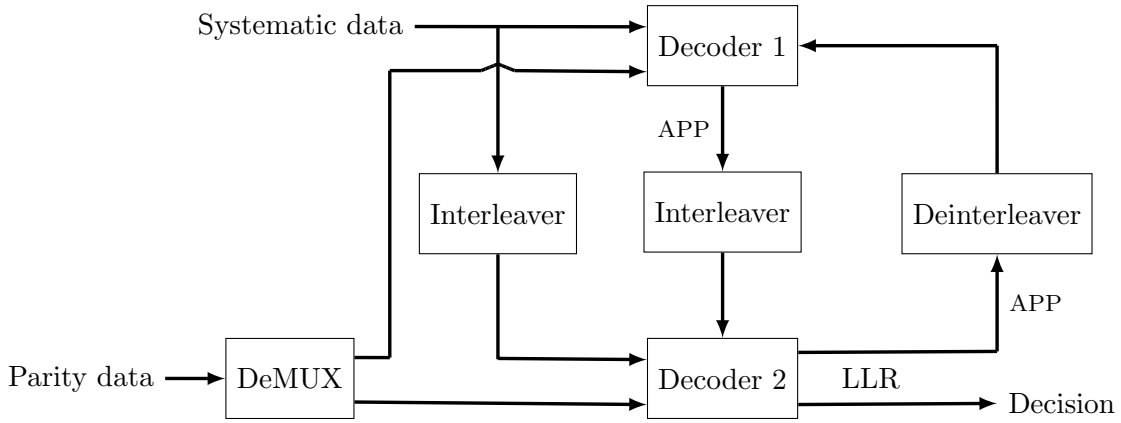

Figure 2.9: Turbo decoder.

2.13.1 Turbo decoding

Figure 2.9 shows the general structure of a turbo decoder. For each turbo encoder used, we have one decoder that estimates the *a posteriori* probability (APP) for every data bit. In the LTE, the turbo decoder is a Soft Input Soft Output (SISO) decoder [29]. The first SISO decoder has two inputs: a systematic data input and an *a priori* Log Likelihood Ratio (LLR) input. The second SISO decoder has the same two inputs, but the first input is an interleaved version of the systematic data. The interleaver and deinterleaver are used in the trubo decoding operations to eliminate the correlation between neighbouring data bits. This decoding process is used in an iterative manner for typically 4 to 8 iterations to improve the performance. In this thesis, we perform 8 iterations for the iterative decoder as shown in [93].

The LLR value λ_b of a data bit b is obtained as the log of the ratio of two probabilities (i.e., for $b = 1$ or $b = 0$)

$$\lambda_b = \ln \Big[\frac{P(b = 1|y)}{P(b = 0|y)}\Big], \tag{2.49}$$

where the two probabilities $P(b = 1|y)$ and $P(b = 0|y)$ correspond to the reliability in the transmitted data bit b being data bit 1 and data bit 0, respectively. These two probabilities are conditioned on a received sequence y (i.e., the systematic data in Figure 2.9). The conditional probabilities $P(b = 1|y)$ and $P(b = 0|y)$ are the APP the turbo decoders estimate for every bit.

Maximum a-posteriori Probability (MAP) decoding algorithm (also known as BCJR algorithm) is a recursive symbol-by-symbol decoding scheme that was initially proposed in [94].

The MAP decoding algorithm provides the optimum decoding performance. However, it is very complicated, especially for large data blocks. Therefore, the data are decoded at the receiver by a simplified versions of the MAP decoding algorithm. This can be achieved by transforming the MAP decoding algorithm to the logarithmic domain in order to reduce its computational complexity. This results in two simplified versions of the MAP algorithm: the Log-MAP and Max-Log-MAP algorithm [95].

In Log-MAP, the Jacobian algorithm can be computed as the following [96]:

$$\begin{aligned} \max^*(x, y) &= \ln(e^x + e^y) \\ &= \max(x, y) + \ln(1 + e^{-|y-x|}) \\ &= \max(x, y) + f_c(|y - x|), \end{aligned} \tag{2.50}$$

where $f_c(|y-x|)$ is a correction function. $f_c(|y-x|)$ can be stored in a simple look-up table [96]. The Log-MAP decoding algorithm computed using (2.50) can achieve the close-to-optimal performance of the MAP decoding algorithm with significantly lower complexity [96].

The Max-Log-MAP can be obtained from (2.50) by omitting the correction function $f_c(|y - x|)$,

$$\max^*(x, y) \approx \max(x, y). \tag{2.51}$$

Max Log-MAP decoding algorithm is much faster than Log-MAP, but this is at the expense of a degradation in the decoding performance. Also, the Max Log-MAP algorithm is sub-optimal at low SNR values. Therefore, we consider Log-MAP decoding algorithm for the turbo decoder in our simulations. In the LTE standard [29], Log-MAP and Max Log-MAP algorithms are supported for the turbo decoding.

2.14 Summary

This chapter can be summarized as the following:

- The combination of MIMO and OFDM technologies for wireless communication systems has been discussed.
- Downlink LTE system specifications and parameters were presented and explained. The

implementation of OFDM in the LTE downlink has been discussed.

- Doubly-selective channels have been introduced. Mathematical representations of Clarke's and Jakes' channel models were presented.
- Pilot-based channel estimation techniques, such as LS and LMMSE channel estimators using BEMs were introduced. The DPSS and parabolic B-spline basis functions were presented for estimation of channel variations in time and frequency.
- An introduction to linear MIMO mismatched detectors such as ZF and MMSE detectors has been provided. The optimal detector that can outperform the mismatched detectors was briefly discussed.
- Channel coding and decoding using turbo codes were presented and explained.
- The techniques considered in this chapter will be used for our design and simulation in the rest of this thesis.

Chapter 3

Data-aided reweighted iterative channel estimation for MIMO OFDM

Contents

3.1 Introduction

In wireless communications, a wide-band mobile radio channel is doubly-selective in time and frequency. The accurate estimation of such channels is challenging. Pilot-based channel estimation is most often used in practice, but it may provide a low estimation performance. Tentative estimates of data symbols can be used to improve the estimation performance in an iterative manner [12,16,17,97]. In [18], a reweighted channel estimator based on tentative data estimates is shown to outperform the unweighted estimation in a multi-user system with Single Carrier Frequency Division Multiple Access (SC-FDMA) modulation in the LTE uplink scenarios. The weights in [18] are optimized for Gaussian data errors, the assumption that holds for the SC-FDMA modulation. In the downlink LTE scenarios, however the OFDM

modulation is used [29], and the Gaussian assumption on data errors is not applicable. As follows from [18], if the residual power for a resource element (defined by time-frequency location of a transmitted symbol) is smaller than the noise variance, the corresponding weight should be unity as in conventional unweighted estimators. However, for higher residual powers, the higher the power the smaller is the weight. Thus the contribution from potentially erroneous data to the channel estimate is reduced. We can expect that any weights that follow this idea should be effective. In particular, weights optimized in [18] for SC-FDMA can also be expected to be efficient for OFDM. In this chapter, we show that indeed by applying such weights, a significant improvement in the performance of MIMO OFDM systems is achieved.

In this chapter, a sequential interference cancellation scheme with reweighted LMMSE channel estimation is proposed for MIMO OFDM systems. In every iteration, the tentative data symbols are recovered without decoding, thus reducing the estimator complexity. It is shown through simulation for downlink LTE scenarios that the reweighted iterative channel estimation significantly outperforms the conventional unweighted iterative estimation.

The organization of the remainder of this chapter is as follows: In Section 3.2, a signal model is introduced. Weighted channel estimation is described in Section 3.3. In Section 3.4, reweighted iterative BEM based channel estimation is presented. In section 3.5, detection and equalization are discussed. Numerical results are given in Section 3.6. A summary of this chapter is given in Section 3.7.

3.2 Signal model

Consider a MIMO OFDM system. In the frequency domain, the $N \times 1$ received signal vector at receive antenna r can be represented with the following model,

$$\mathbf{z}_r = \sum_{k=1}^{N_t} \mathbf{S}_k \mathbf{h}_{r,k} + \mathbf{n}_r, \quad r = 1, ..., N_r, \tag{3.1}$$

where N is the number of data and pilot symbols distributed over time and frequency (OFDM symbols in time and sub-carriers in frequency), N_t is the number of transmit antennas ($k = 1, ..., N_t$), $\mathbf{S}_k$ is an $N \times N$ diagonal matrix of data and pilot symbols transmitted by the kth transmit antenna, $\mathbf{h}_{r,k}$ is an $N \times 1$ vector describing the channel response between the

kth transmit and rth receive antennas, $\mathbf{n}_r$ is an $N \times 1$ complex-valued noise vector with independent Gaussian elements of zero mean and variance σ_n^2 and N_r is the number of receive antennas. We assume that the channel vector $\mathbf{h}_{r,k}$ is represented by an $M \times 1$ vector $\mathbf{a}_{r,k}$ of BEM expansion coefficients, i.e.,

$$\mathbf{h}_{r,k} = \mathbf{B}\mathbf{a}_{r,k}, \tag{3.2}$$

$\mathbf{B}$ is an $N \times M$ matrix with M columns being the basis functions. We assume that the data symbols of $\mathbf{S}_k$ are not accurately known and introduce an error diagonal matrix $\mathbf{E}_k$, i.e., $\mathbf{S}_k = \bar{\mathbf{S}}_k + \mathbf{E}_k$, and thus (3.1) can be rewritten as

$$\mathbf{z}_r = \sum_{k=1}^{N_t} \bar{\mathbf{S}}_k \mathbf{h}_{r,k} + \sum_{k=1}^{N_t} \mathbf{E}_k \mathbf{h}_{r,k} + \mathbf{n}_r, \tag{3.3}$$

where $\bar{\mathbf{S}}_k$ is an $N \times N$ diagonal matrix of tentative data and pilot symbols.

If the diagonal elements (data errors) of the matrix $\mathbf{E}_k$ were described by Gaussian distribution with a zero-mean and variances $\sigma_{e,k}^2$, denoting that $\mathbf{y}_r = \sum_{k=1}^{N_t} \mathbf{E}_k \mathbf{h}_{r,k} + \mathbf{n}_r$ and $\mathbf{a} = [\mathbf{a}_{r,1}^T, ..., \mathbf{a}_{r,k}^T, ..., \mathbf{a}_{r,N_t}^T]^T$, we would arrive at the Probability Density Function (PDF) of the received signal

$$p(\mathbf{z}_r|\mathbf{a}) = \frac{e^{-\mathbf{y}_r^H \mathbf{R}_y^{-1} \mathbf{y}_r}}{\pi^N \det(\mathbf{R}_y)}, \tag{3.4}$$

where $\mathbf{R}_y = \mathbb{E}[\mathbf{y}_r \mathbf{y}_r^H]$ is the covariance matrix of the error and noise.

3.3 Weighted channel estimation

Although for OFDM systems, the expression in (3.4) does not hold, the weighted channel estimation algorithm that results from the Gaussian model is happened to be also useful for OFDM. Therefore, in this section below we revise the estimator in [18] following from the Gaussian model in (3.4).

In general, the channel estimation problem can be represented as maximizing the log-likelihood function $\ln[p(\mathbf{z}_r|\mathbf{a})]$ under some constraints, more specifically,

$$\hat{\mathbf{a}} = \arg \max_{\mathbf{a} \in \mathcal{A}} \ln[p(\mathbf{z}_r|\mathbf{a})], \tag{3.5}$$

where $\mathcal{A}$ is a set of constraints on the vector $\mathbf{a}$. E.g., for the LMMSE estimation, the expansion coefficients $\mathbf{a}$ are assumed to be zero-mean Gaussian with a covariance matrix $\mathbf{R}_a = \mathbb{E}[\mathbf{a}\mathbf{a}^H]$. Using (3.4), the log-likelihood function in (3.5) can be given as [18]:

$$\ln[p(\mathbf{z}_r|\mathbf{a})] = -N\ln[\pi] - \ln[\det(\mathbf{R}_y)] - \mathbf{y}_r^H \mathbf{R}_y^{-1}\mathbf{y}_r. \tag{3.6}$$

Letting,

$$\eta_{r,i} = \sum_{k=1}^{N_t} \left|h_{r,k}^{(i)}\right|^2 \frac{\sigma_{e,k}^2}{\sigma_n^2}, \tag{3.7}$$

$$\ell_{r,i} = \frac{1}{\sigma_n^2}\left| z_{r,i} - \sum_{k=1}^{N_t} h_{r,k}^{(i)} s_{k,i} \right|^2, \tag{3.8}$$

we obtain

$$\ln[\det(\mathbf{R}_y)] = N\ln[\sigma_n^2] + \sum_{i=1}^{N} \ln[\eta_{r,i}+1], \tag{3.9}$$

$$\mathbf{y}_r^H \mathbf{R}_y^{-1}\mathbf{y}_r = \sum_{i=1}^{N} \frac{\ell_{r,i}}{\eta_{r,i}+1}, \tag{3.10}$$

where $h_{r,k}^{(i)}$ is the ith element of the channel vector $\mathbf{h}_{r,k}$, $z_{r,i}$ is the ith element of the received signal vector $\mathbf{z}_r$ and $s_{k,i}$ is the ith element of $\mathbf{s}_k$, $\mathbf{s}_k = \mathrm{diag}(\mathbf{S}_k)$. Then, (3.6) becomes

$$\ln[p(\mathbf{z}_r|\mathbf{a})] = -N\ln[\pi] - N\ln[\sigma_n^2] - \sum_{i=1}^{N} \ln[\eta_{r,i}+1] - \sum_{i=1}^{N} \frac{\ell_{r,i}}{\eta_{r,i}+1}. \tag{3.11}$$

Omitting the terms that do not affect the optimization ($-N\ln[\pi] - N\ln[\sigma_n^2]$), we finally get

$$\ln[p(\mathbf{z}_r|\mathbf{a})] = -\sum_{i=1}^{N} \Big(\ln[\eta_{r,i}+1] + \frac{\ell_{r,i}}{\eta_{r,i}+1} \Big). \tag{3.12}$$

Then, the problem in (3.5) can be rewritten as [18]

$$\hat{\mathbf{a}} = \arg\min_{\mathbf{a}\in\mathcal{A}} \sum_{i=1}^{N} \Big(\ln[\eta_{r,i}+1] + \frac{\ell_{r,i}}{\eta_{r,i}+1} \Big). \tag{3.13}$$

The value $\eta_{r,i}$ is a ratio of powers of the data errors and noise for the ith data element of the rth receive antenna. If $\eta_{r,i} = 0$, the transmitted data are perfectly known, and from (3.13), we arrive at the conventional (unweighted) pilot-based LMMSE BEM estimator: $\hat{\mathbf{a}} = \arg\min_{\mathbf{a}\in\mathcal{A}} \sum_{i=1}^{N} \ell_i$. For non-zero $\eta_{r,i}$, the estimate of the basis expansion coefficients $\hat{\mathbf{a}}$ should be found by solving the complicated non-linear optimization problem in (3.13).

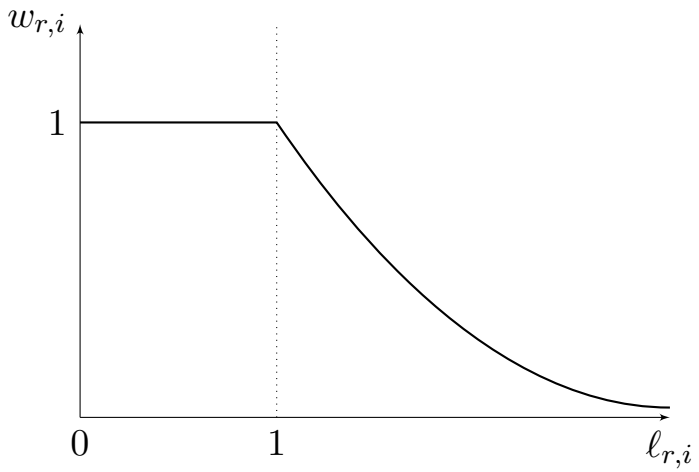

Figure 3.1: The relation between weights $w_{r,i}$ and residual powers $\ell_{r,i}$.

The problem in (3.13) can be represented as an optimization problem over $\eta_{r,i}$,

$$\hat{\mathbf{a}} = \arg \min_{\mathbf{a} \in \mathcal{A}} \min_{\eta_{r,i}} \sum_{i=1}^{N} \Lambda(\eta_{r,i}, \ell_{r,i}), \tag{3.14}$$

where

$$\Lambda(\eta_{r,i}, \ell_{r,i}) = \Big(\ln[\eta_{r,i} + 1] + \frac{\ell_{r,i}}{\eta_{r,i} + 1} \Big). \tag{3.15}$$

The values $\eta_{r,i}$ are unknown since the variances of data errors $\sigma^2_{e,k}$ are unknown. However, we can treat $\eta_{r,i}$ as nuisance parameters and set $\eta_{r,i} \in [0, \infty]$ [18]. Also, the unconstrained minimizer of $\Lambda(\eta_{r,i}, \ell_{r,i})$ is obtained as $\eta_{r,i} = \ell_{r,i} - 1$ by differentiating $\Lambda(\eta_{r,i}, \ell_{r,i})$ over $\eta_{r,i}$,

$$\frac{\partial \Lambda(\eta_{r,i}, \ell_i)}{\partial \eta_{r,i}} = \frac{1}{\eta_{r,i} + 1} - \frac{\ell_{r,i}}{(\eta_{r,i} + 1)^2} = 0. \tag{3.16}$$

Then, we arrive at the weighted optimization problem from (3.14) by letting

$$\Lambda(\eta_{r,i}, \ell_{r,i}) = w_{r,i} \ell_{r,i}, \tag{3.17}$$

then, from (3.15) and (3.17), the weights $w_{r,i}$ are given by [18]

$$w_{r,i} = \frac{\ln[\eta_{r,i} + 1]}{\ell_{r,i}} + \frac{1}{\eta_{r,i} + 1}. \tag{3.18}$$

Using $\eta_{r,i} = \ell_{r,i} - 1$ in (3.18), we arrive at

$$w_{r,i} = \frac{\ln[\ell_{r,i}] + 1}{\ell_{r,i}}. \tag{3.19}$$

Finally, using $\eta_{r,i} = \ell_{r,i} - 1$ and $\eta_{r,i} \in [0, \infty]$, the range for $\ell_{r,i}$ can be set to $\ell_{r,i} \in [1, \infty]$ and then the weights in (3.19) can be rewritten as

$$w_{r,i} = \begin{cases} 1, & \ell_{r,i} \leq 1; \\ \frac{\ln[\ell_{r,i}]+1}{\ell_{r,i}}, & \ell_{r,i} > 1, \end{cases} \tag{3.20}$$

which are independent of $\eta_{r,i}$. Note that in (3.20), for $\ell_{r,i} < 1$, the residual powers $\ell_{r,i}$ are very small, and thus for such case $w_{r,i}$ are set to unity. Figure 3.1 shows the relationship between the weights $w_{r,i}$ and residual powers $\ell_{r,i}$ as described by (3.20). It can be seen that large residual powers $\ell_{r,i}$ are penalized by reducing contribution from the corresponding tentative data symbols into the channel estimate.

The problem in (3.14) can now be solved iteratively by using, at every iteration, weights

$$\hat{w}_{r,i} = \begin{cases} 1, & \hat{\ell}_{r,i} \leq 1; \\ \frac{\ln[\hat{\ell}_{r,i}]+1}{\hat{\ell}_{r,i}}, & \hat{\ell}_{r,i} > 1, \end{cases} \tag{3.21}$$

where

$$\hat{\ell}_{r,i} = \frac{1}{\sigma_n^2} \left| z_{r,i} - \sum_{k=1}^{N_t} \hat{h}_{r,k}^{(i)} \bar{s}_{k,i} \right|^2, \tag{3.22}$$

obtained by replacing the channel response $h_{r,k}^{(i)}$ with the channel estimates $\hat{h}_{r,k}^{(i)}$ and true unknown data symbols $s_{k,i}$ with the tentative data symbol $\bar{s}_{k,i}$.

The approach described in this section is used for designing reweighted iterative LMMSE channel estimator in the MIMO OFDM receiver.

3.4 Reweighted iterative channel estimation

Figure 3.2 shows the block diagram of the proposed reweighted iterative LMMSE channel estimator. In the first step, the channel is estimated using the pilot-based LS BEM channel estimator. Then, tentative data estimates are obtained using the initial channel estimates $\hat{\mathbf{h}}_{r,k}$ in the linear MMSE MIMO detector as described in Chapter 2 (see Subsection 2.11.2). The MMSE soft data estimates obtained are mapped into a constellation (e.g., 16-QAM) to recover the tentative data symbols $\bar{\mathbf{S}}_k$. After that, the weights are computed as described in (3.21) and (3.22). The estimates $\hat{\mathbf{h}}_{r,k}$ and $\bar{\mathbf{S}}_k$ are also used to recover a portion $\hat{\mathbf{z}}_{r,k}$ of the

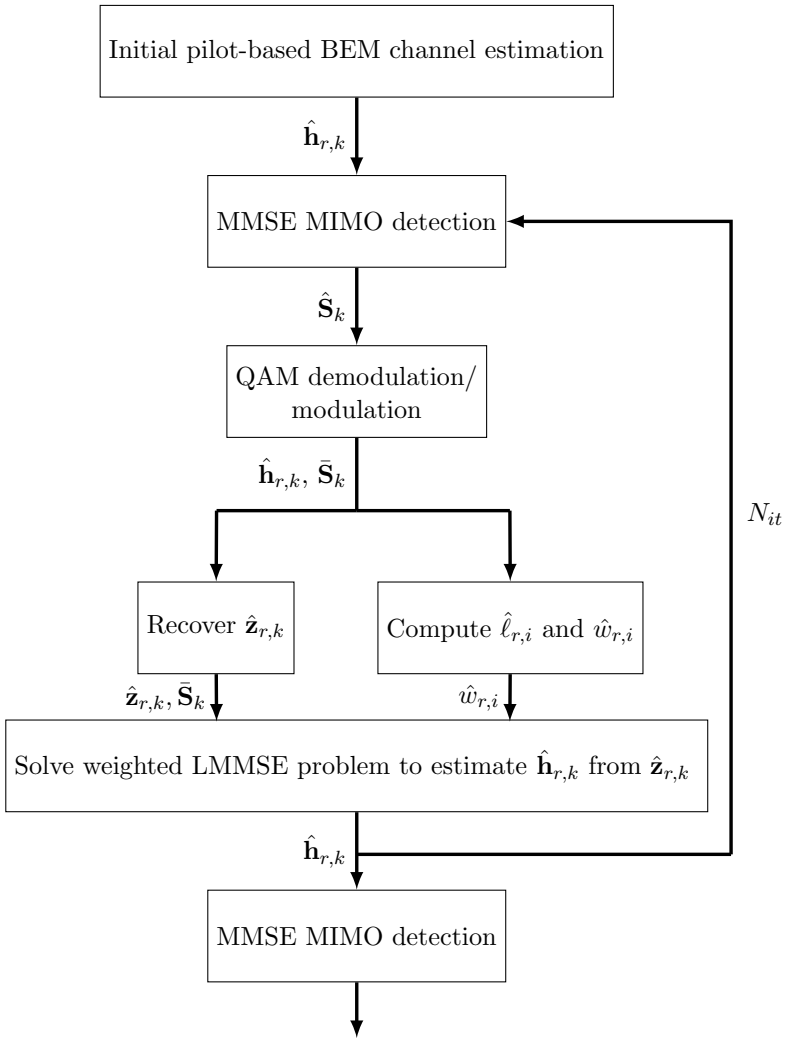

Figure 3.2: Reweighted iterative LMMSE channel estimation.

received signal corresponding to the kth transmit antenna. The recovered signal $\hat{\mathbf{z}}_{r,k}$ is given by

$$\hat{\mathbf{z}}_{r,k} = \mathbf{z}_r - \sum_{\substack{q=1 \\ q \neq k}}^{N_t} \bar{\mathbf{S}}_q \hat{\mathbf{h}}_{r,q}, \tag{3.23}$$

where signals received from the $N_t - 1$ transmit antennas are treated as interference and their estimates are subtracted from the received signal $\mathbf{z}_r$. The weights $\hat{w}_{r,i}$ are then used in the weighted LMMSE channel estimation to re-estimate the channel $\mathbf{h}_{r,k}$. The channel estimation based on the signal estimate $\hat{\mathbf{z}}_{r,k}$ is sub-optimal, but it provides a reduction in the complexity in comparison with a channel estimation joint for all transmit antennas. The updated channel estimates $\hat{\mathbf{h}}_{r,k}$ are used in the next iteration with the total number of N_{it} iterations. The value of N_{it} should not be high. In our experiments, as shown in the next

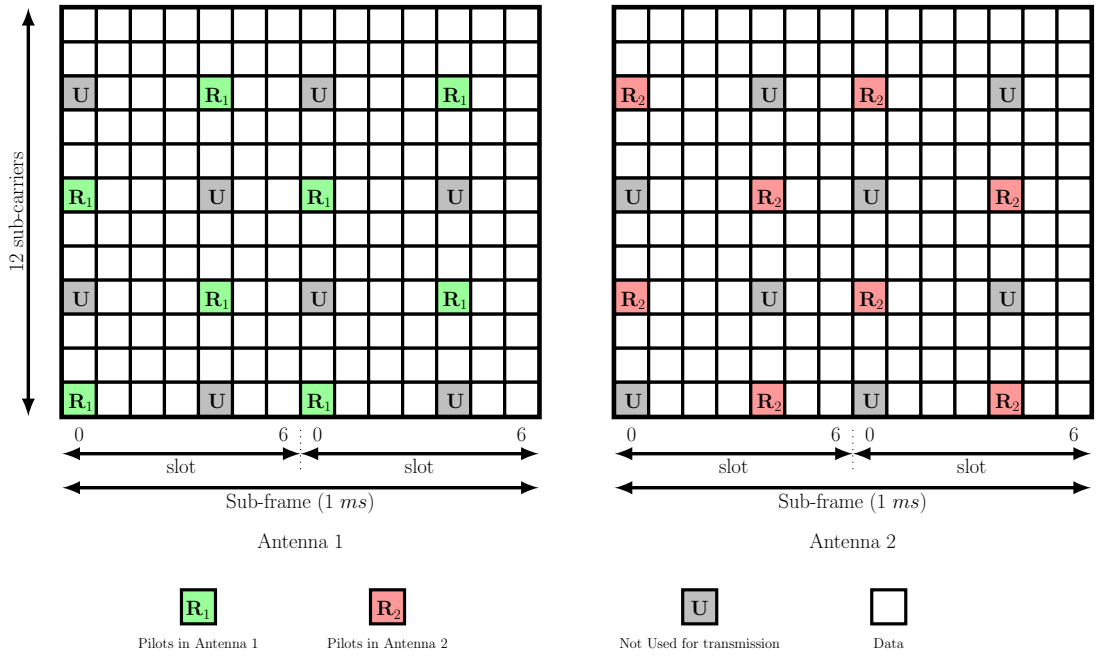

Figure 3.3: LTE downlink sub-frame structure for two transmit antennas.

section, $N_{it} = 3$ iterations are enough to converge.

BEMs are used to estimate the time and frequency variations of fading channels [2–4]. Below we will be using the following BEMs. In frequency (over N_f sub-carriers), we use M_f DPSS [6, 7]. In time (over N_{OFDM} OFDM symbols), we use M_t parabolic B-splines [8–10]. However, other BEMs can also be used. The BEM matrix $\mathbf{B}$ is given by

$$(\mathbf{B})_{i,j} = \varphi_s(g)\psi_m(n) = \xi_j(i), \tag{3.24}$$

where: $M = M_f M_t$, $N = N_f N_{OFDM}$; $i = \{g, n\}$ and $j = \{s, m\}$ are composite indices; $\varphi_s(g)$ is the sth basis function over frequency with $s = 1, ..., M_f$ and $g = 1, ..., N_f$; $\psi_m(n)$ is the mth basis function over time with $m = 1, ..., M_t$ and $n = 1, ..., N_{OFDM}$; $\xi_j(i)$ is the jth time-frequency basis function with $j = 1, ..., M$ and $i = 1, ..., N$.

The initial pilot-based channel estimate is given by

$$\hat{\mathbf{h}}_{r,k} = \mathbf{B}\hat{\mathbf{a}}_{r,k}, \tag{3.25}$$

where an estimate $\hat{\mathbf{a}}_{r,k}$ of the vector of expansion coefficients $\mathbf{a}_{r,k}$ is given by

$$\hat{\mathbf{a}}_{r,k} = (\mathbf{B}^H \mathbf{S}_{n,k}^H \mathbf{S}_{n,k} \mathbf{B} + \mathbf{\Gamma})^{-1} \mathbf{B}^H \mathbf{S}_{n,k}^H \hat{\mathbf{z}}_{r,k}, \tag{3.26}$$

where $\mathbf{S}_{n,k}$ is an $N \times N$ diagonal matrix of pilot symbols transmitted by the kth transmit antenna with zeros at data locations, $\mathbf{\Gamma}$ is an $M \times M$ regularization matrix defined by the set $\mathcal{A}$. At the initialization step, we use $\hat{\mathbf{z}}_{r,k} = \mathbf{z}_r$. Note that in the LTE downlink as seen in Figure 3.3, the pilot symbols occupy different locations for different transmit antennas and the pilot symbols of one transmit antenna are not overlapping with data or pilot symbols of the other transmit antennas. This justifies the relationship $\hat{\mathbf{z}}_{r,k} = \mathbf{z}_r$. When $\mathbf{\Gamma}$ is an $M \times M$ zero matrix, we have the pilot-based LS BEM channel estimator. When $\mathbf{\Gamma} = \sigma_n^2 \mathbf{R}_{\mathbf{a}}^{-1}$, we have the pilot-based LMMSE channel estimator with the covariance $\mathbf{R}_{\mathbf{a}} = \mathbb{E}[\mathbf{a}_{r,k} \mathbf{a}_{r,k}^H]$ computed by

$$\mathbf{R}_{\mathbf{a}} = (\mathbf{B}^H \mathbf{B})^{-1} \mathbf{B}^H \mathbf{\Upsilon} \mathbf{B} (\mathbf{B}^H \mathbf{B})^{-1}, \tag{3.27}$$

where $\mathbf{\Upsilon} = \mathbb{E}[\mathbf{h}_{r,k} \mathbf{h}_{r,k}^H]$ is the channel time-frequency autocorrelation matrix. The matrix $\mathbf{\Upsilon}$ is obtained as the Kronecker product of the channel autocorrelation matrices in frequency and time,

$$\mathbf{\Upsilon} = \mathbf{\Upsilon}_t \otimes \mathbf{\Upsilon}_f, \tag{3.28}$$

where $\mathbf{\Upsilon}_t$ is an $N_{OFDM} \times N_{OFDM}$ channel autocorrelation matrix in time and $\mathbf{\Upsilon}_f$ is an $N_f \times N_f$ channel autocorrelation matrix in frequency. The autocorrelation in time is defined by the Jakes' model [64],

$$\mathbf{\Upsilon}_t = \sigma_h^2 J_0(2\pi f_d \tau), \tag{3.29}$$

where σ_h^2 is the channel variance ($\sigma_h^2 = 1$), $J_0(\cdot)$ is the zero-order Bessel function of the first kind and f_d is the Doppler frequency. The autocorrelation matrix in frequency at two frequencies f_1 and f_2 is obtained as the following

$$\begin{aligned} \mathbf{\Upsilon}_f &= \mathbb{E}[h_{r,k}(f_1) h_{r,k}^*(f_2)] \\ &= \mathbb{E}[\sum_{l=0}^{L-1} b_l e^{-j2\pi f_1 \tau_l} \sum_{m=0}^{L-1} b_m^* e^{-j2\pi f_2 \tau_m}] \\ &= \sum_{l=0}^{L-1} \sum_{m=0}^{L-1} \mathbb{E}[b_l b_m^*] e^{-j2\pi (f_1 \tau_l - f_2 \tau_m)}, \end{aligned} \tag{3.30}$$

when $l \neq m$, $\mathbb{E}[b_l b_m^*] = 0$, and thus (3.30) can be rewritten as

$$\boldsymbol{\Upsilon}_f = \sum_{l=0}^{L-1} p_l e^{-j\tau_l(f_1 - f_2)}, \tag{3.31}$$

where $p_l = \mathbb{E}[|b_l|^2]$ and it is the average power at the lth path. The autocorrelation matrix in frequency is defined by the channel PDP, $\{p_l, \tau_l\}_{l=1}^{L}$.

For the weighted LMMSE channel estimation (the last step before the MIMO detection in Figure 3.2), $\hat{\mathbf{h}}_{r,k}$ is estimated as in (3.25) with $\hat{\mathbf{a}}_{r,k}$ given by

$$\hat{\mathbf{a}}_{r,k} = (\mathbf{B}^H \bar{\mathbf{S}}_k^H \hat{\mathbf{W}}_r \bar{\mathbf{S}}_k \mathbf{B} + \sigma_n^2 \mathbf{R}_{\mathbf{a}}^{-1})^{-1} \mathbf{B}^H \bar{\mathbf{S}}_k^H \hat{\mathbf{W}}_r \hat{\mathbf{z}}_{r,k}, \tag{3.32}$$

where $\bar{\mathbf{S}}_k$ is an $N \times N$ diagonal matrix of tentative data and pilot symbols, $\bar{\mathbf{S}}_k = \text{diag}(\bar{\mathbf{s}}_k)$ and $\hat{\mathbf{W}}_r$ is a diagonal matrix of estimated weights computed from (3.21) for data locations and set to unity for pilot symbol locations, and $\hat{\mathbf{z}}_{r,k}$ is found from (3.23). When $\hat{\mathbf{W}} = \mathbf{I}_N$, we arrive at the conventional unweighted LMMSE BEM channel estimator.

3.5 Numerical results

For simulation, we consider a single-user MIMO downlink LTE scenario [29] with two transmit antennas at the base station and two receive antennas at the UE. This system employs the spatial multiplexing [29]. One sub-frame (as shown in Figure 3.3) consists of two slots with 7 OFDM symbols in each slot. A resource block occupies one slot with 7 OFDM symbols in time and 12 sub-carriers in frequency ($N = 14 \times 12 = 504$ symbols from which 24 symbols are pilots). In our simulation, data are transmitted on 36 sub-carriers (six resource blocks). Other simulation parameters are presented in Table 3.1 [29, 98, 99].

The data are mapped to a 16-QAM constellation. The QAM data symbols are mapped with pilot symbols in time and frequency to construct the LTE subframe structure in Figure 3.3. The pilot symbols are generated from Zadoff-Chu sequences [29] as explained in Chapter 2. Then, IFFT is used to convert the OFDM symbols from the frequency domain to the time domain. The CP is then appended at the beginning of each OFDM symbol to be transmitted through the channel. The number of simulation trials used for the MSE performance results is 10^3 trials. The Block Error rate (BLER) is calculated as the ratio of

Table 3.1: Simulation Parameters

No. of simulated slots	2
Channel bandwidth	5 MHz
Sampling rate	7.68 MHz
Slot length	0.5 ms
No. of used sub-carriers (N_{RB})	36
Frequency spacing between two sub-carriers	15 kHz
IDFT/DFT size	512
Modulation	16-QAM
Delay profile / Doppler frequency	EVA/ETU / 350 Hz
Cyclic Prefix (Normal)	$5.21\mu s$ for Symbol 0 (see Figure 3.3) 4.69 μs for Symbols 1-6
Reference Signal	Cell-specific Reference Signal (CRS) / Zadoff Chu sequence
Coding	Turbo codes: code rate 1/3

the number of transport blocks with errors (with at least one error) to the total number of transmitted transport blocks. The number of simulation trials used for the BLER performance results is 10^4 trials.

Figure 3.4 shows the MSE performance of the LS and LMMSE pilot-based channel estimators versus the number of basis functions in frequency M_f at $M_t = 3, 4, 5$ and SNR = 15 dB. The MSE of the channel estimation is defined by the following

$$\text{MSE} = \frac{\text{tr}\{\mathbb{E}[(\mathbf{h}_{r,k} - \hat{\mathbf{h}}_{r,k})(\mathbf{h}_{r,k} - \hat{\mathbf{h}}_{r,k})^H]\}}{\text{tr}\{\mathbb{E}[\mathbf{h}_{r,k}\mathbf{h}_{r,k}^H]\}}. \tag{3.33}$$

As the reweighted and unweightd iterations are based on the LMMSE channel estimation, we select M_t and M_f that provide the better performance for the LMMSE channel estimator. In Figure 3.4, it can be seen that with higher M_f, the LMMSE channel estimator performance becomes better in the ETU and EVA channels. However, the larger M_f, the more computational load incurred by the estimator. Therefore, we try to select the lowest M_t and M_f that can provide a low approximation error. In the ETU channel (Figure 3.4 (a)), M_t is set to $M_t = 4$ for the basis functions in time, and in frequency, M_f is set to $M_f = 11$. In the EVA channel (Figure 3.4 (b)), M_t and M_f are set to $M_t = 4$ and $M_f = 5$.

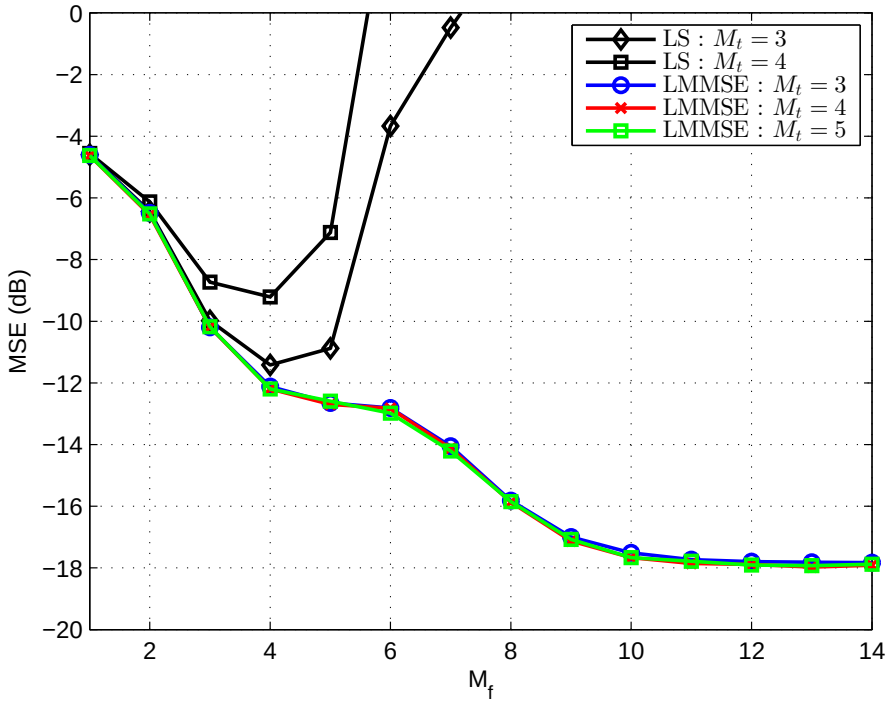

(a)

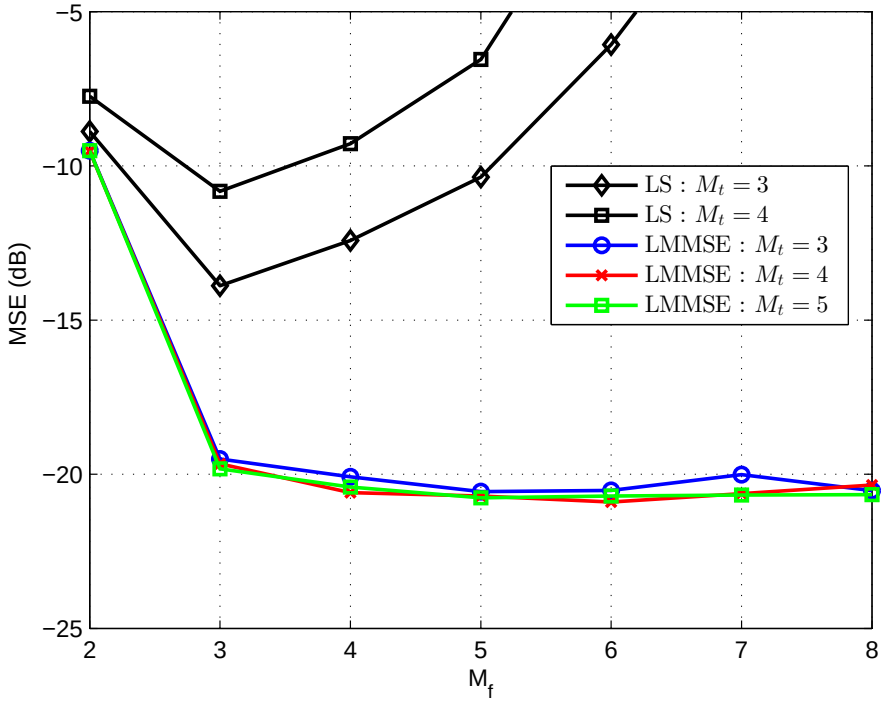

(b)

Figure 3.4: MSE performance of the LS and LMMSE pilot-based BEM channel estimators (for the basis functions in time $M_t = 3, 4, 5$) versus the number of basis functions in frequency M_f in (a) ETU and (b) EVA channels at a 350 Hz Doppler frequency and SNR=15 dB.

Figure 3.5 shows the channel estimation performance of the iterative channel estimators for $N_{it} = 3$ and $N_{it} = 10$ in the EVA channel. When the initial estimates are obtained from the LS channel estimator (Figure 3.5 (a)), the MSE performance of the reweighted estimator for $N_{it} = 3$ is significantly better than that of the unweighted estimator. At $N_{it} = 10$, the performance of the reweighted estimator is better than that of the unweighted estimator by approximately 1 to 3 dB. When the initial estimates are obtained from the LMMSE channel estimator (Figure 3.5 (b)), the MSE performance of the reweighted estimator for $N_{it} = 3$ and $N_{it} = 10$ provides an improvement of about 1 to 2 dB in comparison with the unweighted estimator. The unweighted estimator is affected by the quality of the initial channel estimates. On the other hand, the reweighted estimator is slightly affected by worse initial channel estimate (the LS channel estimates) at $N_{it} = 3$. At $N_{it} = 10$, the reweighted estimator performance is almost the same when the initial LS or LMMSE estimates are used as clearly shown in Figure 3.5 (a) and (b). It shows that at a high number of iterations the reweighted estimator still provides the same performance with better or worse initial channel estimates.

Note that in the ETU channel, $M = M_t M_f = 4 \times 11 = 44$, which is higher than the number of the available pilots (24 pilot symbols). This means that this problem is ill conditioned and the LS channel estimation will result in wrong results. Therefore, we only use the initial LMMSE channel estimates in the reweighted and unweighted estimators in the ETU channel. Figure 3.6 shows the MSE performance of the iterative reweighted channel estimators with the initial LMMSE channel estimates for $N_{it} = 3$ and 10 in the ETU channel at a 350 Hz Doppler frequency. Similar to the EVA channel, the performance of the reweighted estimator is better than that of the unweighted estimator by 1 to 2 dB. Note that, with better initial channel estimates (see Figure 3.5 (b) and Figure 3.6), the difference in the performance of the reweighted estimator between low and high N_{it} is very small. Thus, a small number of iterations can be used in the estimators in such case to achieve close-to-optimal performance.

Figures 3.7 to 3.9 show the BLER performance achieved in the receivers with the reweighted and unweighted LMMSE channel estimators in the EVA and ETU channels. The BLER performance of Perfect Channel Information (PCI) is obtained using the true channel response in the MIMO MMSE detector. In the EVA channel, when the initial channel estimates are obtained using the LS channel estimator (Figure 3.7), the reweighted estimator

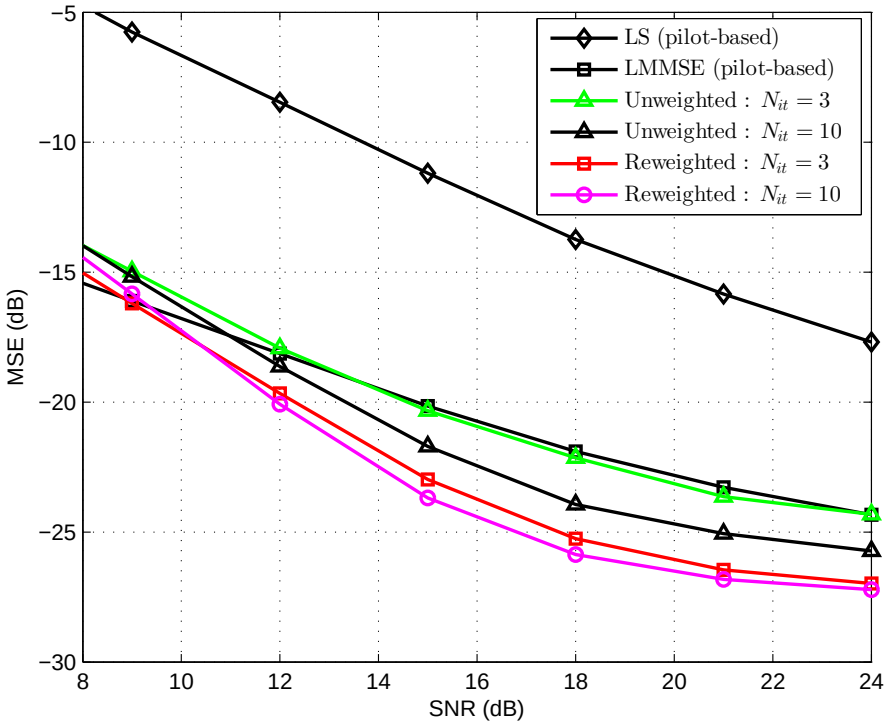

(a)

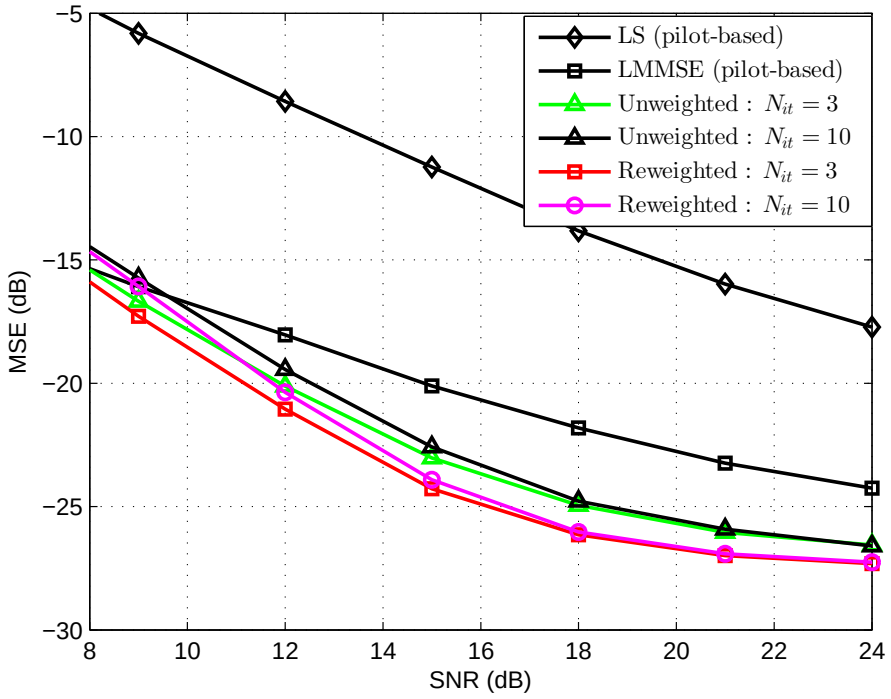

(b)

Figure 3.5: MSE performance of the reweighted and unweighted LMMSE iterative channel estimators with initial (a) LS and (b) LMMSE channel estimates versus SNR in the EVA channel at a 350 Hz Doppler frequency.

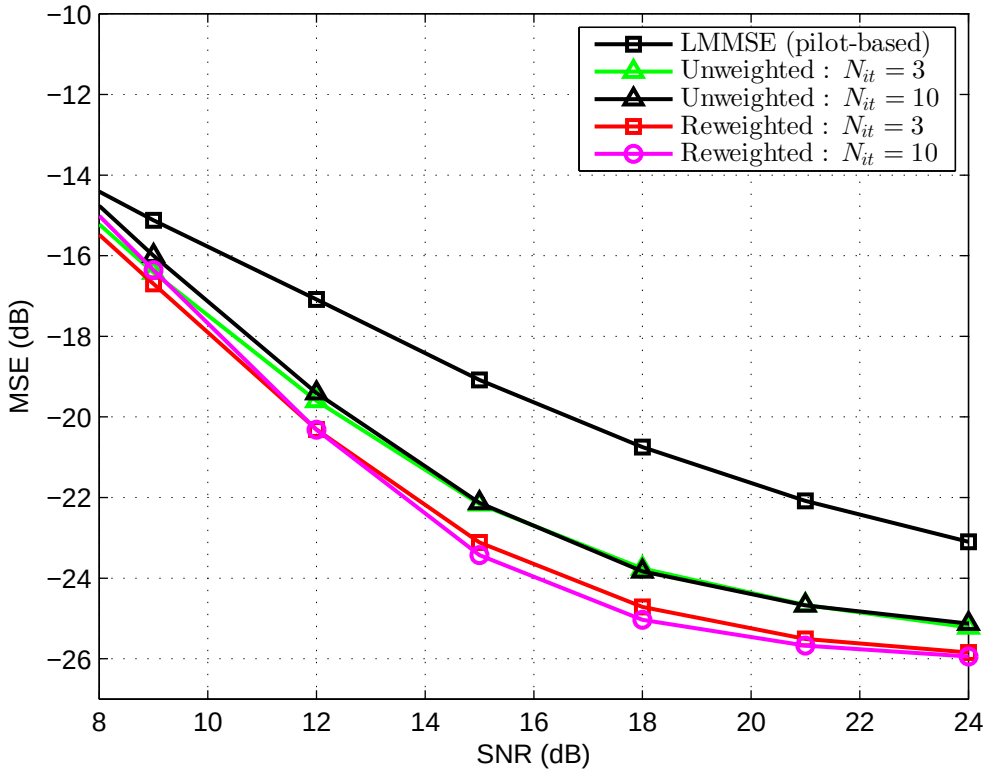

Figure 3.6: MSE performance of the reweighted and unweighted LMMSE iterative channel estimators with LMMSE initial channel estimates versus SNR in the ETU channel at a 350 Hz Doppler frequency.

outperforms the unweighted estimator. When the initial channel estimates are obtained using the LMMSE channel estimation (Figure 3.8), the improvement in the performance becomes very small. It can be seen that, as shown in Figure 3.8, the BLER performance at $N_{it} = 10$ is almost the same for the initial LS and LMMSE channel estimates. Also, the performance with $N_{it} = 3$ and $N_{it} = 10$ is approximately the same when the initial LMMSE channel estimates are used. In the ETU channel (Figure 3.9), the improvement in the performance of the reweighted estimator over that of the unweighted estimator is almost negligible. From Figures 3.7 to 3.9, it can be concluded that in the case of better initial channel estimates (e.g., the LMMSE channel estimates) and a low rate turbo coding, the improvement in the reweighted estimator performance over the unweighed estimator is very small to almost negligible. However, with worse initial channel estimates (e.g., the LS channel estimates), the improvement is significant. This shows that, in scenarios with worse initial channel estimates, the reweighted channel estimator can significantly outperform the unweighted estimator.

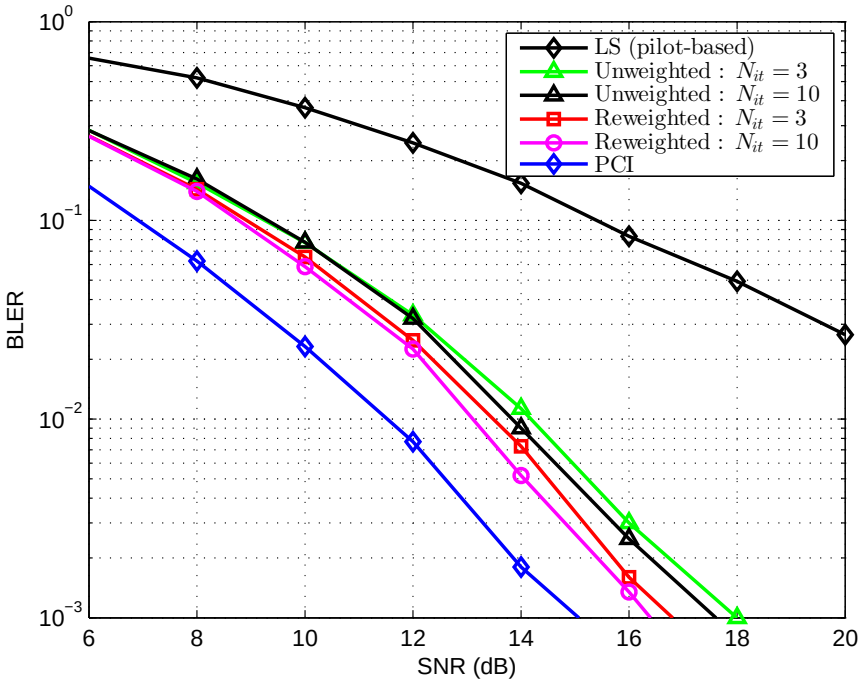

Figure 3.7: BLER performance of the reweighted and unweighted LMMSE iterative channel estimators with initial LS channel estimates versus SNR in the EVA channel at a 350 Hz Doppler frequency.

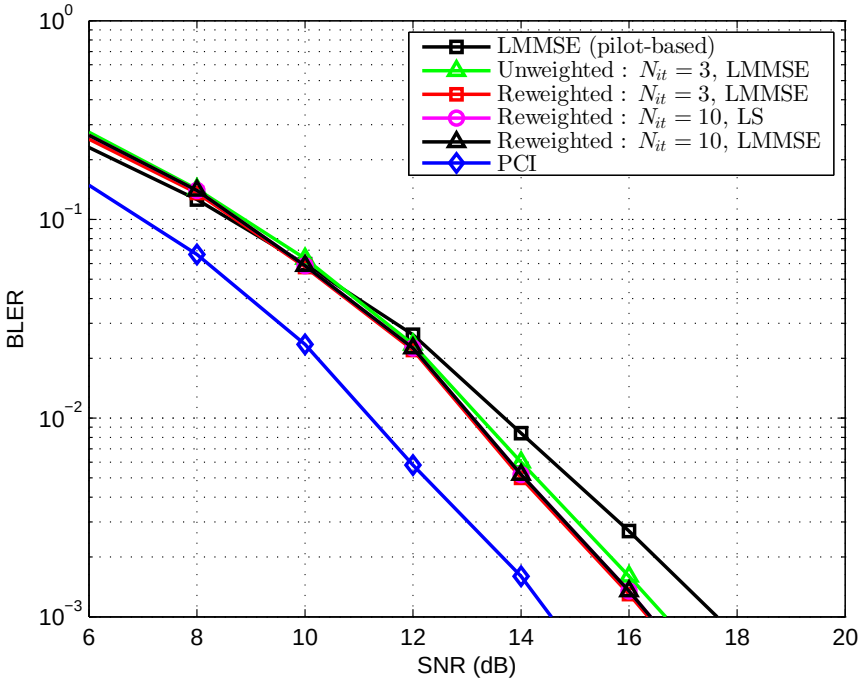

Figure 3.8: BLER performance of the reweighted and unweighted LMMSE iterative channel estimators with initial LS and LMMSE channel estimates versus SNR in the EVA channel at a 350 Hz Doppler frequency.

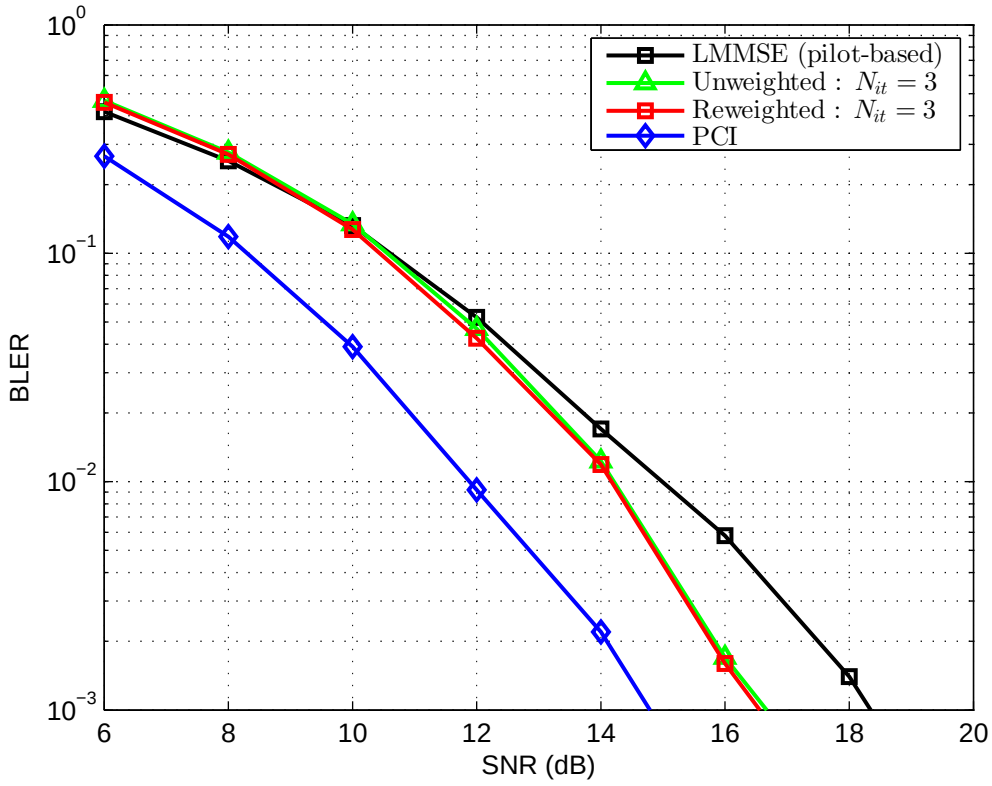

Figure 3.9: BLER performance of the reweighted and unweighted LMMSE iterative channel estimators with initial LMMSE channel estimates versus SNR in the ETU channel at a 350 Hz Doppler frequency.

As can be seen in Figure 3.1, when the weights $w_{r,i}$ are near to unity, we would expect high reliability in the detection of data symbols that correspond to such weights. On the other hand, when $w_{r,i}$ is near zero, the detection of data symbols may result in errors. Therefore, another advantage of the proposed weights is that they can be used as a measure of reliability for the detected received data. In the following chapter, we will exploit the benefit of using the proposed weights as a measure of data reliability and the reweighted channel estimation for complexity reduction of high performance detectors.

3.6 Summary

This chapter can be summarized as the following:

- The optimized weights for uplink LTE scenarios derived in [18] are proposed for using in the LTE downlink. Although, the assumption of Gaussian data errors in [18] is invalid for OFDM, it is shown through simulation results that such weights can pro-

vide improvement in the channel estimation performance over that of the unweighted estimation.

- Data-aided reweighted LMMSE iterative BEM channel estimator for a single-user MIMO OFDM in downlink LTE scenarios was investigated. We have compared the performance of this estimator with that of the conventional unweighted estimator. It has been shown through simulation that the reweighted LMMSE channel estimator with weights from [18] outperforms the unweighted channel estimator in channels with the ETU and EVA PDPs and a high Doppler frequency.

- It has been shown that the performance of the reweighted LMMSE BEM channel estimation is the same with LS or LMMSE pilot-based initial channel estimates if a high number of reweighted iterations is used. This result shows that the effect of worse initial channel estimates on the reweighted LMMSE estimator is almost negligible with high N_{it}. Thus, a lower complexity channel estimation can be used to provide the initial channel estimates in the reweighted LMMSE BEM channel estimator.

- It has been shown that in the case of better initial channel estimates (e.g., the LMMSE channel estimates), a small number of iterations can be used to arrive to the close-to-optimal performance.

Chapter 4

Selective detection with adaptive channel estimation for MIMO OFDM systems

Contents

4.1 Introduction

Detection schemes based on pilot-aided channel estimation are widely used in wireless communication systems. When the estimates are treated as perfect, the detector is a mismatched detector, and it does not provide the best performance [19]. The optimal detector on the other hand uses the received data and pilot symbols jointly to detect the transmitted data without explicit channel estimation [19, 20, 40–42].

Although the optimal detection can provide a significant improvement in the performance, its computational complexity is high and increases exponentially with the size of data package, modulation order and number of transmit antennas. SbS optimal detection can sig-

nificantly reduce the complexity with slight degradation in the performance [20]. However, despite the reduction in complexity, the SbS optimal detection is still very complicated. The SbS optimal detection has been shown to provide a better performance than mismatched detectors with LS or LMMSE channel estimates in time-varying [40] and frequency-selective [20] channels. The improvement in the detection performance becomes more apparent for higher modulation orders and MIMO setup [20, 41]. The SbS optimal detector and the mismatched detector with LMMSE channel estimates in [20,40,41] were implemented assuming full knowledge of the channel PDP and/or Doppler spectrum. However, such information is usually not available and hard to estimate in practice. This chapter addresses: (i) the reduction in complexity of the SbS optimal detection; and (ii) the channel estimation and detection without knowledge of the channel PDP.

The complexity of high performance detectors can be reduced by using a two-stage detection scheme [100, 101]. The first stage involves low complexity channel estimation and detection. The second stage applies a high performance detector to received data that are most likely unreliably detected at the first stage. However, the scheme in [100] is limited to code-division multiple-access systems and BPSK modulation. In [101], a two-stage maximum likelihood detection algorithm was proposed for multiuser detection. This algorithm assumes perfect knowledge of the channel. However, in practice, such information is unavailable. In this chapter, we propose a two-stage detection scheme to reduce the complexity of the SbS optimal detector in a MIMO OFDM system in doubly-selective channels. At the first stage, a re-weighted iterative channel estimation and mismatched detection are used. The re-weighted iterative LMMSE channel estimation is far superior to that of the pilot-based LMMSE channel estimation [18, 25]. At this stage, tentative data estimates [11] are obtained without decoding and used for improving the performance of channel estimation [16, 18]. The weights obtained from the re-weighted channel estimator are used to identify the unreliably detected symbols, to which, at the second stage, the SbS optimal detection is applied.

Both the LMMSE channel estimation and SbS optimal detection require knowledge of the channel statistics. This information is hard to acquire in practice. Model-based (e.g., uniform) channel regularization [21] is more practical for channel estimation, but it requires knowledge of the channel delay spread, which is difficult to estimate. In [21], an adaptive model-based regularization was proposed for multi-carrier systems, such a channel estimator

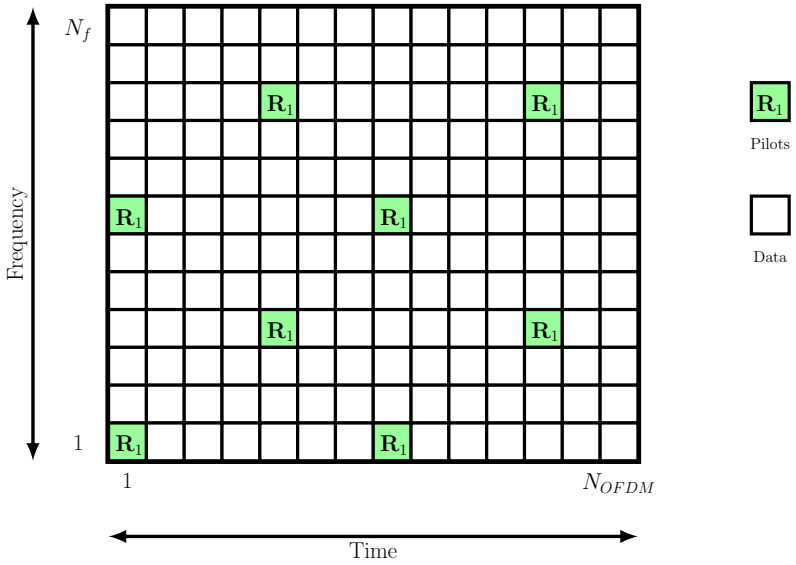

Figure 4.1: Time-frequency grid for one transmit antenna.

was shown to provide a performance close to that of the LMMSE estimator in LTE uplink scenarios without knowledge of the channel statistics. Hence, we investigate the proposed selective detection with the adaptive model-based regularization. The variation of the channel in time and frequency is approximated using BEMs. BEMs are widely used for estimation of doubly-selective channels, since they can provide a high channel estimation performance with low computational complexity [2–10].

In this chapter, A new two stage channel estimation and SbS detection receiver is proposed to reduce the complexity of the SbS optimal detector (i.e., selective SbS optimal detector) while maintaining its high detection performance. We show that the selective SbS detector can provide a performance close to that of the SbS optimal detector with significantly lower complexity. We show that detectors using the adaptive model-based regularization can provide a performance close to that of the detectors with known channel statistics.

This chapter is organized as follows. Signal and channel models are presented in Section 4.2. In Section 4.3, the optimal detection with imperfect channel knowledge and mismatched detection are revised. In Section 4.4, the new receiver is proposed. Numerical results are given in Section 4.5. Section 4.6 provides a brief summary of the chapter.

4.2 Signal and channel models

We first consider the time-frequency structure of a data package transmitted from a single transmit antenna, see Figure 4.1 as an example. In the data package, there are N_{OFDM} OFDM symbols and N_f subcarriers. A single subcarrier of a single OFDM symbol represents a resource element (RE), e.g., such as a QAM symbol; thus the data package contains $N = N_{OFDM}N_f$ REs. Every RE is occupied by either data or pilot symbol; it is also possible that some REs are zeros. In a MIMO system, from every transmit antenna, a signal is transmitted with a structure similar to that in Figure 4.1. The difference in data packages transmitted by different antennas can be in positions of pilot symbols. For example, in the LTE downlink, positions of pilot symbols of different transmit antennas are not overlapping and data symbols being zeros at these positions (see Figure 3.3), thus providing an opportunity for independent estimation of the multiple channels between transmit and receive antennas.

In a MIMO OFDM system, the signal model can be described as

$$\mathbf{z} = \mathbf{\Psi}\mathbf{a} + \mathbf{n}, \tag{4.1}$$

where $\mathbf{z}$ is an $NN_r \times 1$ vector of received signals, $\mathbf{z} = [\mathbf{z}_1^T, ..., \mathbf{z}_r^T, ..., \mathbf{z}_{N_r}^T]^T$, $\mathbf{z}_r$ is an $N \times 1$ signal vector at the rth receive antenna, N_r is the number of receive antennas, $\mathbf{\Psi}$ is an $NN_r \times MN_tN_r$ matrix so that $\mathbf{\Psi} = \mathbf{I}_{N_r} \otimes [\mathbf{S}_1\mathbf{B}, ..., \mathbf{S}_k\mathbf{B}, ..., \mathbf{S}_{N_t}\mathbf{B}]$, $\mathbf{S}_k$ is an $N \times N$ diagonal matrix of data and pilot symbols transmitted by the kth transmit antenna, N_t is the number of transmit antennas, $\mathbf{B}$ is an $N \times M$ matrix of basis functions (see below), $\mathbf{a} = [\mathbf{a}_1^T, ..., \mathbf{a}_r^T, ..., \mathbf{a}_{N_r}^T]^T$, $\mathbf{a}_r = [\mathbf{a}_{r,1}^T, ..., \mathbf{a}_{r,k}^T, ..., \mathbf{a}_{r,N_t}^T]^T$, $\mathbf{a}_{r,k}$ is an $M \times 1$ vector of BEM expansion coefficients for the channel between the kth transmit antenna and the rth receive antenna, $\mathbf{n} \sim \mathcal{N}_C(0, \sigma_n^2\mathbf{I}_{NN_r})$ is an $NN_r \times 1$ vector of complex-valued Gaussian noise with variance σ_n^2, $\mathbf{n} = [\mathbf{n}_1^T, ..., \mathbf{n}_r^T, ..., \mathbf{n}_{N_r}^T]^T$, and $\mathbf{n}_r$ is an $N \times 1$ noise vector on the rth receive antenna.

Let $\mathbf{h}_{r,k}$ be an $N \times 1$ vector representing the channel response between the kth transmit and rth receive antennas at positions of the N REs within the data package. It is assumed that, in a doubly-selective channel, the channel response can be represented as $\mathbf{h}_{r,k} = \mathbf{B}\mathbf{a}_{r,k}$. We consider here two-dimensional (time-frequency) basis functions, represented by the $N \times M$

matrix $\mathbf{B}$ defined as

$$\mathbf{B} = \mathbf{B}_t \otimes \mathbf{B}_f. \tag{4.2}$$

The $N_{OFDM} \times M_t$ matrix $\mathbf{B}_t$ represents M_t basis functions across time, i.e., across the N_{OFDM} OFDM symbols. The $N_f \times M_f$ matrix $\mathbf{B}_f$ represents M_f basis functions across frequency, i.e., across the N_f sub-carriers. Thus, we have $M = M_t M_f$. We assume that $\mathbf{h}_{r,k} \sim \mathcal{N}_C(\mathbf{0}_N, \boldsymbol{\Upsilon})$. The $N \times N$ channel covariance matrix $\boldsymbol{\Upsilon} = \mathbb{E}\{\mathbf{h}_{r,k}\mathbf{h}_{r,k}^H\}$ is defined through the channel PDP and Doppler spectrum [102]; we assume here the Jakes' Doppler spectrum. The covariance matrix $\mathbf{R}_a$ of the expansion coefficients $\mathbf{a}_{r,k}$ can then be represented as

$$\mathbf{R}_a = \mathbb{E}\{\mathbf{a}_{r,k}\mathbf{a}_{r,k}^H\} = (\mathbf{B}^H\mathbf{B})^{-1}\mathbf{B}^H\boldsymbol{\Upsilon}\mathbf{B}(\mathbf{B}^H\mathbf{B})^{-1}. \tag{4.3}$$

The received data and pilots can be equivalently represented as

$$\mathbf{z}_d = \boldsymbol{\Psi}_d\mathbf{a} + \mathbf{n}_d, \tag{4.4}$$

$$\mathbf{z}_p = \boldsymbol{\Psi}_p\mathbf{a} + \mathbf{n}_p, \tag{4.5}$$

where $\mathbf{z}_d$ is an $N_dN_r \times 1$ vector of received data, $\mathbf{z}_d = [\mathbf{z}_{d,1}^T, ..., \mathbf{z}_{d,r}^T, ..., \mathbf{z}_{d,N_r}^T]^T$, $\mathbf{z}_{d,r}$ is an $N_d \times 1$ vector of received data at the rth receive antenna, N_d is the number of data symbols, $\boldsymbol{\Psi}_d = \mathbf{I}_{N_r} \otimes [\mathbf{S}_{d,1}\mathbf{B}_d, ..., \mathbf{S}_{d,k}\mathbf{B}_d, ..., \mathbf{S}_{d,N_t}\mathbf{B}_d]$ is $N_dN_r \times MN_rN_t$ matrix, $\mathbf{S}_{d,k}$ is an $N_d \times N_d$ diagonal matrix obtained from $\mathbf{S}_k$ at data locations, $\mathbf{B}_d$ is an $N_d \times M$ matrix of basis functions ($\mathbf{B}$ at data locations), $\mathbf{n}_d$ is an $N_dN_r \times 1$ vector of complex-valued Gaussian noise, $\mathbf{z}_p$ is an $N_pN_r \times 1$ vector of received pilot symbols, N_p is the number of pilot symbols, $\boldsymbol{\Psi}_p = \mathbf{I}_{N_r} \otimes [\mathbf{S}_{p,1}\mathbf{B}_p, ..., \mathbf{S}_{p,k}\mathbf{B}_p, ..., \mathbf{S}_{p,N_t}\mathbf{B}_p]$ is $N_pN_r \times MN_rN_t$ matrix, $\mathbf{S}_{p,k}$ is an $N_p \times N_p$ diagonal matrix obtained from $\mathbf{S}_k$ at pilot locations, $\mathbf{B}_p$ is an $N_p \times M$ matrix of basis functions ($\mathbf{B}$ at pilot locations), $\mathbf{n}_p$ is an $N_pN_r \times 1$ vector of complex-valued Gaussian noise. We assume that the N_d data symbols for each of N_t transmit antennas are obtained independently from data symbols for the other transmit antennas by interleaving and encoding N_t binary data packages, and further mapping the encoded bits into the QAM constellation.

4.3 Optimal and mismatched detection

A mismatched detector assumes that channel estimates (e.g., LMMSE channel estimates) are perfect [19]. The optimal detector does not make such an assumption and jointly processes the received data and pilot symbols to detect the transmitted data, without an explicit chan-

nel estimation. The optimal detector minimizes the probability of detection error, and thus provides better performance than mismatched detectors.

Now we describe the optimal detection with imperfect channel estimation by modifying results presented in [20] to adjust them to the signal model and the doubly-selective channel model described in Section 4.2. The optimal detector is a maximizer of the log-likelihood function $\lambda_{\text{opt}}(\mathbf{s}_d) = \ln[p(\mathbf{z}_d|\mathbf{s}_d, \mathbf{z}_p)]$:

$$\hat{\mathbf{s}}_{d,\text{opt}} = \arg \max_{\mathbf{s}_d \in \mathcal{A}^{N_D N_t \times 1}} \lambda_{\text{opt}}(\mathbf{s}_d), \tag{4.6}$$

where $\mathbf{s}_d = \text{diag}(\mathbf{S}_d)$, $\mathcal{A}$ is the QAM constellation and N_D is the number of data symbols simultaneously detected. In the optimal detector, all ($N_D = N_d$) data symbols are jointly detected. The PDF $p(\mathbf{z}_d|\mathbf{s}_d, \mathbf{z}_p)$ is found by integrating the PDF $p(\mathbf{z}_d|\mathbf{s}_d, \mathbf{a})$ over the nuisance parameters $\mathbf{a}$:

$$p(\mathbf{z}_d|\mathbf{s}_d, \mathbf{z}_p) = \int p(\mathbf{z}_d|\mathbf{s}_d, \mathbf{a}) f(\mathbf{a}|\mathbf{z}_p) d\mathbf{a}, \tag{4.7}$$

where

$$\begin{aligned}
p(\mathbf{z}_d|\mathbf{s}_d, \mathbf{a}) &= \mathcal{N}_C(\mathbf{\Psi}_d \mathbf{a}, \mathbf{R}_d), && (4.8)\\
f(\mathbf{a}|\mathbf{z}_p) &= \mathcal{N}_C(\mathbf{m}_a, \mathbf{C}_a), && (4.9)\\
\mathbf{R}_d &= \mathbb{E}\{\mathbf{n}_d \mathbf{n}_d^H\} = \sigma_n^2 \mathbf{I}_{N_d N_r} && (4.10)\\
\mathbf{m}_a &= \mathbf{C}_a \mathbf{L}_p, && (4.11)\\
\mathbf{C}_a &= \mathbf{R}_c (\mathbf{\Gamma}_p \mathbf{R}_c + \mathbf{I}_{MN_r N_t})^{-1}, && (4.12)\\
\mathbf{L}_p &= \sigma_n^{-2} \mathbf{\Psi}_p^H \mathbf{z}_p, && (4.13)\\
\mathbf{\Gamma}_p &= \sigma_n^{-2} \mathbf{\Psi}_p^H \mathbf{\Psi}_p, && (4.14)\\
\mathbf{R}_c &= \mathbf{I}_{N_r} \otimes \mathbf{I}_{N_t} \otimes \mathbf{R}_a, && (4.15)\\
\mathbf{L}_d &= \sigma_n^{-2} \mathbf{\Psi}_d^H \mathbf{z}_d, && (4.16)\\
\mathbf{\Gamma}_d &= \sigma_n^{-2} \mathbf{\Psi}_d^H \mathbf{\Psi}_d, && (4.17)
\end{aligned}$$

$\mathbf{R}_d$ is the noise covariance matrix for data REs and $\mathbf{R}_c$ is an $MN_tN_r \times MN_tN_r$ covariance matrix of the expansion coefficients for channels between all transmit and all receive antennas.

By using complex multivariate normal distributions for $p(\mathbf{z}_d|\mathbf{s}_d, \mathbf{a})$ and $f(\mathbf{a}|\mathbf{z}_p)$, we obtain

$$\begin{aligned} p(\mathbf{z}_d|\mathbf{s}_d, \mathbf{a}) &= \frac{1}{\pi^{N_d}|\mathbf{R}_d|} \exp(-(\mathbf{z}_d - \mathbf{\Psi}_d\mathbf{a})^H \mathbf{R}_d^{-1}(\mathbf{z}_d - \mathbf{\Psi}_d\mathbf{a})) \\ &= \frac{1}{\pi^{N_d}|\mathbf{R}_d|} \exp(-\mathbf{z}_d^H \mathbf{R}_d^{-1}\mathbf{z}_d + 2\Re(\mathbf{a}^H \mathbf{\Psi}_d^H \mathbf{R}_d^{-1}\mathbf{z}_d) - \mathbf{a}^H \mathbf{\Psi}_d^H \mathbf{R}_d^{-1}\mathbf{\Psi}_d\mathbf{a}), \end{aligned} \tag{4.18}$$

Replacing some of the parameters with $\mathbf{R}_d$, $\mathbf{L}_d$ and $\mathbf{\Gamma}_d$, we arrive at

$$p(\mathbf{z}_d|\mathbf{s}_d, \mathbf{a}) = \frac{\sigma_n^{-2}}{\pi^{N_d}} \exp(-\sigma_n^{-2}|\mathbf{z}_d|^2 + 2\Re(\mathbf{a}^H \mathbf{L}_d) - \mathbf{a}^H \mathbf{\Gamma}_d \mathbf{a}). \tag{4.19}$$

$$\begin{aligned} f(\mathbf{a}|\mathbf{z}_p) &= \frac{1}{\pi^N|\mathbf{C}_a|} \exp(-(\mathbf{a} - \mathbf{m}_a)^H \mathbf{C}_a^{-1}(\mathbf{a} - \mathbf{m}_a)) \\ &= \frac{1}{\pi^N|\mathbf{C}_a|} \exp(-\mathbf{a}^H \mathbf{C}_a^{-1}\mathbf{a} + 2\Re(\mathbf{a}^H \mathbf{C}_a^{-1}\mathbf{m}_a) - \mathbf{m}_a^H \mathbf{C}_a^{-1}\mathbf{m}_a). \end{aligned} \tag{4.20}$$

By substituting (4.19) and (4.20) in (4.7) and integrating over the real and imaginary parts of $\mathbf{a}$, we arrive at

$$\begin{aligned} p(\mathbf{z}_d|\mathbf{s}_d, \mathbf{z}_p) = c \int &\exp(2\Re(\mathbf{a}^H \mathbf{L}_d) - \mathbf{a}^H \mathbf{\Gamma}_d \mathbf{a}) \\ &\exp(-\mathbf{a}^H \mathbf{C}_a^{-1}\mathbf{a} + 2\Re(\mathbf{a}^H \mathbf{C}_a^{-1}\mathbf{m}_a)) d\Re(\mathbf{a}) d\Im(\mathbf{a}), \end{aligned} \tag{4.21}$$

where c is a constant,

$$c = \frac{\sigma_n^{-2} \exp(-\sigma_n^{-2}|\mathbf{z}_d|^2) \exp(-\mathbf{m}_a^H \mathbf{C}_a^{-1}\mathbf{m}_a)}{\pi^{N_d}|\mathbf{C}_a|} > 0. \tag{4.22}$$

Solving (4.21) with $\mathbf{L}_p = \mathbf{C}_a^{-1}\mathbf{m}_a$, we get

$$p(\mathbf{z}_d|\mathbf{s}_d, \mathbf{z}_p) = c \int \exp(2\Re(\mathbf{a}^H(\mathbf{L}_d + \mathbf{L}_p)) - \mathbf{a}^H(\mathbf{\Gamma}_d + \mathbf{C}_a^{-1})\mathbf{a}) d\Re(\mathbf{a}) d\Im(\mathbf{a}). \tag{4.23}$$

Lemma 4.1 [40]:

If $\mathbf{q}$ and $\mathbf{y}$ are complex M-dimensional vectors and $\mathbf{\Gamma}$ is an $M \times M$ definite positive Hermitian matrix, then

$$\int \exp(2\Re(\mathbf{q}^H \mathbf{y}) - \mathbf{q}^H \mathbf{\Gamma}^{-1}\mathbf{q}) d\Re(\mathbf{q}) d\Im(\mathbf{q}) = \pi^M |\mathbf{\Gamma}| \exp(\mathbf{y}^H \mathbf{\Gamma} \mathbf{y}). \tag{4.24}$$

Applying Lemma 4.1 to (4.23), we get

$$p(\mathbf{z}_d|\mathbf{s}_d,\mathbf{z}_p)=\frac{c}{|\mathbf{C}_a\mathbf{\Gamma}_d+\mathbf{I}_{MN_rN_t}|}\exp\{(\mathbf{L}_d+\mathbf{L}_p)^H(\mathbf{\Gamma}_d+\mathbf{C}_a^{-1})^{-1}(\mathbf{L}_d+\mathbf{L}_p)\}. \tag{4.25}$$

Using (4.25), the metric $\lambda_{opt}(\mathbf{s}_d)$ is given by

$$\begin{aligned}\lambda_{opt}(\mathbf{s}_d)&=\ln[p(\mathbf{z}_d|\mathbf{s}_d,\mathbf{z}_p)],\\&=\ln\Big[\frac{c}{|\mathbf{C}_a\mathbf{\Gamma}_d+\mathbf{I}_{MN_rN_t}|}\exp\{(\mathbf{L}_d+\mathbf{L}_p)^H(\mathbf{\Gamma}_d+\mathbf{C}_a^{-1})^{-1}(\mathbf{L}_d+\mathbf{L}_p)\}\Big],\\&=\ln[c]-\ln[|\mathbf{C}_a\mathbf{\Gamma}_d+\mathbf{I}_{MN_rN_t}|]+((\mathbf{L}_d+\mathbf{L}_p)^H(\mathbf{\Gamma}_d+\mathbf{C}_a^{-1})^{-1}(\mathbf{L}_d+\mathbf{L}_p)),\end{aligned} \tag{4.26}$$

Omitting terms that do not affect the optimization (i.e., $\ln[c]$) and replacing some parameters by (4.12) to (4.17), we arrive at the optimal metric:

$$\begin{aligned}&\lambda_{\text{opt}}(\mathbf{s}_d)=\{\sigma_n^{-2}(\mathbf{\Psi}_d^H\mathbf{z}_d+\mathbf{\Psi}_p^H\mathbf{z}_p)^H\\\times\;&(\mathbf{\Psi}_d^H\mathbf{\Psi}_d+\mathbf{\Psi}_p^H\mathbf{\Psi}_p+\sigma_n^2\mathbf{R}_c^{-1})^{-1}(\mathbf{\Psi}_d^H\mathbf{z}_d+\mathbf{\Psi}_p^H\mathbf{z}_p)\\-\;&\ln|\mathbf{\Psi}_d^H\mathbf{\Psi}_d+\mathbf{\Psi}_p^H\mathbf{\Psi}_p+\sigma_n^2\mathbf{R}_c^{-1}|\}.\end{aligned} \tag{4.27}$$

Note that the optimal detector maximizing the metric $\lambda_{\text{opt}}(\mathbf{s}_d)$ in (4.27) simultaneously for all N_d symbols in the data package is extremely complicated. It has been shown in [20] that, with a slightly reduced detection performance, the optimization can be done in a SbS fashion (i.e., by setting $N_D=1$), thus significantly reducing the complexity of the detector.

In the SbS optimal detection, $\mathbf{z}_d$ is simplified to $\mathbf{z}_d=[z_{d,1}^{(g)},...,z_{d,r}^{(g)},...,z_{d,N_r}^{(g)}]^T$, which is an $N_r\times 1$ vector of received data at the gth RE, $z_{d,r}^{(g)}$ is the gth element of the vector $\mathbf{z}_{d,r}$, $g=1,...,N_d$, $\mathbf{\Psi}_d$ is simplified to $\mathbf{\Psi}_d=\mathbf{I}_{N_r}\otimes[s_{d,1}^{(g)}\mathbf{b}_d,...,s_{d,k}^{(g)}\mathbf{b}_d,...,s_{d,N_t}^{(g)}\mathbf{b}_d]$, $s_{d,k}^{(g)}$ is the kth element of the vector $\mathbf{s}_d^{(g)}=[s_{d,1}^{(g)},...,s_{d,k}^{(g)},...,s_{d,N_t}^{(g)}]$ and gth element of the vector $\mathbf{s}_{d,k}=[s_{d,k}^{(1)},...,s_{d,k}^{(g)},...,s_{d,k}^{(N_d)}]^T$, $\mathbf{S}_{d,k}=\text{diag}(\mathbf{s}_{d,k})$, $\mathbf{b}_d$ is an $1\times M$ vector obtained as the gth row of the matrix $\mathbf{B}_d$.

It can be seen that the optimal metric depends on the covariance matrix $\mathbf{R}_c$ of channel expansion coefficients $\mathbf{a}$. This covariance is unknown in practice. Besides, the SbS optimal detector is still complicated. Therefore, two problems should be addressed: (i) to reduce complexity of the detector, and (ii) to make the detector operating without the perfect knowledge of the channel statistics.

For N_t transmit antennas, $N_D = N_d$ data symbols and a modulation with 2^K constellation points, the optimal metric $\lambda_{\text{opt}}(\mathbf{s}_d)$ in (4.27) is calculated $2^{KN_dN_t}$ times, which results in a high computational load. In the SbS optimal detector ($N_D = 1$), the optimal metric is calculated 2^{KN_t} times for every symbol and $N_d 2^{KN_t}$ times for all symbols. Since $N_d \ll 2^{N_d}$, this significantly reduces the overall complexity of the detector. However, the SbS optimal detector is still complicated for implementation. To analyse the SbS optimal detector complexity, we consider the case of $N_t = N_r = 1$ (i.e., single input single output system) and known data and pilot basis functions $\mathbf{B}_d$ and $\mathbf{B}_p$, noise power σ_n^2 and covariance $\mathbf{R}_c$. For such case, the following parameters are simplified: $\mathbf{s}_d = s_d$, $\mathbf{z}_d = z_d$ and $\mathbf{\Psi}_d = s_d\mathbf{b}_d$. Then, the metric in (4.27) can be rewritten as (see [20] for more details)

$$\lambda_{\text{opt}}(\mathbf{s}_d) = \{\sigma_n^{-2}|s_d|^2|z_d|^2\varrho + 2\sigma_n^{-2}\Re\{s_d z_d^* \epsilon z_p\} + \sigma_n^{-2}\mathbf{z}_p^H \mathbf{\Xi}\mathbf{z}_p + \ln|\mathbf{Y}|\}. \tag{4.28}$$

where $\varrho = \mathbf{b}_d\mathbf{Y}\mathbf{b}_d^H$, $\epsilon = \mathbf{b}_d\mathbf{Y}\mathbf{\Psi}_p$, $\mathbf{\Xi} = \mathbf{\Psi}_p\mathbf{Y}\mathbf{\Psi}_p^H$ and $\mathbf{Y} = (\mathbf{\Psi}_d^H\mathbf{\Psi}_d + \mathbf{\Psi}_p^H\mathbf{\Psi}_p + \sigma_n^2\mathbf{R}_c^{-1})^{-1}$. In (4.28), ϱ, ϵ, $\mathbf{\Xi}$, $\mathbf{Y}$ and $[\ln|\mathbf{Y}|]$ can be precomputed and saved in the memory. The terms $[\epsilon z_p]$ and $[\sigma_n^{-2}\mathbf{z}_p^H\mathbf{\Xi}\mathbf{z}_p]$ can be computed once for all data symbols. However, the terms $[|s_d|^2|z_d|^2]$ and $[s_d z_d^*]$ are to be computed on SbS basis. Using (4.28), $\left[\frac{2N_p^2+2N_p+D}{N_d} + 2^K + D\right]$ real-time complex multiplications are required to detect one data symbol ($N_d = 1$) [20], where D represents all possible values of $|s_d|$ (e.g., for 16-QAM, $D = 4$). For N_d data symbols, $\left[N_d\left(\frac{2N_p^2+2N_p+D}{N_d} + 2^K + D\right)\right]$ complex multiplications are required to be computed. For high N_d, N_t and modulation order, the complex multiplications required will increase significantly.

The main objective of the selective receiver proposed in the following section is to significantly reduce the number of data symbols processed in the SbS optimal detector. In other words, calculating the optimal metric $N_{sel}2^{KN_t}$ times instead of $N_d 2^{KN_t}$ times, with N_{sel} are the number of data symbols processed in the SbS optimal detector and $N_{sel} \ll N_d$. This significantly reduce the overall complexity of the receiver, while keeping its high detection performance. For the case of $N_t = N_r = 1$, $\left[N_{sel}\left(\frac{2N_p^2+2N_p+D}{N_d} + 2^K + D\right)\right]$ complex multiplications only are required to be computed by the selective receiver. We will show through simulation that using the proposed selection scheme, N_{sel} symbols (which represent a small percentage of N_d symbols) are only selected for processing in the SbS optimal detector. The most of the received symbols are processed in a more simple mismatched detector, e.g., such as the MMSE detector. The complexity of an MMSE detector for one symbol is only $\mathcal{O}(N_t^3)$

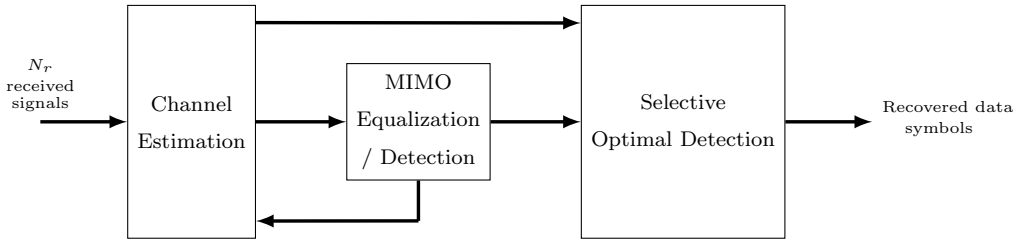

Figure 4.2: Proposed channel estimation and detection architecture at the receiver.

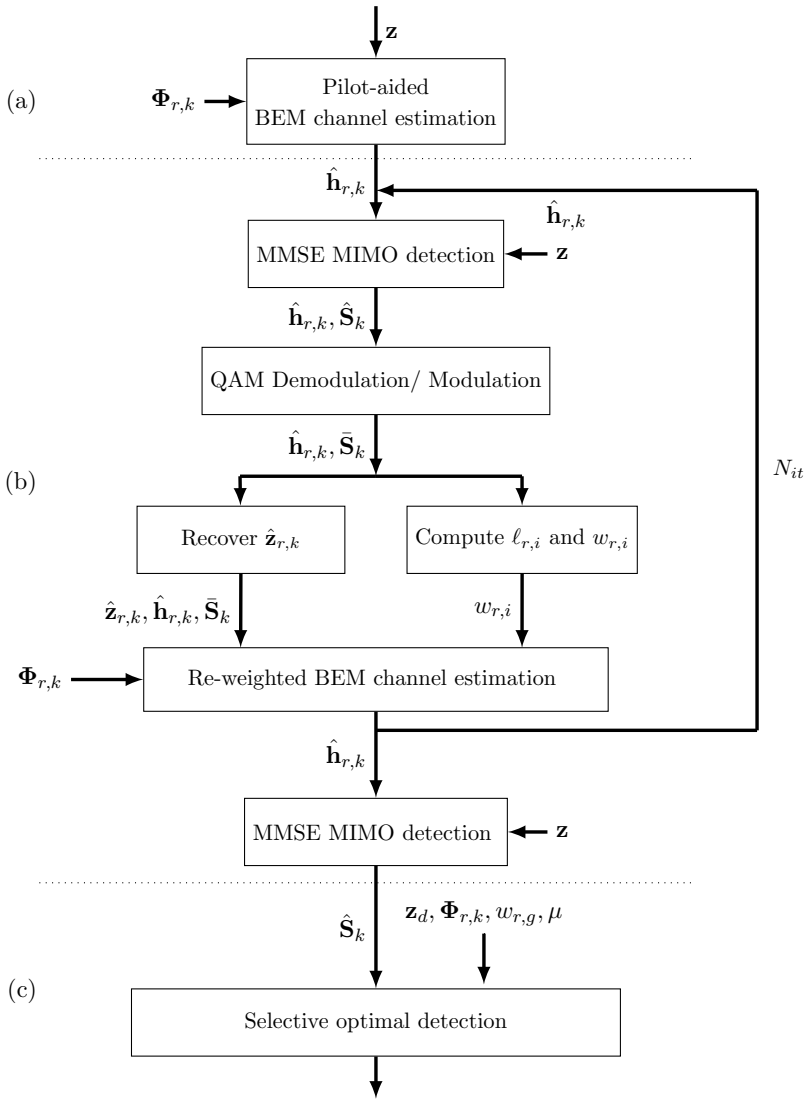

Figure 4.3: Proposed receiver: (a) pilot-based BEM channel estimation (b) re-weighted iterative BEM channel estimation (c) selective SbS optimal detection.

arithmetic operations, which is significantly lower than that of the SbS optimal detector.

4.4 Proposed receiver

In the proposed receiver, the SbS optimal and mismatched detection are combined into a two-stage detection scheme. Firstly, the mismatched detection is applied to all data symbols in the data package and unreliably detected symbols are identified. The mismatched detection is based on the re-weighted channel estimation (see below) which, as a by-pass product, for every data symbol, generates weights characterizing the reliability of the symbol estimates. These weights are exploited in a selection scheme that identifies *unreliable* symbols. Only these symbols are processed in the SbS optimal detector. This approach allows reduction in the receiver complexity.

However, for operation of the SbS optimal receiver, the problem of the knowledge of channel statistics should also be addressed. To deal with this problem, we propose the following approach. In the channel estimator operating with the mismatched detector, we propose to use an adaptive regularization, i.e., finding a regularization matrix that results in the most accurate channel estimate. This allows an improved detection performance in the mismatched detector. However, it also provides an estimate of the channel statistics for operation of the SbS optimal detector. Since the optimal regularization matrix is the inverse of the channel covariance matrix, the adaptively found regularization matrix can be treated as an estimate of the covariance inverse and be directly applied in the SbS optimal detector.

Although the optimal regularization can be found jointly for all $N_t N_r$ channels between the N_t transmit and N_r receive antennas, it is more practical (and significantly less complicated) to find it separately for every channel. Besides, the complexity of the joint channel estimation for all channels would be $\mathcal{O}(N_r(MN_t)^3)$ arithmetic operations, which is high. On the other hand, the complexity of independently estimating the multiple channels between transmit and receive antennas is only $\mathcal{O}(N_r N_t M^3)$ operations. Thus, the proposed receiver should recover the received signals corresponding to the channels to enable the separate channel estimation.

Figure 4.3 describes the channel estimation and detection stages of the proposed receiver. The pilot-based BEM channel estimation is used to provide initial channel estimates [see Figure 4.3 (a)]. The re-weighted iterative BEM channel estimation [Figure 4.3 (b)] is used to

improve the channel estimation performance and provide information that is necessary to implement the selective optimal detector. The selective detector [Figure 4.3 (c)] selects the received data that are assumed to be detected unreliably at stage (b) and applies the SbS optimal detector to these symbols. Below, these stages are explained in more details.

4.4.1 Pilot-based BEM channel estimation

For better explanation of how the proposed receiver operates, we consider an equivalent model of the received signal. The received signal $\mathbf{z}_r$ at the rth receive antenna can be expressed as

$$\mathbf{z}_r = \sum_{k=1}^{N_t} \mathbf{S}_k \mathbf{h}_{r,k} + \mathbf{n}_r, \quad r = 1, ..., N_r. \tag{4.29}$$

The initial pilot-based channel estimate $\hat{\mathbf{h}}_{r,k}$ is given by

$$\hat{\mathbf{h}}_{r,k} = \mathbf{B}\hat{\mathbf{a}}_{r,k}, \tag{4.30}$$

where the estimate $\hat{\mathbf{a}}_{r,k}$ of the expansion coefficients $\mathbf{a}_{r,k}$ is given by

$$\hat{\mathbf{a}}_{r,k} = (\mathbf{B}^H \mathbf{S}_{n,k}^H \mathbf{S}_{n,k} \mathbf{B} + \mathbf{\Phi}_{r,k})^{-1} \mathbf{B}^H \mathbf{S}_{n,k}^H \tilde{\mathbf{z}}_{r,k}, \tag{4.31}$$

$\mathbf{S}_{n,k}$ is an $N \times N$ diagonal matrix of symbols transmitted by the kth transmit antenna with zeros at data REs, $\mathbf{\Phi}_{r,k}$ is an $M \times M$ regularization matrix for the channel between the kth transmit antenna and the rth receive antenna and $\tilde{\mathbf{z}}_{r,k}$ is an $N \times 1$ vector of received pilot symbols from the kth transmit antenna with zeros at data locations. The matrix $\mathbf{S}_{n,k}$ is obtained from $\mathbf{S}_k$ by zeroing the data symbols. In the LTE downlink [29] (which we adopt for our simulation), as shown in Figure 3.3, pilot symbols transmitted from one transmit antenna are not overlapping with data or pilot symbols from the other transmit antennas. Thus, the received pilot symbols from the kth transmit antenna will be free from the multi-antenna interference and can be recovered separately. This justifies the estimation of $\mathbf{a}_{r,k}$ from $\tilde{\mathbf{z}}_{r,k}$ as in (4.31). If $\mathbf{\Phi}_{r,k} = \sigma_n^2 \mathbf{R}_a^{-1}$ with $\mathbf{R}_a = \mathbb{E}(\mathbf{a}_{r,k} \mathbf{a}_{r,k}^H)$, we arrive at the pilot-based LMMSE channel estimation. The covariance matrix $\mathbf{R}_a$ of the expansion coefficients can be computed from the channel covariance (defined by the PDP and the Doppler spectrum) as in (4.3). As the true channel PDP is unavailable in practice, we use a more practical approach for finding the regularization matrix, as suggested in [21].

If $\mathbf{\Phi}_{r,k} = \sigma_n^2 \mathbf{R}_\xi^{-1}$, where $\mathbf{R}_\xi$ is an $M \times M$ covariance matrix for a model PDP, we arrive at the pilot-based channel estimation with model-based regularization. If $\mathbf{\Phi}_{r,k} = \sigma_n^2 \mathbf{I}_M$, we arrive at the pilot-based channel estimation with diagonal loading, which only requires the knowledge of the noise variance σ_n^2. However, it causes a significant degradation in the estimation performance as will be seen from numerical results.

4.4.2 Re-weighted iterative BEM channel estimation

In stage (b) of the proposed receiver, see Figure 4.3, tentative soft data estimates $\hat{\mathbf{S}}_k$ are obtained in the MMSE MIMO detector using the initial channel estimates $\hat{\mathbf{h}}_{r,k}$. The tentative data symbols $\bar{\mathbf{S}}_k$ are recovered by mapping the soft data estimates onto the QAM constellation. Then, for the rth receive antenna, the weights $w_{r,i}$ are computed by [18]

$$w_{r,i} = \begin{cases} 1, & \ell_{r,i} \leq 1; \\ \frac{\ln(\ell_{r,i})+1}{\ell_{r,i}}, & \ell_{r,i} > 1, \end{cases} \tag{4.32}$$

where

$$\ell_{r,i} = \frac{1}{\sigma_n^2} \left| z_{r,i} - \sum_{k=1}^{N_t} \hat{h}_{r,k}^{(i)} \bar{s}_{k,i} \right|^2, \tag{4.33}$$

$w_{r,i}$ is the ith element of the rth weight vector $\mathbf{w}_r = [w_{r,1}, ..., w_{r,i}, ..., w_{r,N}]$, $z_{r,i}$ is the ith element of the received signal vector $\mathbf{z}_r$, $\hat{h}_{r,k}^{(i)}$ is the ith element of the estimated channel vector $\hat{\mathbf{h}}_{r,k}$, and $\bar{s}_{k,i}$ is the ith element of the tentative data and pilot vector $\bar{\mathbf{s}}_k$. From (4.32), it can be seen that the weight $w_{r,i}$ is in the range $(0, 1]$. When the weight is unity, the received symbol is perfectly known. For pilot symbols, the weights $w_{r,i}$ are set to unity (since the pilot symbols are perfectly known). Equation (4.32) implies that when the normalized residual power $\ell_{r,i}$ is high, the contribution (weight) of the corresponding tentative data symbols $\bar{s}_{k,i}$ into the channel estimate is reduced.

A portion $\hat{\mathbf{z}}_{r,k}$ of the received signal corresponding to the kth transmit antenna is recovered as

$$\hat{\mathbf{z}}_{r,k} = \mathbf{z}_r - \sum_{j=1, j\neq k}^{N_t} \bar{\mathbf{S}}_j \hat{\mathbf{h}}_{r,j}, \tag{4.34}$$

where signals received from other transmit antennas are treated as interference and their estimates are subtracted from the received signal $\mathbf{z}_r$. After the interference cancellation, the

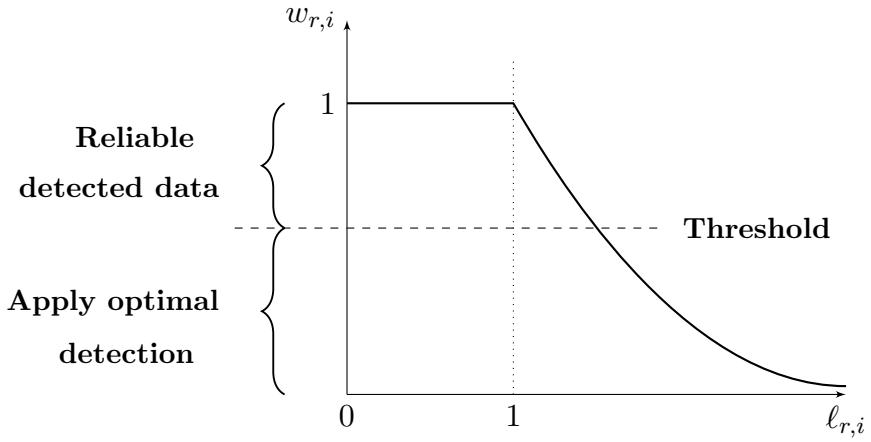

Figure 4.4: Selection scheme.

channel is re-estimated from $\hat{\mathbf{z}}_{r,k}$, and the re-weighted estimate of $\mathbf{a}_{r,k}$ is given by

$$\hat{\mathbf{a}}_{r,k} = (\mathbf{B}^H \bar{\mathbf{S}}_k^H \mathbf{W}_r \bar{\mathbf{S}}_k \mathbf{B} + \mathbf{\Phi}_{r,k})^{-1} \mathbf{B}^H \bar{\mathbf{S}}_k^H \mathbf{W}_r \hat{\mathbf{z}}_{r,k}, \tag{4.35}$$

where $\bar{\mathbf{S}}_k$ is an $N \times N$ diagonal matrix of tentative data and pilot symbols, $\bar{\mathbf{S}}_k = \text{diag}(\bar{\mathbf{s}}_k)$, and $\mathbf{W}_r = \text{diag}(\mathbf{w}_r)$ is the diagonal matrix of weights computed using (4.32). If $\mathbf{W}_r = \mathbf{I}_N$, we arrive at the conventional unweighted BEM channel estimator, which however has inferior performance compared to the re-weighted estimation [18].

Note that, the channel estimate obtained from $\hat{\mathbf{z}}_{r,k}$ is sub-optimal as the channel estimation is performed independently instead of jointly for all transmit antennas. However, this approach reduces the complexity and it simplifies the adaptive regularization, which is described in Subsection 4.4.4. The updated channel estimates $\hat{\mathbf{h}}_{r,k}$ are used in the next re-weighted iteration of a total number of N_{it}. Note that the accuracy of tentative data estimates can be improved if decoding is used in the iterative re-weighted estimator. However, this will result in higher complexity of the receiver. Thus, we obtain the tentative data estimates without decoding as shown in Figure 4.3 (b). In the final iteration, the channel estimates $\hat{\mathbf{h}}_{r,k}$ are used in the MIMO MMSE detector to obtain soft estimates of data symbols in $\hat{\mathbf{S}}_k$. Then, the weights $w_{r,i}$ are used to construct the SbS selection scheme for the optimal detection.

4.4.3 The selection scheme

Figure 4.4 shows the relationship between the weights $w_{r,i}$ and the residual powers $\ell_{r,i}$ as in (4.32). For a single receive antenna, the idea of the proposed selection scheme is based on setting a threshold for the weights $w_{r,i}$. The weights that are below the threshold correspond to unreliable data symbols while weights above the threshold correspond to reliable data symbols. Using the weights as a measure of the data reliability, we can combine detectors with high complexity and high detection performance (i.e., the SbS optimal detection) with detectors that have lower complexity and lower detection performance (i.e., the re-weighted channel estimation with the MMSE detection). At first, the detection is performed by the lower complexity detector. Then, based on the weights and a threshold, the unreliable received data are processed in the higher complexity detector, thus reducing the complexity of the better detector (as it is applied on a small percentage of the received data) and having its high detection performance. The threshold value μ that provides a trade-off between the complexity and the detection performance in the worse channel case (i.e., the ETU channel) is selected from the values $\mu \in (0, 1]$.

Now we describe the selection scheme for the case of multiple receive antennas. Let $w_{r,g}$ be the weights at data locations, where $w_{r,g}$ is obtained from $w_{r,i}$ by only selecting the data locations (g is the index i at data locations). For different receive antennas, the weight $w_{r,g}$ can be different. Consider the first receive antenna ($r = 1$), let $v_1 = w_{1,g}$ be the weight that corresponds to the gth received data element $z_{d,1}^{(g)}$ ($z_{d,r}^{(g)}$ at $r = 1$). For the second receive antenna ($r = 2$), let $v_2 = w_{r,g}$ be the weight that corresponds to the gth received data element $z_{d,2}^{(g)}$. Let μ be a threshold value in the range $(0, 1]$. When v_1 and v_2 are below μ, we can assume that the received data $\mathbf{z}_d$ at this location has not been detected reliably. Then, the scheme selects this $\mathbf{z}_d$ for detection by the SbS optimal detector. If one of the weights or both the weights are greater than or equal to μ, the scheme decides that the received data have already been detected correctly. Note that, the selective detector is applied only on a small percentage of the received data symbols (see Section 4.5) which significantly reduces the detector complexity in comparison with the SbS optimal detector.

4.4.4 Adaptive model-based regularization

The model-based regularization is computed assuming a model PDP with uniformly distributed delays within a delay spread τ_{max}. The model PDP can differ from the true channel

PDP. The model-based regularization requires the knowledge of the delay spread. However, in practice, it is unknown and difficult to estimate. Our approach is to use an adaptive model-based regularization with a set of delay spreads given by [21]

$$\tau_{max} \in \{\tau_1, ..., \tau_\xi, ..., \tau_Q\}, \tag{4.36}$$

where τ_ξ is the ξth maximum delay spread and Q is its total number. The step $\Delta\tau$ between delay spreads in the set can be selected to about uniformly cover the maximum channel delays for the worst channel (e.g., for the ETU model [98]). For example, one can set $\Delta\tau = \frac{\tau_Q}{Q}$ and τ_Q is greater than the maximum delay spread of the ETU channel. As long as the set in (4.36) sufficiently covers the possible delay spreads of the high, medium and low delay spread channels, any $\Delta\tau$ can be selected.

For the ξth delay spread τ_ξ, an $M \times M$ model-based covariance matrix $\mathbf{R}_\xi$ is pre-computed, thus providing a set $\{\mathbf{R}_\xi\}_{\xi=1}^{Q}$. In order to select the best covariance matrix for channel estimation from this set, we use the GCV method [103]. The GCV method has been previously used for selection of smoothing parameters of a spline fitting without the knowledge of noise variance [21, 104]. In the GCV method, one sample of observed data (in our case, one RE) is removed and the remaining samples are used to estimate this sample; this procedure is repeated for all samples. When a smoothing parameter is the best fit for the estimation for all these samples, the overall prediction error (i.e., the GCV) is minimized.

Using the GCV method, for every ξ, the cross-validation parameter is computed [21,103], which in application to the channel estimation problem amounts to:

$$V_{r,k}(\xi) = \frac{||\tilde{\mathbf{z}}_{r,k} - \mathbf{G}_{n,k}^{(\xi)}\tilde{\mathbf{z}}_{r,k}||^2}{(N_p - \mathrm{tr}\{\mathbf{G}_{n,k}^{(\xi)}\})^2}, \tag{4.37}$$

$$\mathbf{G}_{n,k}^{(\xi)} = \mathbf{S}_{n,k}\mathbf{B}(\mathbf{B}^H\mathbf{S}_{n,k}^H\mathbf{S}_{n,k}\mathbf{B} + \sigma_n^2\mathbf{R}_\xi^{-1})^{-1}\mathbf{B}^H\mathbf{S}_{n,k}^H, \tag{4.38}$$

where $V_{r,k}(\xi)$ is a ξth cross-validation parameter for the channel between the rth receive antenna and kth transmit antenna. The covariance matrix $\mathbf{R}_\xi$ that provides the minimum value of $V_{r,k}(\xi)$ from the set of matrices $\{\mathbf{R}_\xi\}_{\xi=1}^{Q}$ is selected for the BEM channel estimation.

Note that the covariance matrix $\mathbf{R}_\xi$ is computed without the knowledge of the true

channel PDP. However, the Doppler frequency in our investigation is assumed perfectly known when computing the matrix $\mathbf{R}_{\xi}$. We make this assumption to simplify the presentation. Indeed, the adaptive regularization can be easily extended to the case of unknown Doppler frequency. Besides, there are techniques that can be used to estimate the Doppler frequency [105–110].

4.4.5 Complexity reduction

In the proposed receiver, the overall complexity is reduced, compared to the optimal detector, because of the following:

- The SbS optimal detector is used which significantly reduces the complexity in comparison to the optimal detector that jointly processes all symbols in the data package as explained in Section 4.3.
- The number of data symbols to which the SbS optimal detector is applied is significantly reduced as detailed in Section 4.3.
- Decoding is not used in the iterations involving the re-weighted channel estimation and mismatched detection.
- Pilot-based and re-weighted channel estimation is performed independently (not jointly) for the multiple $N_t \times N_r$ channels of the MIMO system as discussed in Section 4.4.

4.5 Numerical results

In the simulation, we consider a single-user MIMO downlink LTE scenario [29] in the spatial multiplexing transmission mode with two transmit antennas at the base station and two receive antennas at the user side. The channel frequency-selectivity is defined by the EPA, EVA, or ETU PDP [98]. The ETU channel has a high delay spread (slightly longer than the cyclic prefix length), while EVA and EPA channels have medium and low delay spreads, respectively. The multipath time-variant channel is described by Jakes' model with Doppler frequencies of 5 Hz for EPA and 350 Hz for EVA and ETU channels.

A transport block of one sub-frame (see Figure 3.3) with six resource blocks (36 subcarriers) is transmitted. A resource block occupies one slot of duration 0.5 ms and contains

7 OFDM symbols in time and 12 sub-carriers in frequency. The cyclic prefix duration is 5.2 μs for the first OFDM symbol in a slot and 4.69 μs for the rest of the OFDM symbols, each having the useful length 66.7 μs. The pilot symbols are generated from Zadoff-Chu sequences [29]. Data are encoded by turbo codes with 1/3-code rate [99]. The modulation scheme is 16-QAM.

For the adaptive regularization, the channel covariance for a set of uniform PDPs is precomputed with the following delay spreads ($Q = 8$):

$$\frac{\tau_{max}}{\tau_{CP}} \in \{1, 6, 14, 22, 30, 38, 44, 50\}/36, \quad \tau_{CP} = 4.69 \ \mu\text{s}. \tag{4.39}$$

With the adaptive regularization, no knowledge of the true channel PDP is assumed. The number of basis functions in time M_t and frequency M_f are set large enough to guarantee a low approximation error for the worst-case channel (the ETU channel with a Doppler frequency of 350 Hz). The receiver adopts these M_t and M_f for other channels. In this case, the receiver does not need to change its configuration for different channels which would be difficult to achieve in practice. Figure 4.5 shows the MSE performance of the pilot-based LMMSE BEM channel estimation for different values of basis functions M_t and M_f in the ETU channel with a Doppler frequency of 350 Hz at SNR=18 dB. It can be seen that $M_t = 4$ and $M_f = 11$ allow negligible approximation errors (i.e., the lowest M_t and M_f that can provide close-to-optimal MSE performance).

For the simulations, the following receivers are considered:

(1) Receiver 1 (R1): The MMSE detection with the pilot-based channel estimation. In this receiver, the pilot-based channel estimation in (4.31) is implemented with one of the following regularization schemes:

- LMMSE: $\mathbf{\Phi}_{r,k} = \sigma_n^2 \mathbf{R}_a^{-1}$.
- Adaptive: $\mathbf{\Phi}_{r,k} = \sigma_n^2 \mathbf{R}_\xi^{-1}$, $\xi = 1, \ldots, Q$.
- Diagonal loading: $\mathbf{\Phi}_{r,k} = \sigma_n^2 \mathbf{I}_M$.
- ETU: In this scheme, the channel covariance matrix is computed using the ETU PDP.

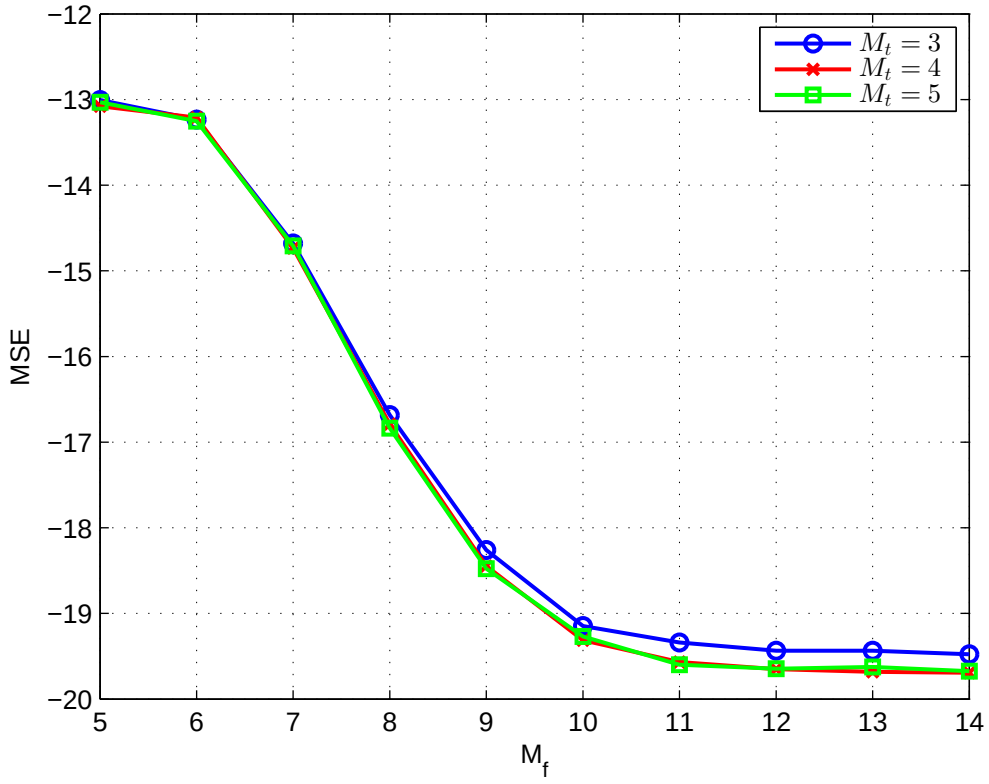

Figure 4.5: MSE performance of the pilot-based LMMSE BEM channel estimation for basis functions in time $M_t = 3, 4$ and 5 versus the number of basis functions in frequency M_f in a fading channel with the ETU PDP and a 350 Hz Doppler frequency at SNR = 18 dB.

(2) Receiver 2 (R2): The MMSE detection with the re-weighted channel estimation. In this receiver, the initial channel estimates are obtained via the pilot-based channel estimation in (4.31). For the iterative re-weighted channel estimation in (4.35), the number of iterations is set to $N_{it} = 3$. The channel estimates are based on the following regularization schemes:

- LMMSE: $\mathbf{\Phi}_{r,k} = \sigma_n^2 \mathbf{R}_a^{-1}$.
- Adaptive: $\mathbf{\Phi}_{r,k} = \sigma_n^2 \mathbf{R}_\xi^{-1}$, $\xi = 1, \ldots, Q$.
- Diagonal loading: $\mathbf{\Phi}_{r,k} = \sigma_n^2 \mathbf{I}_M$.

(3) Receiver 3 (R3): The SbS optimal receiver (4.6) with $N_D = 1$. In this receiver, the optimal detector exploits full knowledge of the channel covariance matrix (i.e., the true channel PDP) with $\mathbf{R}_c = \mathbf{I}_{N_r} \otimes \mathbf{I}_{N_t} \otimes \mathbf{R}_a$ in (4.15).

(4) Receiver 4 (R4): The SbS sub-optimal receiver. This receiver is the same as R3, but with an approximation to the true $\mathbf{R}_a$ in (4.15). Thus, the detector becomes sub-optimal. Depending on the covariance matrix replacing $\mathbf{R}_a$ in (4.15), the following sub-optimal detectors are considered:

- Adaptive: $\mathbf{\Phi}_{r,k} = \sigma_n^2 \mathbf{R}_\xi^{-1}$, $\xi = 1, \ldots, Q$.
- Model-based: In this case, the covariance matrix is computed for a uniform PDP with the delay spread of the true channel, i.e., the channel delay spread is assumed perfectly known.
- Diagonal loading: $\mathbf{\Phi}_{r,k} = \sigma_n^2 \mathbf{I}_M$.

(5) Receiver 5 (R5): The selective SbS optimal receiver (see Figure 4.3). In this receiver, the re-weighted channel estimation with the LMMSE regularization matrix is used.

(6) Receiver 6 (R6): The selective SbS sub-optimal receiver (see Figure 4.3). This receiver is the same as R5, but uses the adaptive regularization for the re-weighted channel estimation and for detection.

After the last stage in the receivers, the turbo decoding is performed. The LLR values for the data detected in the re-weighted channel estimation/detection iterations are calculated directly using the soft information obtained at the output of the MIMO MMSE detector [111]. The LLR λ_b for each bit of the data detected by the SbS optimal detector are computed as [40]:

$$\lambda_b = \ln \sum_{\mathcal{A}_k^+} e^{-\lambda_{opt}(\mathbf{s}_d)} - \ln \sum_{\mathcal{A}_k^-} e^{-\lambda_{opt}(\mathbf{s}_d)}, \tag{4.40}$$

where $\mathcal{A}_k^{\pm} = \{\mathbf{s}_d \in \mathcal{A} | b = \pm 1\}$. More details on the LLR calculation in the optimal detector can be found in [40, 112].

We first investigate the performance of the adaptive regularization. Figure 4.6 shows the BLER performance of the receiver (R1) with the pilot-based channel estimates in the EPA channel. The BLER performance of the receiver with the channel estimation using the diagonal loading (R1: Diagonal loading) shows a relatively poor performance. The channel estimation with the ETU regularization (R1: ETU reg.), i.e., the worst-case regularization, also causes a significant degradation in the performance. Thus, the often attractive approach

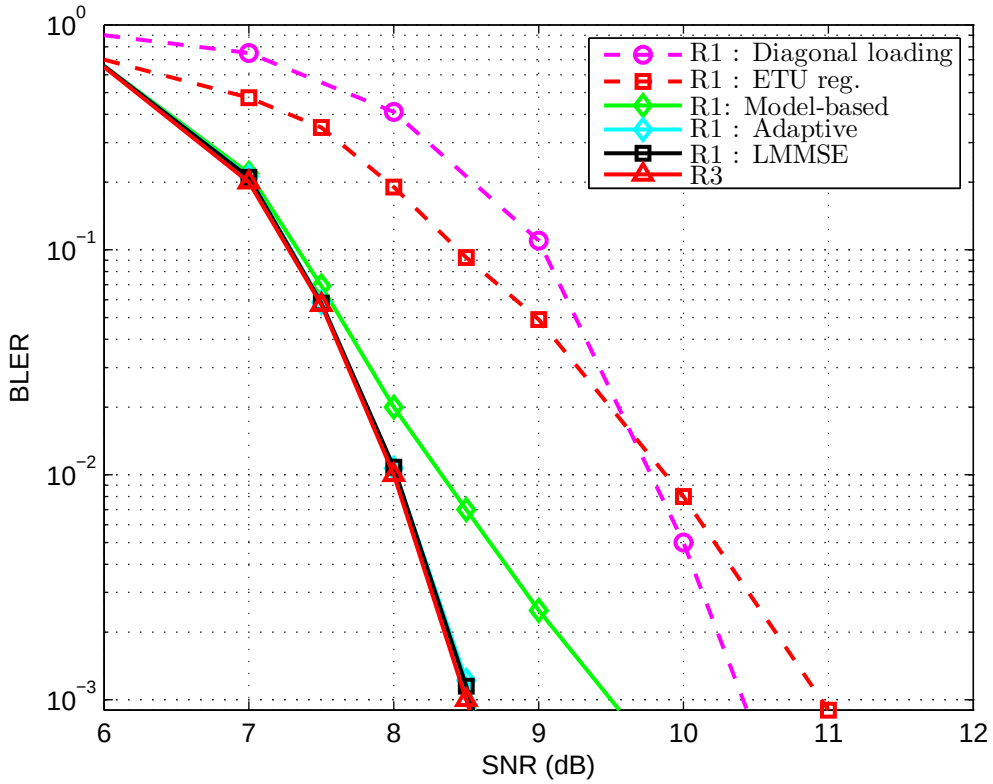

Figure 4.6: BLER performance of the receivers in the EPA channel with a Doppler frequency of 5 Hz.

of the estimation tuned to the worst-case scenario does not work well here. The MMSE detection with the pilot-based LMMSE channel estimation (R1: LMMSE) provides a performance that is very close to that of the SbS optimal detection (R3). The receiver with the adaptive regularization (R1: Adaptive) is more practical than the receiver with the LMMSE regularization as it can be applied without the knowledge of the channel PDP; but it also provides a performance very close to that of the SbS optrimal receiver with full knowledge of channel statistics (R3). Interestingly, the receiver with the model-based regularization (R1: Model-based), though based on perfect knowledge of the channel delay spread, shows an inferior performance when compared to the receiver with adaptive regularization.

In the EPA channel, where the channel is almost frequency-flat, the pilot-based channel estimation is enough to produce close-to-optimal detection performance. In the channels with longer delay spreads, such as the ETU and EVA channels, in addition to the pilot symbols, tentative data estimates need to be used for the channel estimation to achieve the close-to-optimal detection performance. Figure 4.7 shows the BLER performance of the receivers in

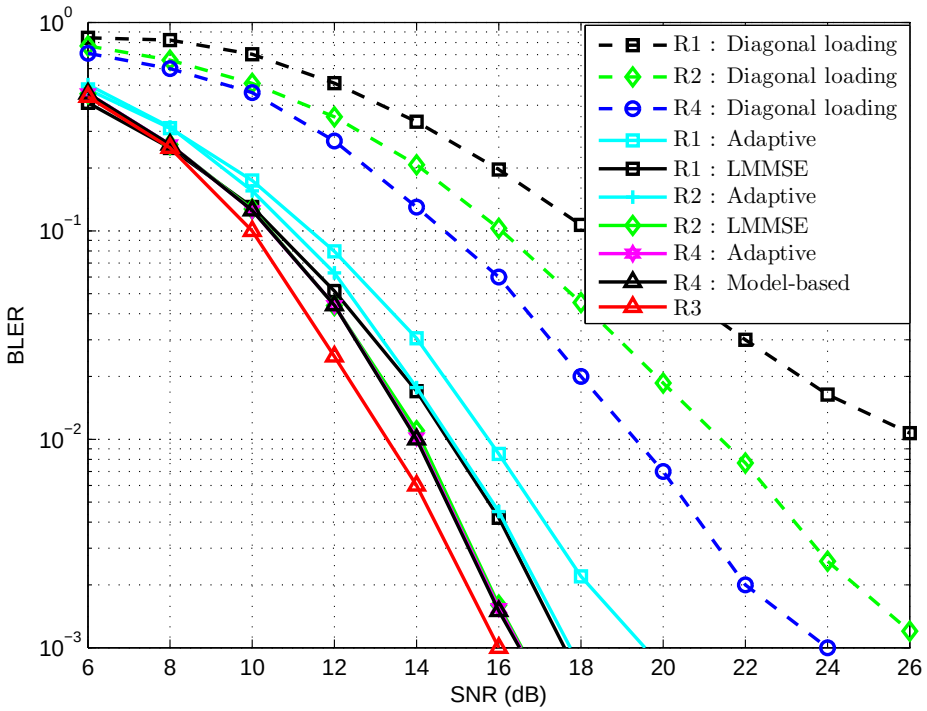

Figure 4.7: BLER performance of the receivers in the ETU channel with a Doppler frequency of 350 Hz.

the ETU channel. It is seen that the performance of all receivers with the diagonal loading is significantly inferior to that of the receivers with other regularization schemes. However, it is also seen that the use of the tentative data estimates for channel estimation (R2) provides a significant improvement in the performance compared to the pilot-based channel estimation (R1). It can also be seen that the sub-optimal receiver with the diagonal loading (R4: diagonal loading) results in a much better performance, compared to receivers R1 and R2 with diagonal loading. The receiver with the re-weighted channel estimation and adaptive regularization (R2: Adaptive) shows a good performance and is only about 0.7 dB away from that of the receiver with the re-weighted LMMSE channel estimation (R2: LMMSE) at a BLER of 10^{-2}. The sub-optimal receiver with adaptive regularization (R4: Adaptive) has almost the same performance as that of the receiver with the model-based regularization requiring perfect knowledge of the channel delay spread (R4: Model-based). The sub-optimal receiver with the adaptive regularization (R4: Adaptive) is about 0.7 dB away from the SbS optimal receiver with perfect knowledge of the channel statistics (R3). Thus, the sub-optimal receiver with the adaptive regularization provides a performance close to that of the optimal receiver.

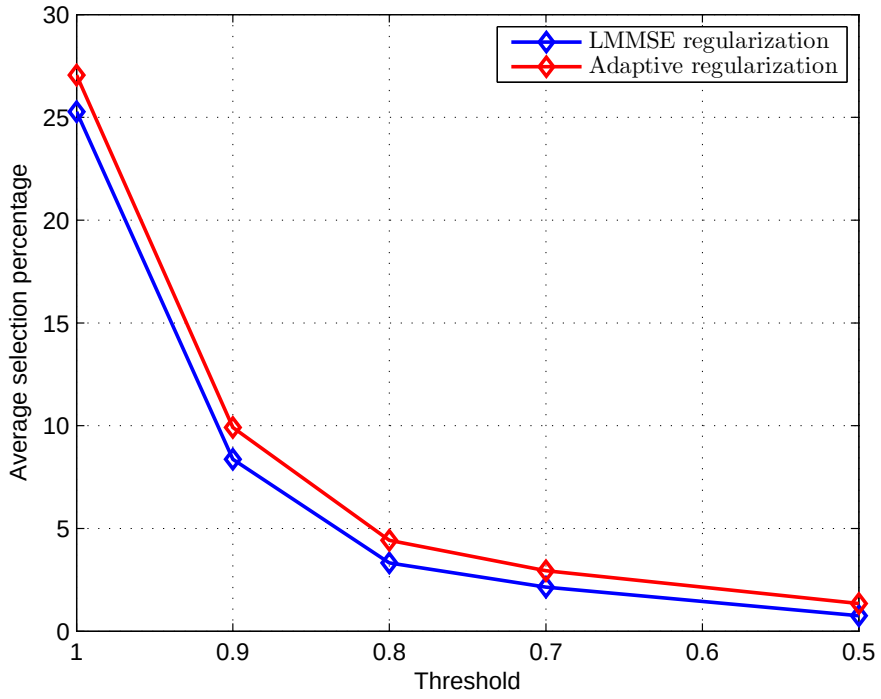

Figure 4.8: Average percentage of selection of received data elements versus the threshold μ for the selective detection with channel estimation using the LMMSE regularization and the adaptive regularization at SNR = 18 dB in the ETU channel with a Doppler frequency of 350 Hz.

Figure 4.8 shows the average percentage of selected unreliably received data elements versus the threshold μ for the cases of the LMMSE and adaptive regularization in the ETU channel. This represents the percentage of received data symbols selected for the optimal detection of the total number of data symbols N_d, averaged over 10^4 sub-frames. Figure 4.8 also shows that the percentage for the adaptive regularization is close to that of the LMMSE regularization. When the threshold value is reduced from $\mu = 1$ to $\mu = 0.5$, the percentage is significantly reduced and fewer received symbols are selected for the optimal detection. The less the percentage, the less complicated is the receiver, but with a drop in the performance.

Figure 4.9 shows the BLER performance of the receiver with the selective optimal detection (R5) for different values of the threshold ($\mu = 1$, 0.8, 0.7, 0.5) in the ETU channel. The selective optimal receiver with $\mu = 0.8$ has almost the same BLER performance as that of the optimal receiver (R3). The threshold value $\mu = 0.8$ provides a good performance-complexity trade-off. As shown in Figure 4.8, for $\mu = 0.8$, as few as 3.3 % of received data symbols are processed in the SbS optimal detector, while 4.4 % are processed in the case of the adaptive

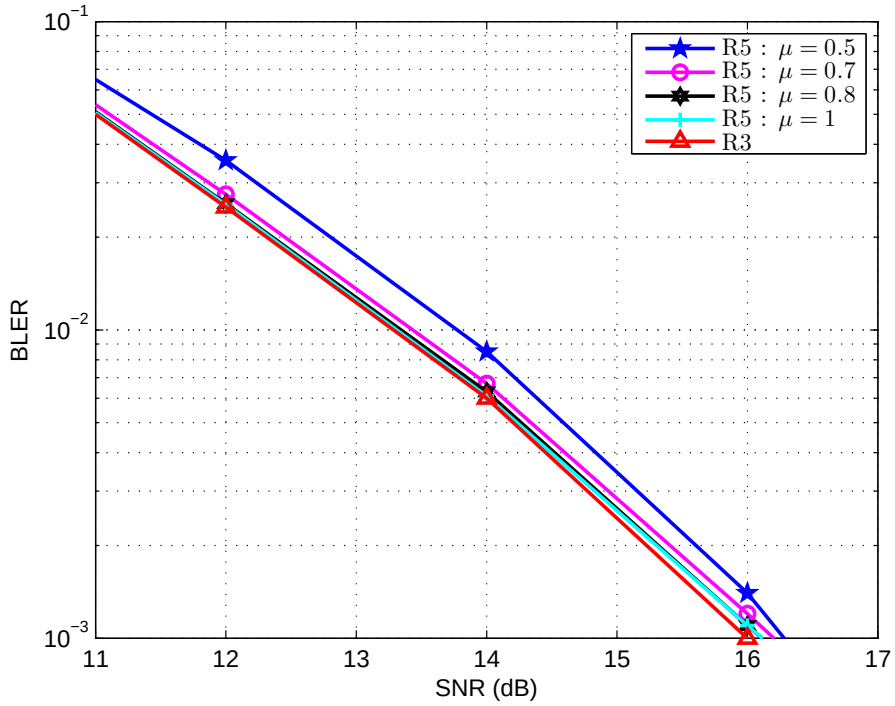

Figure 4.9: BLER performance of the selective detection versus the selection threshold μ in the ETU channel with a Doppler frequency of 350 Hz.

regularization. Thus, the complexity is reduced by approximately 30 times in comparison to applying the SbS optimal detection to all received data for the case of the known channel statistics and 23 times for the case of the adaptive regularization.

Figure 4.10 compares the BLER performance of the selective detection (optimal receiver R5 and sub-optimal receiver R6, $\mu = 0.8$) and the SbS optimal receiver (R3) with the LMMSE and adaptive regularization in the ETU channel. It can be seen that the selective receiver with the LMMSE regularization (R5) provides almost the same performance as that of the optimal receiver (R3). The selective receiver with the adaptive regularization (R6) has almost the same performance as the SbS sub-optimal receiver with the adaptive regularization (R4), but the complexity of the receiver R6 is significantly lower, as was explained in Sections 4.3 and 4.4.

Figure 4.11 shows the BLER performance of the receivers in the EVA channel. Similar to the ETU channel, the performance of the receivers with the channel estimation using the diagonal loading is inferior to that of the receivers with the other regularization schemes. The SbS sub-optimal receiver with adaptive regularization (R4: Adaptive) has almost the same performance as that with the model-based regularization (R4: Model-based) and only about

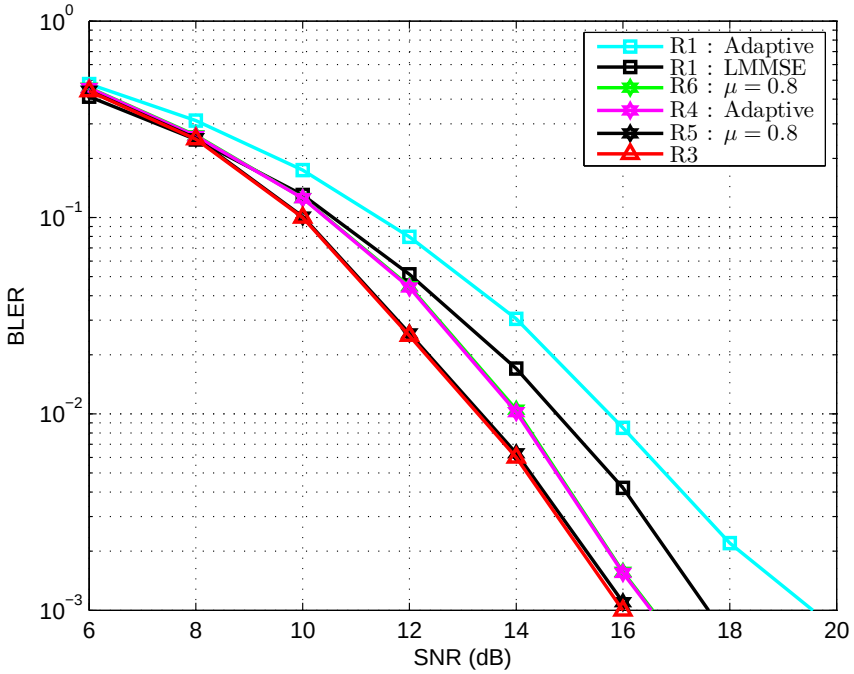

Figure 4.10: BLER performance of the selective detection (R5 and R6, $\mu = 0.8$) with LMMSE and adaptive regularization in the ETU channel with a Doppler frequency of 350 Hz.

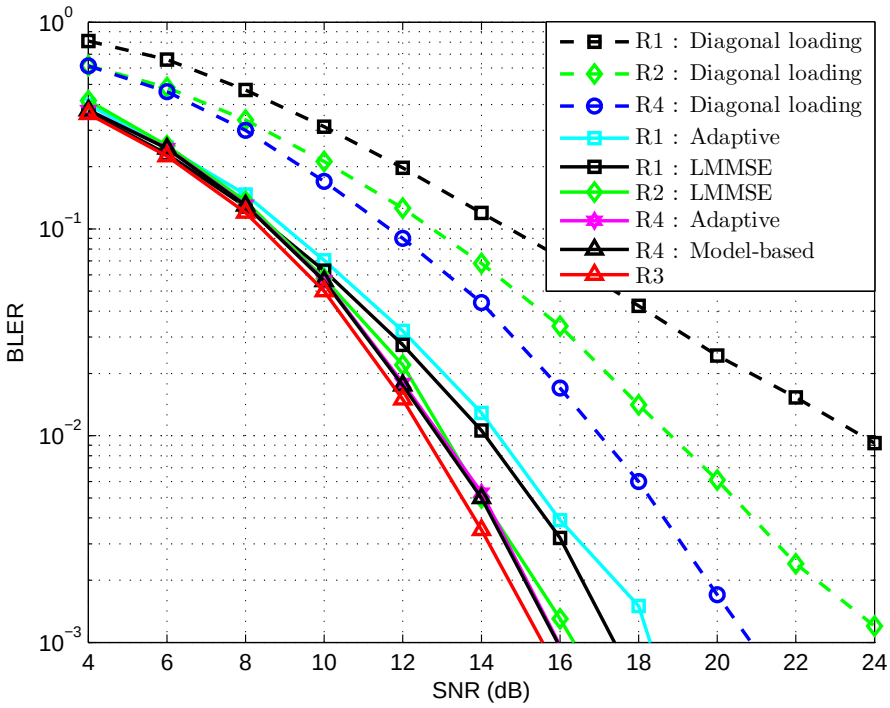

Figure 4.11: BLER performance of the receivers in the EVA channel with a Doppler frequency of 350 Hz.

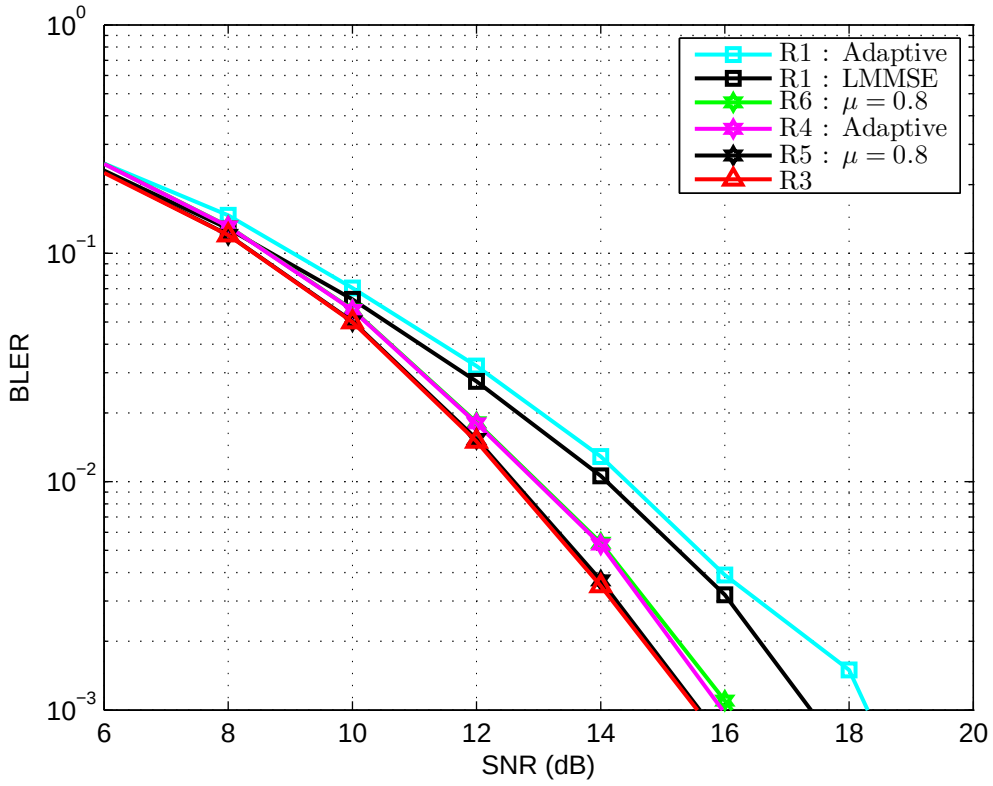

Figure 4.12: BLER performance of the selective detection receivers (R5 and R6, $\mu = 0.8$) using the LMMSE and the adaptive regularization in the EVA channel with a Doppler frequency of 350 Hz.

0.4 dB away from the SbS optimal detector (R3). Thus, the detection with the adaptive regularization again provides a performance close to that of the optimal detection.

As in the ETU channel, based on simulation that is not shown here, $\mu = 0.8$ provides a good performance-complexity trade-off in the EVA channel. For the LMMSE regularization, only 1.5 % of the received data are processed in the SbS optimal detector, and thus the complexity is reduced by approximately 65 times in comparison to applying the optimal detector to all received data. For the adaptive regularization, 2.4 % or received data are processed, and thus the complexity is reduced by approximately 42 times.

Figure 4.12 compares the BLER performance of the selective optimal receiver (R5) and selective sub-optimal receiver (R6) in the EVA channel. It can be seen again that the selective SbS optimal receiver (R5) provides almost the same performance as that of the optimal receiver (R3), whereas the selective receiver with the adaptive regularization (R6) shows a

performance very close to that of the SbS sub-optimal receiver with adaptive regularization (R4: Adaptive).

4.6 Summary

This chapter can be summarized as the following:

- A selective symbol-by-symbol detection with adaptive channel estimation was proposed for MIMO OFDM systems in doubly-selective channels.
- The proposed selective detection allows significantly lower complexity with almost the same detection performance in comparison with the symbol-by-symbol optimal receiver applied to all received data symbols.
- The performance of receivers with the adaptive regularization without knowledge of channel statistics is close to that of receivers with full knowledge of channel statistics.

Chapter 5

Joint Doppler-delay spread and channel estimation in doubly-selective channels

Contents

5.1 Introduction

Channel estimation is an important step in receivers of wireless communication systems. Pilot-based channel estimation, using BEMs, is often used for this purpose [2–10]. BEMs can provide high channel estimation performance with a low computational complexity [8,9]. However, the channel estimation may result in a poor estimation performance if ignoring the channel response smoothness (correlation) and noise. The estimation can be improved by taking these into account, which can be achieved by the use of a regularization. The best

estimation performance can be achieved if the regularization is based on the perfect knowledge of channel statistics, such as the Doppler spectrum and PDP. However, these are often unavailable in practice. For channel estimation, the Doppler spectrum is well described by such a parameter as the Doppler spread (or Doppler frequency). The PDP, for the purpose of channel estimation, can be represented by the delay spread. Therefore, in this chapter, we address the joint pilot-based estimation of the Doppler frequency, delay spread and BEM coefficients.

Several techniques for estimation of the Doppler frequency [105, 106, 110, 113] and delay spread [82, 114–116] with and without the channel estimation have been proposed in the literature for doubly-selective channels. However, only a few papers have addressed the joint estimation of the Doppler frequency, delay spread and the channel [117–120]. In [117], the channel was estimated for medium to high Doppler frequencies assuming some estimates of the Doppler frequency in doubly-selective channels. However, it does not consider the channel estimation at low Doppler frequencies. In [118], a Doppler frequency estimator with delay-subspace tracking was shown to provide high accuracy in the estimation of medium to high Doppler frequencies. However, this estimator utilizes a high number of pilot symbols and has high estimation errors at low Doppler frequencies. In [119] and [120], the estimation performance was investigated at low Doppler frequencies only. In this chapter, we are motivated to find a joint estimator for the Doppler frequency, delay spread and channel that outperforms existing estimators in doubly-selective channels at low to high Doppler frequencies.

In [21], the channel estimation with adaptive model-based regularization was proposed. This approach selects, using a cross-validation (CV) criterion, a regularization matrix from a set of regularization matrices defined by a set of delay spreads. Such an estimation achieves a performance close to that of the channel estimation with the knowledge of the true channel delay spread. However, it does assume that the Doppler frequency is known, which however is unavailable in practice. Here, we extend the approach in [21] to jointly estimate the Doppler frequency, delay spread and channel response.

In the joint estimation, a large set of regularization matrices defined by the Doppler frequency and delay spread (i.e., two-dimensional set) is required. This involves a large number of matrices to be precomputed and stored, which may occupy a large space in the memory.

Also, when the CV approach [103,121] uses the exhaustive search to find the optimal solution from this set, it results in a high computational load. To reduce the memory load, we use properties of the BEM matrices. The dichotomous search [122] can be used instead of the exhaustive search to reduce the complexity.

In general, Doppler frequency estimators designed for a specific Doppler spread model will have large modelling errors when in reality a different Doppler model describes the real channel [105]. For example, in macro-cells, the Doppler spectrum is well described by Jakes' Doppler spectrum [123]. On the other hand, in indoor environments, the Doppler spectrum is often uniform [124]. When the Doppler frequency estimator designed for an environment with the uniform Doppler spectrum is applied on an environment described by the Jakes' Doppler spectrum, this may cause high estimation errors. This may also affect the performance of the joint estimation. In our investigation, the Doppler model mismatch is investigated.

In this chapter, a new joint Doppler-delay spread and channel estimation is proposed for doubly-selective channels. This estimator exploits the GCV, dichotomous search and some properties of the BEM matrices to achieve high estimation performance with a reduced memory space and reduced complexity. A MIMO OFDM system in downlink LTE scenarios [29] is used to investigate the performance of the proposed joint estimator. In this chapter, more emphasis is put on uncertainty in the Doppler spread and channel estimation. The performance of the Doppler frequency estimation by the proposed estimator is compared with that obtained by a conventional Doppler frequency estimator [22]. The performance of channel estimates obtained by the proposed approach is compared with that of the LMMSE channel estimates. It is shown that the proposed estimator provides channel estimates without the knowledge of the channel statistics with accuracy, which are close to those obtained with perfect knowledge of channel statistics.

The remainder of this chapter is organized as follows: signal and channel models are introduced in Section 5.2. Pilot-based BEM channel estimation is described in Section 5.3. The conventional Doppler frequency estimation is described in Section 5.4. In Section 5.5, the new joint estimator is presented. In Section 5.6, the complexity reduction of the joint estimator is discussed. In Section 5.7, a re-adjustable estimation is proposed to provide further improvement to the joint Doppler-delay spread and channel estimation. Numerical

results are given in Section 5.8. Section 5.9 concludes the chapter.

5.2 Signal and channel models

Consider a single-user MIMO OFDM system. At the rth receive antenna, the received signal $\mathbf{y}_r$ is modelled as

$$\mathbf{z}_r = \sum_{k=1}^{N_t} \mathbf{S}_k \mathbf{h}_{r,k} + \mathbf{n}_r, \;\; r = 1, ..., N_r, \tag{5.1}$$

where $\mathbf{S}_k$ is an $N \times N$ diagonal matrix of data and pilot symbols transmitted by the kth transmit antenna, N is the number of data and pilot symbols, $\mathbf{h}_{r,k}$ is an $N \times 1$ vector describing the channel time-frequency response between the kth transmit and rth receive antennas, $\mathbf{n}_r$ is an $N \times 1$ complex noise vector with independent Gaussian elements of zero mean and variance σ_n^2, N_t is the number of transmit antennas and N_r is the number of receive antennas.

It is assumed that the channel vector $\mathbf{h}_{r,k}$ is represented by an $M \times 1$ vector $\mathbf{a}_{r,k}$ of BEM coefficients,

$$\mathbf{h}_{r,k} = \mathbf{B}\mathbf{a}_{r,k}, \tag{5.2}$$

where $\mathbf{B}$ is an $N \times M$ matrix of basis functions with M being the number of basis functions. The two-dimensional (time and frequency) BEM matrix $\mathbf{B}$ is computed as

$$\mathbf{B} = \mathbf{B}_t \otimes \mathbf{B}_f, \tag{5.3}$$

where $\mathbf{B}_t$ is an $N_{OFDM} \times M_t$ matrix of basis functions in time, N_{OFDM} is the number of OFDM symbols, M_t is the number of basis functions in time, $\otimes$ denotes the Kronecker product, $\mathbf{B}_f$ is an $N_f \times M_f$ matrix of basis functions in frequency, N_f is the number of subcarriers, M_f is the number of basis functions in frequency, and $M = M_t M_f$. Different basis functions can be used to approximate the channel variations in frequency and time [2–10]. In our simulations, the discrete prolate spheroidal sequences [6,7] are used as the basis functions in frequency. In time, parabolic B-splines [8–10] are used.

5.3 Pilot-based BEM channel estimation

The pilot-based channel estimation is considered. With BEMs, the estimated channel vector $\hat{\mathbf{h}}_{r,k}$ is given by

$$\hat{\mathbf{h}}_{r,k} = \mathbf{B}\hat{\mathbf{a}}_{r,k}, \tag{5.4}$$

where the estimate $\hat{\mathbf{a}}_{r,k}$ of the expansion coefficients $\mathbf{a}_{r,k}$ is found as [18]

$$\hat{\mathbf{a}}_{r,k} = (\mathbf{B}^H \mathbf{S}_{n,k}^H \mathbf{S}_{n,k} \mathbf{B} + \mathbf{\Gamma}_{r,k})^{-1} \mathbf{B}^H \mathbf{S}_{n,k}^H \tilde{\mathbf{z}}_{r,k}, \tag{5.5}$$

$\mathbf{S}_{n,k}$ is an $N \times N$ diagonal matrix of pilot symbols transmitted by the kth transmit antenna with zeros at data locations, and it is obtained from $\mathbf{S}_k$ by selecting N_p pilot symbols, $\mathbf{\Gamma}_{r,k}$ is an $M \times M$ regularization matrix for the channel between the kth transmit antenna and the rth receive antenna and $\tilde{\mathbf{z}}_{r,k}$ is an $N \times 1$ vector of received pilots from the kth transmit antenna with zeros at data locations. In the LTE downlink [29], as shown in Figure 3.3, a single RE represents a single OFDM symbol in time and a single subcarrier in frequency. REs with pilot symbols from one transmit antenna are not overlapping with non-zero REs transmitted from the other transmit antennas [29]. Hence, the pilot symbols received from the kth transmit antenna can be recovered without the multi-antenna interference, and this justifies the estimation of $\mathbf{a}_{r,k}$ as in (5.5).

When $\mathbf{\Gamma}_{r,k} = \sigma_n^2 \mathbf{R}_c^{-1}$, where $\mathbf{R}_c = \mathbb{E}[\mathbf{a}_{r,k}\mathbf{a}_{r,k}^H]$, we arrive at the pilot-based LMMSE channel estimation. The $M \times M$ covariance matrix of the expansion coefficients $\mathbf{R}_c$ can be computed from [40]

$$\mathbf{R}_c = \mathbb{E}[\mathbf{a}_{r,k}\mathbf{a}_{r,k}^H] = (\mathbf{B}^H\mathbf{B})^{-1}\mathbf{B}^H \mathbf{\Upsilon} \mathbf{B} (\mathbf{B}^H\mathbf{B})^{-1}, \tag{5.6}$$

where $\mathbf{\Upsilon} = \mathbb{E}[\mathbf{h}_{r,k}\mathbf{h}_{r,k}^H]$ is the channel time-frequency auto-correlation matrix defined by the channel PDP and Doppler spectrum. The matrix $\mathbf{\Upsilon}$ is given by

$$\mathbf{\Upsilon} = \mathbf{\Upsilon}_t \otimes \mathbf{\Upsilon}_f, \tag{5.7}$$

where the channel auto-correlation in time $\mathbf{\Upsilon}_t$, as an example, is based on Jakes' model [64],

$$[\mathbf{\Upsilon}_t]_{p,q} = \rho_t((p-q)T_{OFDM}), \tag{5.8}$$

where

$$\rho_t(\tau) = J_0(2\pi f_d \tau), \quad p, q = 1, ..., N_{OFDM}, \tag{5.9}$$

$J_0(\cdot)$ denotes the zero order Bessel function of first kind, f_d is the Doppler frequency, τ is a delay and T_{OFDM} is the duration of a single OFDM symbol. The channel auto-correlation in frequency $\boldsymbol{\Upsilon}_f$ is given by [102]

$$[\boldsymbol{\Upsilon}_f]_{p,q} = \rho_f((p-q)\Delta f), \tag{5.10}$$

where

$$\rho_f(F) = \sum_{l=1}^{L} \sigma_l^2 e^{-2\pi j F \tau_l}, \quad p, q = 1, ..., N_f, \tag{5.11}$$

where σ_l^2 is the average power of the lth path, τ_l is the delay of the lth path, $l = 1, ..., L$, L is the number of paths and Δf is the frequency spacing between two consecutive sub-carriers (in the LTE downlink, Δf=15 kHz [29]). The powers σ_l^2 and delays τ_l define the channel PDP.

When $\boldsymbol{\Gamma}_{r,k} = \sigma_n^2 \mathbf{R}_{\xi}^{-1}$ and $\mathbf{R}_{\xi}$ is an $M \times M$ model (not true) covariance matrix defined by a model PDP and a model Doppler spectrum, we arrive at a model-based regularization. When $\boldsymbol{\Gamma}_{r,k} = \sigma_n^2 \mathbf{I}_M$ and $\mathbf{I}_M$ is an $M \times M$ identity matrix, we arrive at the channel estimation with the diagonal loading, which is a popular regularization technique [21,125,126]. It however cannot provide the channel estimation performance close to that with the LMMSE regularization.

5.4 Conventional Doppler frequency estimation

The time-frequency auto-correlation function is given by

$$\rho(\tau, F) = \mathbb{E}[h_{r,k}^{(u)} h_{r,k}^{(v)*}] = \rho_t(\tau)\rho_f(F), \tag{5.12}$$

where the positions of the two elements $h_{r,k}^{(u)}$ and $h_{r,k}^{(v)}$ are separated in time by τ and in frequency by F; $(\cdot)^*$ denotes the complex conjugate. In [22], Lin and Proakis proposed to estimate the Doppler frequency by fitting the auto-correlation of channel estimates using the optimization:

$$\hat{f}_d = \arg\min_{f_d} [J_0(2\pi f_d \tau) - \hat{\rho}_t(\tau)]^2, \tag{5.13}$$

where $\hat{\rho}_t(\tau)$ is an estimate of the channel time auto-correlation. In application to the LTE downlink scenarios, the channel time auto-correlation estimate can be obtained as

$$\hat{\rho}_t(\tau) = \frac{\hat{\rho}_1 + \hat{\rho}_2}{2}, \tag{5.14}$$

where

$$\hat{\rho}_1 = \frac{\Re(\tilde{\mathbf{h}}_1^T)\Re(\tilde{\mathbf{h}}_2)}{\sqrt{\Re(\mathbf{h}_{p1}^T)\Re(\tilde{\mathbf{h}}_1)}\sqrt{\Re(\tilde{\mathbf{h}}_2^T)\Re(\tilde{\mathbf{h}}_2)}}, \tag{5.15}$$

$$\hat{\rho}_2 = \frac{\Im(\tilde{\mathbf{h}}_1)^T\Im(\tilde{\mathbf{h}}_2)}{\sqrt{\Im(\tilde{\mathbf{h}}_1)^T\Im(\tilde{\mathbf{h}}_1)}\sqrt{\Im(\tilde{\mathbf{h}}_2)^T\Im(\tilde{\mathbf{h}}_2)}}, \tag{5.16}$$

$\Re[\cdot]$ and $\Im[\cdot]$ are the real and imaginary parts of a complex number, respectively, $\tilde{\mathbf{h}}_1$ is an $\frac{N_p}{2} \times 1$ vector of LS channel estimates obtained at pilot locations in slot 1 (see Figure 3.3) and $\tilde{\mathbf{h}}_2$ is an $\frac{N_p}{2} \times 1$ vector of LS channel estimates obtained at pilot locations in slot 2. The value of τ, in this case, is equal to $\tau = T_{slot}$, where T_{slot} is the slot duration (in the LTE downlink, $T_{slot} = 0.5$ms [29]). The LS channel estimate $\tilde{\mathbf{h}}_1$ for the first slot is given by

$$\tilde{h}_1(g) = \frac{\tilde{z}_r(g)}{\tilde{s}_k(g)}, \tag{5.17}$$

where $\tilde{z}_r(g)$ and $\tilde{s}_k(g)$ are elements of the received and transmitted pilot symbols, respectively, that correspond to the gth element of $\tilde{\mathbf{h}}_1$, $g = 1, ..., \frac{N_p}{2}$. The LS channel estimate $\tilde{\mathbf{h}}_2$ for the second slot can be obtained in the same manner as in (5.17).

The optimization problem in (5.13) provides a biased solution and it can be modified as suggested in [106] by introducing a correction term, taking into account the SNR:

$$\hat{f}_d = \arg\min_{f_d} \Big[\frac{J_0(2\pi f_d \tau)}{1 + 1/SNR} - \hat{\rho}_t(\tau)\Big]^2. \tag{5.18}$$

The solution to the optimization problem in (5.18) is used as the conventional Doppler frequency estimate.

The conventional Doppler frequency estimator based on (5.18) corresponds to an environment with Jakes' Doppler spectrum. As another example, the time auto-correlation

function can be considered [127]

$$\rho_t(\tau) = \text{sinc}(2f_d\tau). \tag{5.19}$$

The auto-correlation function in (5.19) corresponds to an environment with a Doppler spectrum that is uniform over the frequency interval $[-f_d, f_d]$. In the following sections, the performance of the conventional and proposed estimators designed based on a Doppler model that is different from the true Doppler model is investigated.

5.5 Joint Doppler-delay spread and channel estimation

In the proposed estimator, regularization matrices for a two-dimensional set of Doppler frequencies and delay spreads are precomputed and stored. In this set, the estimator finds a regularization matrix that minimizes the GCV. The Doppler frequency and delay spread defining this matrix are considered as their estimates. The exhaustive search over all regularization matrices in the set will require a high complexity, especially for a high number of Doppler frequencies and delay spreads. To reduce the complexity, the estimator uses the dichotomous search [122].

In the frequency domain, the model-based regularization matrices are defined by a set of Doppler frequencies :

$$f_d \in \{f_{d,1}, ..., f_{d,j}, ..., f_{d,P}\}, \quad j = 1, ..., P, \tag{5.20}$$

where $f_{d,j+1} = f_{d,j} + \Delta f_d$ and Δf_d defines the Doppler frequency resolution. In time, these matrices are defined by a set of root mean squares (rms) delay spreads :

$$\tau_{rms} \in \{\tau_{rms,1}, ..., \tau_{rms,i}, ..., \tau_{rms,Q}\}, \quad i = 1, ..., Q, \tag{5.21}$$

where $\tau_{rms,i+1} = \tau_{rms,i} + \Delta\tau$ and $\Delta\tau$ defines the rms delay spread resolution.

The $P \times Q$ set of Doppler-delay regularization matrices is denoted as $\{\sigma_n^2 \mathbf{R}_{j,i}^{-1}\}_{(j=1,i=1)}^{(P,Q)}$. The covariance matrix of expansion coefficients $\mathbf{R}_{j,i}$ is computed using (5.6) and (5.7), where the matrix $\boldsymbol{\Upsilon}_t$ is computed using (5.9) for every Doppler frequency in (5.20), while the matrix

$\boldsymbol{\Upsilon}_f$ is computed for every rms delay spread in (5.21). For modelling PDPs, the exponentially decaying model is used, for N_m multipath components, as the following [128]:

$$\theta(\tau_k) = e^{-\tau_k/\tau_{rms}}, \tag{5.22}$$

where τ_k is a random delay and the probability density function of the delays τ_k is given by

$$f_{\tau_k}(\tau_k) = \begin{cases} 1/T_d & \text{if } \tau_k \in [0, T_d] \\ 0 & \text{otherwise} \end{cases}, \tag{5.23}$$

where T_d is set to be greater than the expected maximum delay spread. The frequency auto-correlation for this model can be obtained in a closed form as [128]

$$[\boldsymbol{\Upsilon}_f]_{p,q} = \frac{1 - e^{-T_d\left(\frac{1}{\tau_{rms}} + 2\pi j(p-q)\Delta f\right)}}{\left(1 - e^{-(\frac{T_d}{\tau_{rms}})}\right)\left(1 + 2\pi j(p-q)\Delta f \tau_{rms}\right)}, \tag{5.24}$$

where (5.24) corresponds to a truncated exponentially decaying PDP in the range $[0, T_d]$.

The optimal regularization matrix of expansion coefficients from the set $\{\sigma_n^2 \mathbf{R}_{j,i}^{-1}\}_{(j=1,i=1)}^{(P,Q)}$ is found in the proposed estimator by using the GCV method [103, 121]. The (j,i)th cross-validation $V_{r,k}$ is computed for the channel between the kth transmit and rth receive antennas [103, 121]:

$$V_{r,k}(j,i) = \frac{||\tilde{\mathbf{z}}_{r,k} - \mathbf{G}_k^{(j,i)} \tilde{\mathbf{z}}_{r,k}||^2}{(N_p - \alpha \text{tr}\{\mathbf{G}_k^{(j,i)}\})^2}, \tag{5.25}$$

$$\mathbf{G}_k^{(j,i)} = \mathbf{S}_{n,k}\mathbf{B}(\mathbf{B}^H \mathbf{S}_{n,k}^H \mathbf{S}_{n,k}\mathbf{B} + \sigma_n^2 \mathbf{R}_{j,i}^{-1})^{-1}\mathbf{B}^H \mathbf{S}_{n,k}^H, \tag{5.26}$$

where α is an adjusted parameter, $1 \leq \alpha \leq 2$. The regularization matrix that provides the minimum of $V_{r,k}(j,i)$ is selected for the channel estimation,

$$\{j, i\} = \arg\min_{p,q} V_{r,k}(p,q), \tag{5.27}$$

where the optimal regularization matrix is $\boldsymbol{\Gamma}_{r,k} = \sigma_n^2 \mathbf{R}_{j,i}^{-1}$, and its corresponding Doppler frequency and delay spread are considered as estimates of these parameters.

The search for the optimal solution through the computation of the GCV for all matrices in the set $\{\sigma_n^2 \mathbf{R}_{j,i}^{-1}\}_{(j=1,i=1)}^{(P,Q)}$ using an exhaustive search results in high complexity. To reduce

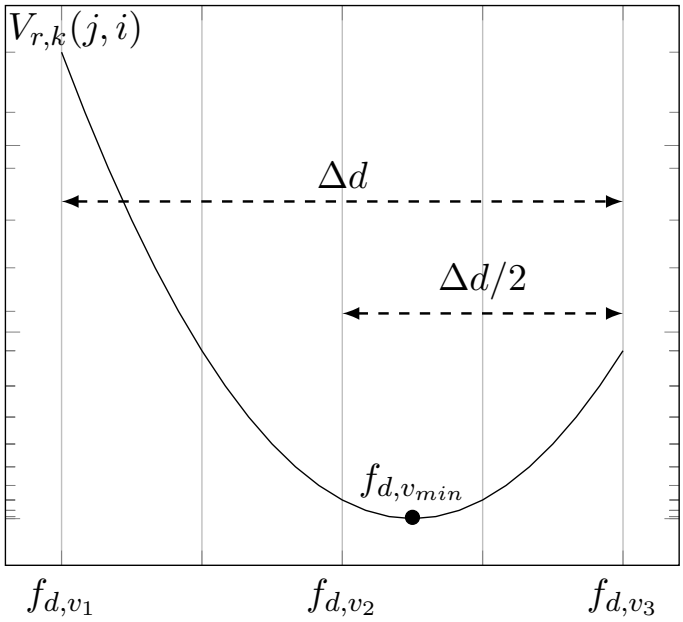

Figure 5.1: The dichotomous search.

the complexity, the dichotomous search is used in the proposed estimator. The GCV with the dichotomous search can be performed jointly on the two-dimensional set of Doppler frequencies and delay spreads or independently on one of these sets. In this chapter, the search is performed on the set of Doppler frequencies. Below, the dichotomous search is introduced and its use with the GCV method is explained.

Figure 5.1 shows an example of using the dichotomous search to find a minimum of $V_{r,k}(j,i)$ for a set of Doppler frequencies f_d and a known PDP. At the first iteration, the values f_{d,v_1}, f_{d,v_2} and f_{d,v_3} are available, v_1, v_2 and v_3 are indices of Doppler frequencies, $V_{r,k}(j = v_1, i) > V_{r,k}(j = v_2, i)$ and $V_{r,k}(j = v_3, i) > V_{r,k}(j = v_2, i)$. The dichotomous search finds the minimum of $V_{r,k}(j,i)$ from two samples f_{d,v_1} and f_{d,v_3}. If $V_{r,k}(j = v_1, i) < V_{r,k}(j = v_3, i)$, the search at the next iteration is performed between points v_1 and v_2, thus reducing the search size by half. If $V_{r,k}(j = v_1, i) > V_{r,k}(j = v_3, i)$, the search is performed between v_2 and v_3; point v_2 becomes v_1 and the function $V_{r,k}(j,i)$ is computed at a new point $v_2 = (v_1 + v_3)/2$. This procedure is repeated D_{it} times, reducing the search area by half at every iteration. D_{it} is found by increasing the number of iterations until we arrive at $v_3 - v_1 = 1$ (last two elements to be compared). Note that the problem in Figure 5.1 represents a convex optimization problem. However, the optimization problem in reality is non-convex and this may cause a wrong selection of the search area, especially at the first iteration. Therefore, the dichotomous search is modified only at the first iteration by adding

more samples between v_1 and v_3 to guarantee more accurate selection of the initial search area.

In the proposed estimator, the GCV with the dichotomous iterations is performed over Doppler frequencies. At the first iteration, N_s Doppler frequencies $\{f_{d,1}, ..., f_{d,n}, ..., f_{d,N_s}\}$ are selected from (5.20), where $f_{d,1} = f_{d,j=1}$, $f_{d,N_s} = f_{d,j=P}$ and $n = 1, ..., N_s$. Note that the higher N_s, the better the accuracy in the selection of the initial search area. For every Doppler frequency $f_{d,n}$, the GCV is computed for all Q delay spreads in (5.21) and thus an $N_s \times Q$ set of $V_{r,k}(n, i)$ values is obtained. Then, the minimum $V_{r,k}(n, i)$ over i is found for every Doppler frequency f_{d,j_n} as the following

$$i_n = \arg \min_{i=1:Q} V_{r,k}(n, i), \quad n = 1, ..., N_s. \tag{5.28}$$

This results in N_s values of $V_{r,k}(n, i_n)$. The minimum of $V_{r,k}(n, i_n)$ is found and its corresponding delay spread is selected as the estimated delay spread. Note that the optimal delay spread from the set in (5.21) can be obtained with already a high accuracy at the first iteration (see Section 5.8) without necessarily having the optimal Doppler frequency, which is only found at the final iteration. For $D_{it} > 1$, the search is performed using the classical dichotomous search as the optimization problem at this stage is almost a convex problem (see Figure 5.1). At the output of the first iteration, v_1 and v_3 are obtained as the following:

$$v_1 = \begin{cases} 1 & \text{if} \quad n = 1, \\ N_s - 1 & \text{if} \quad n = N_s, \\ n - 1 & \text{if} \quad V_{r,k}(n-1, i_n) < V_{r,k}(n+1, i_n), \quad n \neq 1 \quad \text{and} \quad n \neq N_s, \\ n & \text{if} \quad V_{r,k}(n-1, i_n) > V_{r,k}(n+1, i_n), \quad n \neq 1 \quad \text{and} \quad n \neq N_s, \end{cases} \tag{5.29}$$

$$v_3 = \begin{cases} 2 & \text{if} \quad n = 1, \\ N_s & \text{if} \quad n = N_s, \\ n & \text{if} \quad V_{r,k}(n-1, i_n) < V_{r,k}(n+1, i_n), \quad n \neq 1 \quad \text{and} \quad n \neq N_s, \\ n + 1 & \text{if} \quad V_{r,k}(n-1, i_n) > V_{r,k}(n+1, i_n), \quad n \neq 1 \quad \text{and} \quad n \neq N_s. \end{cases} \tag{5.30}$$

At iterations $D_{it} > 1$, the GCV is only computed at f_{d,v_2} with the estimated delay spread obtained from the first iteration. The indices v_1 and v_3 at the output of the second iteration

and subsequent iterations, are obtained as the following:

$$v_1 = \begin{cases} v_1 & \text{if} \quad V_{r,k}(v_1, i_n) < V_{r,k}(v_3, i_n), \\ v_2 & \text{if} \quad V_{r,k}(v_1, i_n) > V_{r,k}(v_3, i_n), \end{cases} \tag{5.31}$$

$$v_3 = \begin{cases} v_2 & \text{if} \quad V_{r,k}(v_1, i_n) < V_{r,k}(v_3, i_n), \\ v_3 & \text{if} \quad V_{r,k}(v_1, i_n) > V_{r,k}(v_3, i_n), \end{cases} \tag{5.32}$$

where v_2 is the half distance between v_1 and v_3, $v_2 = \frac{v_1+v_3}{2}$. At the final iteration, the optimal regularization matrix and the estimate of Doppler frequency are given by

$$\mathbf{\Gamma}_{r,k} = \begin{cases} \{\sigma_n^2 \mathbf{R}_{j,i}^{-1}\}_{j=v_1,i_n} & \text{if} \quad V_{r,k}(v_1, i_n) < V_{r,k}(v_3, i_n), \\ \{\sigma_n^2 \mathbf{R}_{j,i}^{-1}\}_{j=v_3,i_n} & \text{if} \quad V_{r,k}(v_1, i_n) > V_{r,k}(v_3, i_n), \end{cases} \tag{5.33}$$

$$\hat{f}_d = \begin{cases} f_{d,v_1} & \text{if} \quad V_{r,k}(v_1, i_n) < V_{r,k}(v_3, i_n), \\ f_{d,v_3} & \text{if} \quad V_{r,k}(v_1, i_n) > V_{r,k}(v_3, i_n). \end{cases} \tag{5.34}$$

The adaptive regularization matrix obtained in (5.33) is used for the pilot-based channel estimation in (5.5).

5.6 Complexity reduction

When the GCV method is applied using the two-dimensional regularization set, PQ GCV computations are necessary to find the minimum of the cross-validation parameter. For high P and Q, this results in a high computational load. To reduce the complexity, the GCV method is implemented using the dichotomous search. Using N_s samples at the first iteration and D_{it} iterations in the GCV with the dichotomous search, the number of GCV computations is reduced from PQ to $N_sQ + (D_{it} - 1)$. For example, for $P = 230$, $Q = 20$, $N_s = 11$ and $D_{it} = 6$, the number of GCV computations is reduced from $PQ = 4600$ to $N_sQ + (D_{it} - 1) = 225$, and thus, for this example, the complexity is reduced by approximately 20.4 times.

The resolution of the joint estimator depends on the selected values Δf_d and $\Delta\tau$. The lower Δf_d and $\Delta\tau$, the better the estimation accuracy, the larger the set of regularization ma-

trices and higher computational load. Implementing the GCV method with the dichotomous search provides more freedom in selection of Δf_d and $\Delta\tau$ to achieve a desired estimation performance.

For storing the precomputed regularization matrices, a large memory space may be required. To reduce the memory, the following properties of the BEM matrix $\mathbf{B}$ and channel covariance $\boldsymbol{\Upsilon}$ are used. Let $\mathbf{B}^+ = (\mathbf{B}^H\mathbf{B})^{-1}\mathbf{B}^H$, then (5.6) can be rewritten as

$$\mathbf{R}_c = \mathbf{B}^+\boldsymbol{\Upsilon}(\mathbf{B}^+)^H. \tag{5.35}$$

Using $\mathbf{B} = \mathbf{B}_t \otimes \mathbf{B}_f$, $\boldsymbol{\Upsilon} = \boldsymbol{\Upsilon}_t \otimes \boldsymbol{\Upsilon}_f$ and the property of the Kronecker product, we have $\mathbf{B}^+ = \mathbf{B}_t^+ \otimes \mathbf{B}_f^+$, and (5.35) becomes [129]

$$\begin{aligned}
\mathbf{R}_c &= [\mathbf{B}_t^+ \otimes \mathbf{B}_f^+][\boldsymbol{\Upsilon}_t \otimes \boldsymbol{\Upsilon}_f][\mathbf{B}_t^+ \otimes \mathbf{B}_f^+]^H \\
&= [\mathbf{B}_t^+\boldsymbol{\Upsilon}_t \otimes \mathbf{B}_f^+\boldsymbol{\Upsilon}_f][(\mathbf{B}_t^+)^H \otimes (\mathbf{B}_f^+)^H] \\
&= (\mathbf{B}_t^+\boldsymbol{\Upsilon}_t(\mathbf{B}_t^+)^H) \otimes (\mathbf{B}_f^+\boldsymbol{\Upsilon}_f(\mathbf{B}_f^+)^H) \\
&= \mathbf{R}_t \otimes \mathbf{R}_f.
\end{aligned} \tag{5.36}$$

The inverse of (5.36) is then given by

$$\mathbf{R}_c^{-1} = \mathbf{R}_t^{-1} \otimes \mathbf{R}_f^{-1}, \tag{5.37}$$

where $\mathbf{R}_t = \mathbf{B}_t^+\boldsymbol{\Upsilon}_t(\mathbf{B}_t^+)^H$ is an $M_t \times M_t$ time covariance matrix of expansion coefficients, $\mathbf{B}_t^+ = (\mathbf{B}_t^H\mathbf{B}_t)^{-1}\mathbf{B}_t^H$, and $\mathbf{R}_f = \mathbf{B}_f^+\boldsymbol{\Upsilon}_f(\mathbf{B}_f^+)^H$ is an $M_f \times M_f$ frequency covariance matrix of expansion coefficients, $\mathbf{B}_f^+ = (\mathbf{B}_f^H\mathbf{B}_f)^{-1}\mathbf{B}_f^H$. Using (5.37), instead of storing PQ regularization matrices $\{\sigma_n^2\mathbf{R}_{j,i}^{-1}\}_{(j=1,i=1)}^{(P,Q)}$, each of size $M_tM_f \times M_tM_f$, we only store P inverse time covariance matrices, each of size $M_t \times M_t$ and Q inverse frequency covariance matrices, each of size $M_f \times M_f$. As a result, the memory is reduced from PQM^2 to $PM_t^2 + QM_f^2$. For example, if $P = 230$, $Q = 20$, $M_t = 4$ and $M_f = 11$, as in our simulation scenarios, the memory is reduced from $PQM^2 \approx 8.9 \times 10^6$ elements to $PM_t^2 + QM_f^2 \approx 6.1 \times 10^3$ elements. In this example, the memory is reduced by about 1.5×10^3 times, which is a very significant reduction in the memory size.

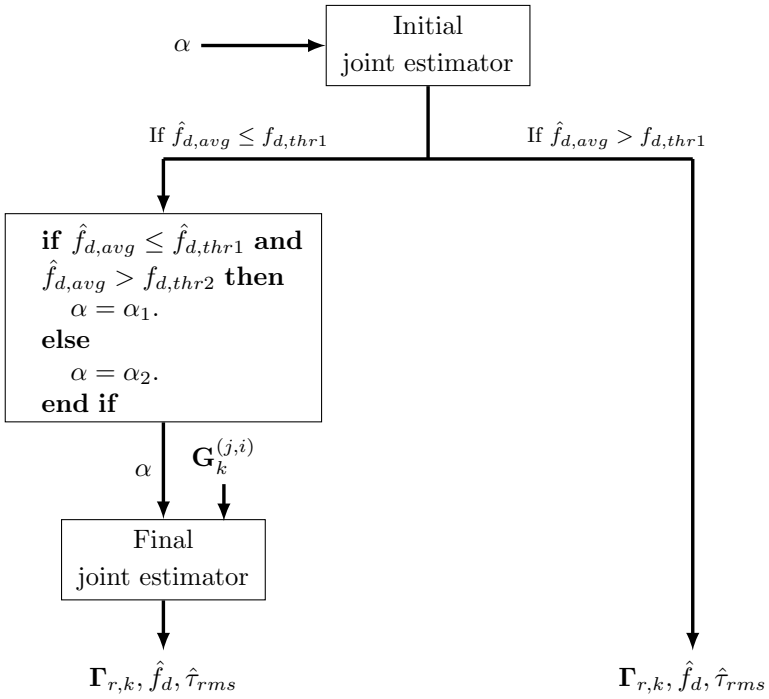

Figure 5.2: Re-adjustable joint estimator.

5.7 Re-adjustable joint Doppler-delay spread and channel estimation

The constant α in (5.25), providing the best Doppler-delay spread and channel estimation performance can be different over different range of Doppler frequencies (as will be shown in Section 5.8). Therefore, the division of Doppler frequencies into low, medium and high range and apply different α at each Doppler frequency range to improve the estimation performance is proposed. To do this, an initial estimate of the Doppler frequency is required. This can be achieved first applying the joint estimator as described in Section 5.5 with an initial α over all Doppler frequencies. Then, the initial Doppler frequency estimate is used to set the value of α.

Figure. 5.2 shows the block diagram of the proposed re-adjustable joint estimator. Initial joint estimator is designed as described in Section 5.5. Let $\hat{f}_{d,avg}$ be the estimated Doppler frequency in the initial joint estimator, averaged over all multiple $N_t N_r$ channels in the MIMO system, and $f_{d,thr1}$ and $f_{d,thr2}$ are Doppler frequency thresholds defining the low, medium and high Doppler frequencies. If $\hat{f}_{d,avg} > f_{d,thr1}$, then the estimated Doppler frequency is in the high frequency range and there is no need for re-adjustment (as will be shown in Section 5.8). If $\hat{f}_{d,avg} \leq f_{d,thr1}$, then α is re-adjusted for the final joint estimator (which is designed as

described in Section 5.5). If $f_{d,avg} \leq f_{d,thr1}$ and $\hat{f}_{d,avg} > f_{d,thr2}$, α is re-adjusted as $\alpha = \alpha_1$ for the medium frequency range. If $\hat{f}_{d,avg} \leq f_{d,thr2}$, the estimated Doppler frequency is in the low frequency range and therefore α is re-adjusted as $\alpha = \alpha_2$. In the proposed re-adjustable estimator, in the final joint estimator, $\mathbf{G}_k^{(j,i)}$ is not computed. This is because it has already been saved from the initial joint estimator. In the following section, an example to show how the values of $f_{d,thr1}$, $f_{d,thr2}$ and α are found is presented for the re-adjustable estimator.

5.8 Numerical results

A single-user MIMO-OFDM system is considered in the LTE downlink scenarios [29], with two transmit antennas at the base station and two receive antennas at the user side. The MIMO system is in a spatial multiplexing transmission mode [29]. Jakes' channel with ETU or EVA [98] PDP is used; such PDPs correspond to high and medium delay spreads, respectively, in comparison to the length of the cyclic prefix.

A transport block containing one sub-frame (see Figure 3.3) with 36 sub-carriers in frequency and 14 OFDM symbols in time is transmitted (it carries $N = 14 \times 36 = 504$ symbols of which $N_p = 24$ are pilot symbols). The number of basis functions in time is $M_t = 4$ and in frequency $M_f = 11$ [23]. The modulation scheme is 16-QAM. The pilot symbols are generated using the Zadoff-Chu sequences [29].

The number of pilots used is $N_p = 24$ while the total number of basis functions is $M = M_t M_f = 4 \times 11 = 44$. Thus, the number of parameters to estimate is higher than the number of available measurements. Hence, this problem is ill conditioned. For example, this means that the LS BEM channel estimation (obtained when $\mathbf{\Gamma}_{r,k}$ is an $M \times M$ zero matrix in (5.5)) could not provide reliable results. The only way around this is the channel estimation with regularization. Therefore, the regularization is extremely important. Also, it motivates us to compare the adaptive regularization (obtained in the proposed estimator without knowledge of the channel statistics) with the diagonal loading regularization and the LMMSE regularization.

In the dichotomous search, the number of iterations is set to $D_{it} = 6$ and number of samples at the first iteration $N_s = 11$. The following Doppler frequencies and delay spreads

are considered:

$$f_d \in \{1, 3, 5, 7, 9, ..., 459\} \text{ Hz}, \tag{5.38}$$

$$\tau_{rms} \in \left\{0.2, 0.4, ..., 4\right\}\mu s, \tag{5.39}$$

where $\Delta f_d = 2$ Hz and $\Delta\tau = 0.2\mu s$. T_d is set to 1.3 the length of the cyclic prefix, i.e., $T_d = 1.3 \times 4.69\mu s \approx 6.1\mu s$. The reason for this is that the delay spread of some channels (such as the ETU channel) may exceed the cyclic prefix duration, and thus T_d must be large enough to take this into account.

In the simulations, the joint estimator using the GCV method with the exhaustive search is referred to as GCV-E, while the GCV with the dichotomous search is referred to as GCV-D. Two sets of scenarios are considered: (i) known PDP and (ii) unknown PDP. The investigation of the scenarios with known PDP can help us find the best performance achieved when the Doppler frequency and channel are jointly estimated. Such estimation performance is then compared with that of the estimation with unknown PDP.

5.8.1 PDP is known

In this scenario, the channel delay spread is perfectly known and the joint estimator is simplified to a one dimensional search over Doppler frequencies only. First, the best value of parameter α is to be found. Figure 5.3 shows the performance of Doppler frequency estimation for different α. In simulation, the mean of the Doppler frequency estimates is found as

$$\bar{f}_d = \frac{1}{N_{trial}} \sum_{m=1}^{N_{trial}} \hat{f}_d^{(m)}, \tag{5.40}$$

where $\hat{f}_d^{(m)}$ is the Doppler frequency estimate in the mth trial; averaged over the $N_t N_r$ channels in the MIMO system. For the simulation trials, N_{trial} is set to $N_{trial} = 10^3$ trials. In Figure 5.3, as α increases, the estimation accuracy improves at low Doppler frequencies. On the other hand, the higher the value of α, the more degraded the Doppler frequency estimation is at high Doppler frequencies. Overall, $\alpha = 1.1$ can provide a trade-off in the estimation performance for the ETU and EVA channels over all Doppler frequencies. Therefore, $\alpha = 1.1$ is set for the simulation.

Figure 5.4 compares the performance of the proposed Doppler frequency estimator with

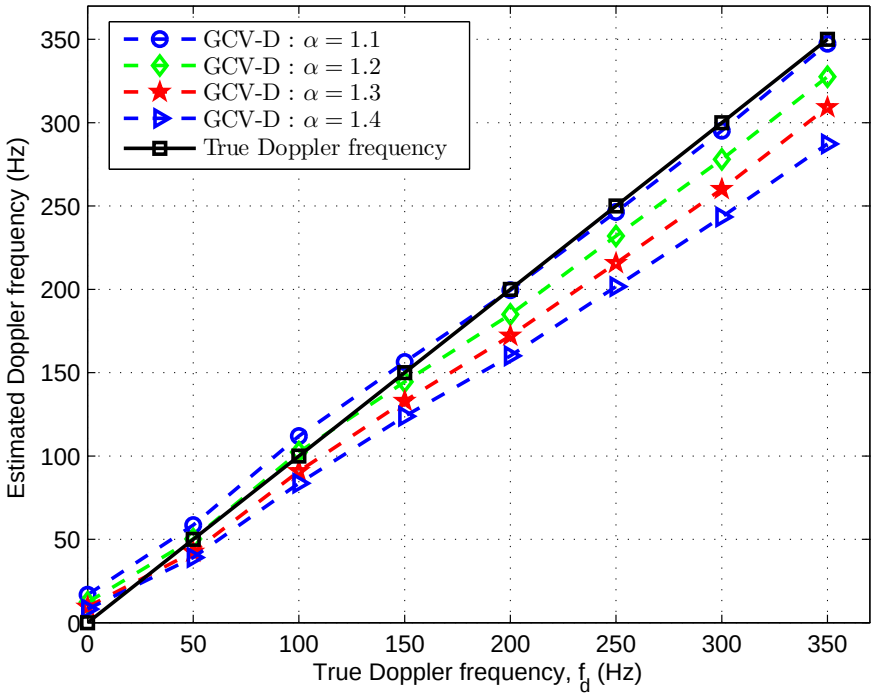

(a)

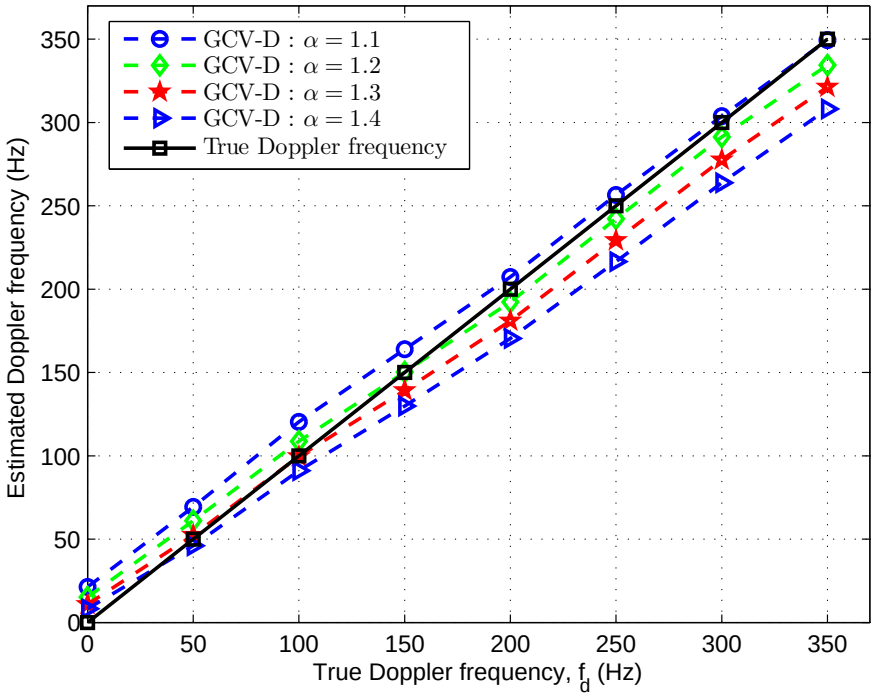

(b)

Figure 5.3: Performance of Doppler frequency estimation of the proposed estimator in a scenario with known PDP; (a) ETU channel; (b) EVA channel. SNR=15 dB.

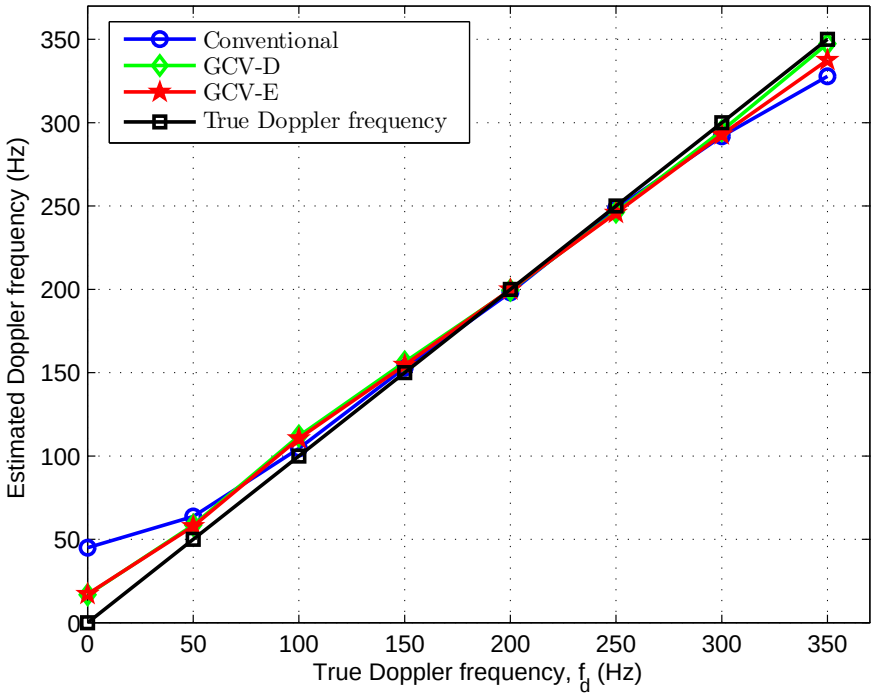

(a)

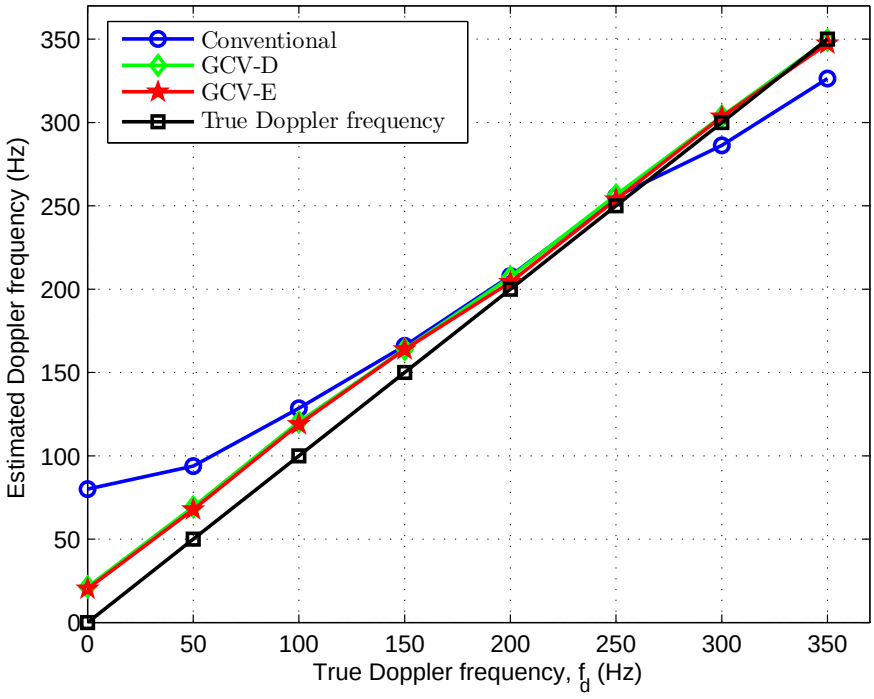

(b)

Figure 5.4: Performance of Doppler frequency estimation of the conventional estimator and the proposed estimator in (a) ETU and (b) EVA channels. SNR=15 dB and $\alpha = 1.1$.

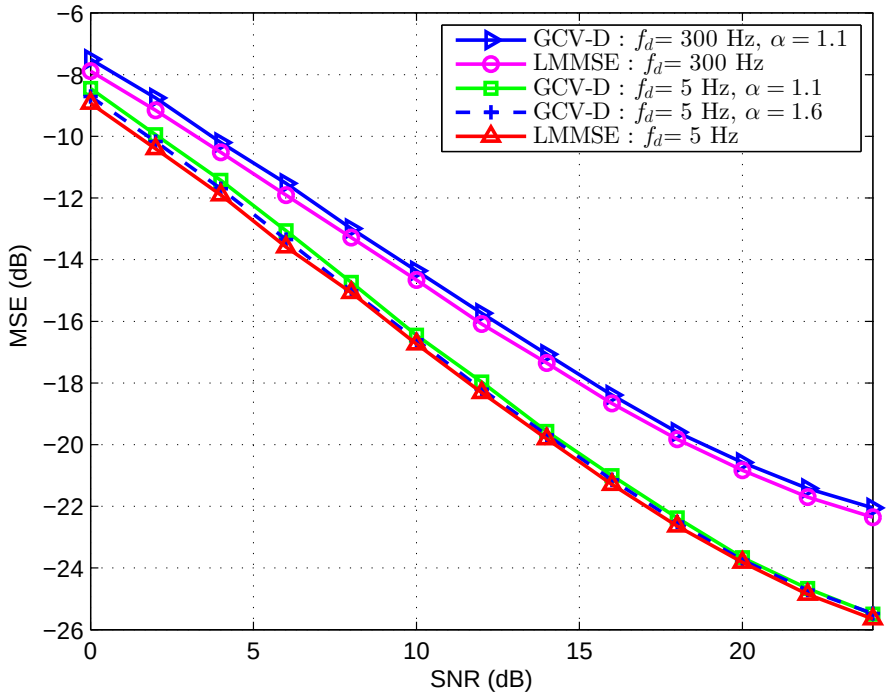

(a)

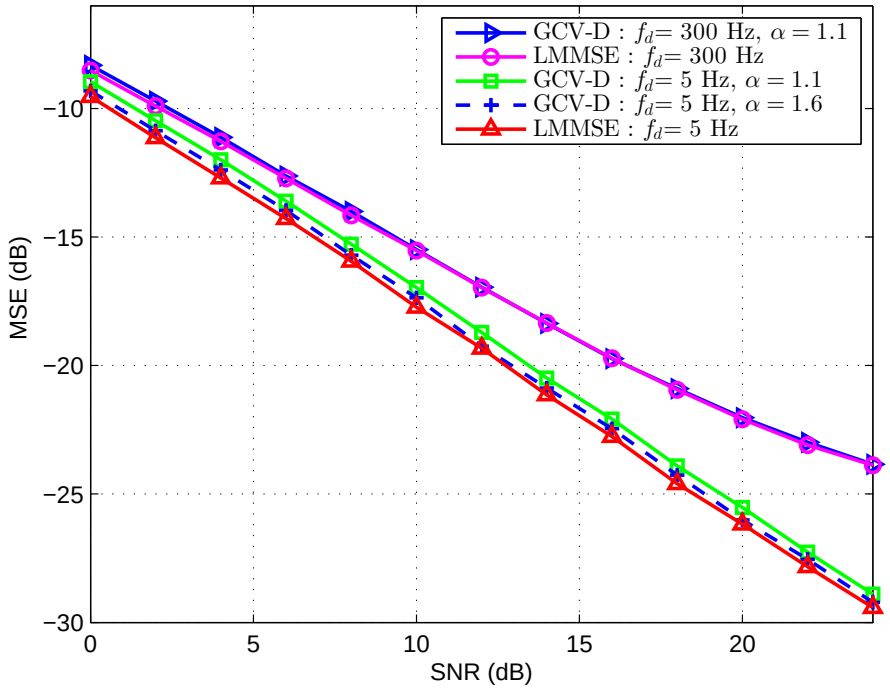

(b)

Figure 5.5: MSE performance of the proposed channel estimator in scenarios with known PDP in (a) ETU and (b) EVA channels.

the exhaustive search (GCV-E) and dichotomous search (GCV-D) with that of the conventional estimator. The GCV with dichotomous search has almost the same performance as that of the GCV with exhaustive search. Thus, the dichotomous search provides reduction in the estimator complexity without loss in the performance. It is also seen that the proposed estimator outperforms the conventional estimator, especially at low Doppler frequencies.

Figure 5.5 shows the MSE performance of channel estimation. The frequency f_d denotes the true Doppler frequency. The MSE is defined as

$$\mathrm{MSE_h} = \frac{\mathrm{tr}\{\mathbb{E}[(\mathbf{h}_{r,k} - \hat{\mathbf{h}}_{r,k})(\mathbf{h}_{r,k} - \hat{\mathbf{h}}_{r,k})^H]\}}{\mathrm{tr}\{\mathbb{E}[\mathbf{h}_{r,k}\mathbf{h}_{r,k}^H]\}}. \tag{5.41}$$

In simulation, this is estimated as

$$\widehat{\mathrm{MSE}}_\mathrm{h} = \frac{\sum_{m=1}^{N_{trial}} \sum_{r=1}^{N_r} \sum_{k=1}^{N_t} ||\mathbf{h}_{r,k} - \hat{\mathbf{h}}_{r,k}||^2}{\sum_{m=1}^{N_{trial}} \sum_{r=1}^{N_r} \sum_{k=1}^{N_t} ||\mathbf{h}_{r,k}||^2}, \tag{5.42}$$

where $\hat{\mathbf{h}}_{r,k}$ is the estimated frequency channel response. As shown in Figure 5.5, the MSE performance of the channel estimator is very close to that of the LMMSE channel estimator (i.e., with knowledge of the true Doppler frequency and true channel PDP).

5.8.2 PDP is unknown

In this scenario, the proposed technique estimates the Doppler-delay spread and channel as described in Section 5.5. First, the effect of unknown PDP on the performance of Doppler frequency estimation is investigated. In Figure 5.6, it can be seen that the Doppler frequency estimates without PDP knowledge are almost as accurate as in the case of known PDP.

Figure 5.7 compares the performance of the proposed delay spread estimation with that of the theoretical rms delay spread. The rms delay spread of a given PDP is computed as [82, 130]

$$\tau_{rms} = \sqrt{\bar{\tau^2} - (\bar{\tau})^2}, \tag{5.43}$$

where

$$\bar{\tau^2} = \frac{\sum_l \tau_l^2 \sigma_l^2}{\sum_l \sigma_l^2}, \tag{5.44}$$

$$\bar{\tau} = \frac{\sum_l \tau_l \sigma_l^2}{\sum_l \sigma_l^2}. \tag{5.45}$$

In simulation, the mean of the rms delay spread estimates is found as

$$\hat{\tau}_{rms} = \frac{1}{N_{trial}} \sum_{m=1}^{N_{trial}} \hat{\tau}_{rms}^{(m)}, \tag{5.46}$$

where $\hat{\tau}_{rms}^{(m)}$ is the rms delay spread estimate in the mth trial; averaged over the $N_t N_r$ channels in the MIMO system. It can be seen from Figure 5.7 that the delay spread estimate at the first iteration $D_{it} = 1$ is almost as accurate as that obtained from the final iteration $D_{it} = 6$ (over all Doppler frequencies). In the ETU channel, the estimated delay spread is around $19 \sim 24\%$ greater than the theoretical delay spread at $f_d \in [50, 350]$ Hz. At $f_d \in [0, 50)$ Hz, $\hat{\tau}_{rms}$ is about $24 \sim 32\%$ greater than the theoretical values. In the EVA channel, the estimated delay spread is about $12 \sim 22\%$ greater than the theoretical values at $f_d \in [50, 350]$ Hz and $22 \sim 33\%$ at $f_d \in [0, 50)$ Hz. This shows that the proposed estimator provides good estimates of the delay spread, especially at medium to high Doppler frequencies.

Now, the performance of the conventional and proposed estimators when the Doppler model used in designing the estimators is different from the true Doppler model is compared. The *sinc* auto-correlation function in (5.19) is used in designing the estimators (which corresponds to uniform Doppler model). The estimation performance using the uniform Doppler model is investigated in Jakes' channel. The value $\alpha = 1.3$ is used for the proposed estimator (see Appendix A for more details) when using (5.19) for computing $\boldsymbol{\Upsilon}_t$. In Figure 5.8, it can be seen that the conventional Doppler frequency estimator with the *sinc* time auto-correlation function degrades due to the Doppler modelling errors. In comparison, the difference in the performance of the proposed joint estimator when using Jakes' or the *sinc* time auto-correlation functions in designing the estimator is very small. This shows that the proposed estimator is robust to the choice of the Doppler model.

Figure 5.9 shows the MSE performance of the channel estimator using different regularization schemes. The channel estimator with the diagonal loading is inferior to the channel estimator with the adaptive regularization. It can be also seen that the proposed channel estimator without knowledge of PDP provides only slightly degraded performance in comparison to the proposed estimator with known PDP. Overall, the performance of the channel estimator with the adaptive regularization is close to that of the LMMSE channel estimator (with perfect knowledge of channel statistics). When using Jakes' or *sinc* functions in the

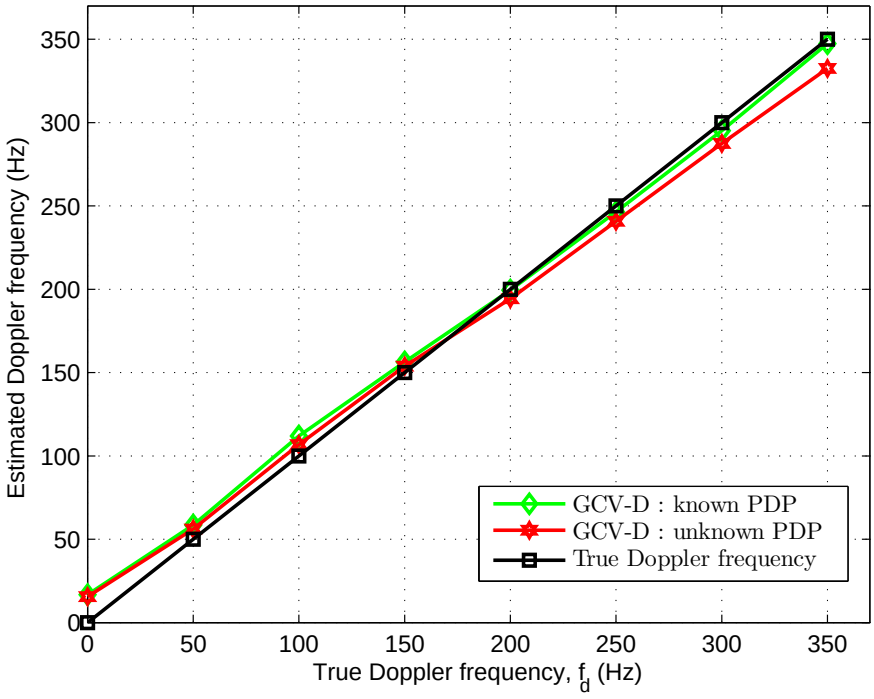

(a)

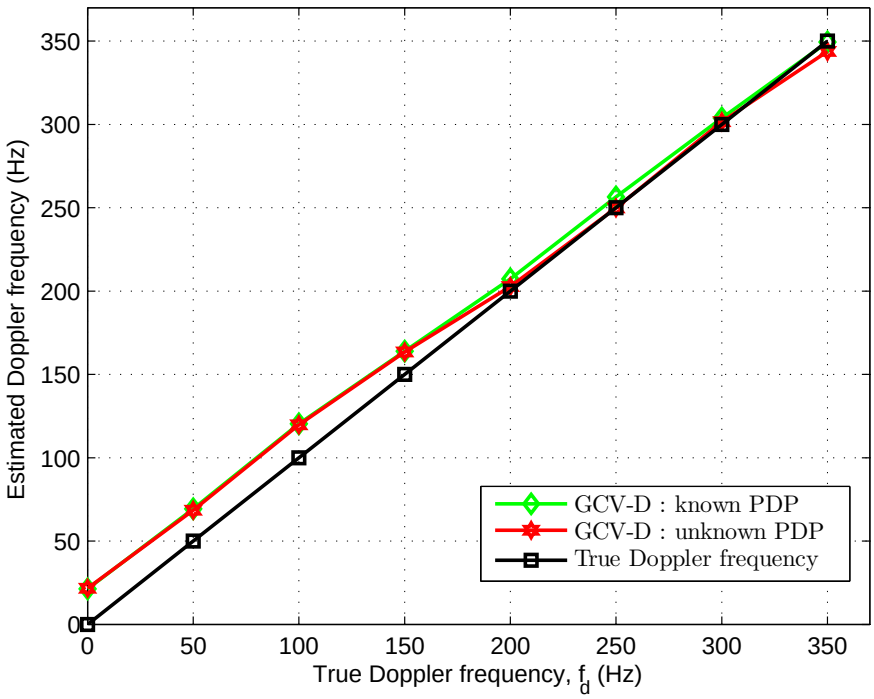

(b)

Figure 5.6: Performance of Doppler frequency estimation of the the proposed estimator in scenarios with known and unknown PDP; (a) ETU channel; (b) EVA channel. SNR=15 dB and $\alpha = 1.1$.

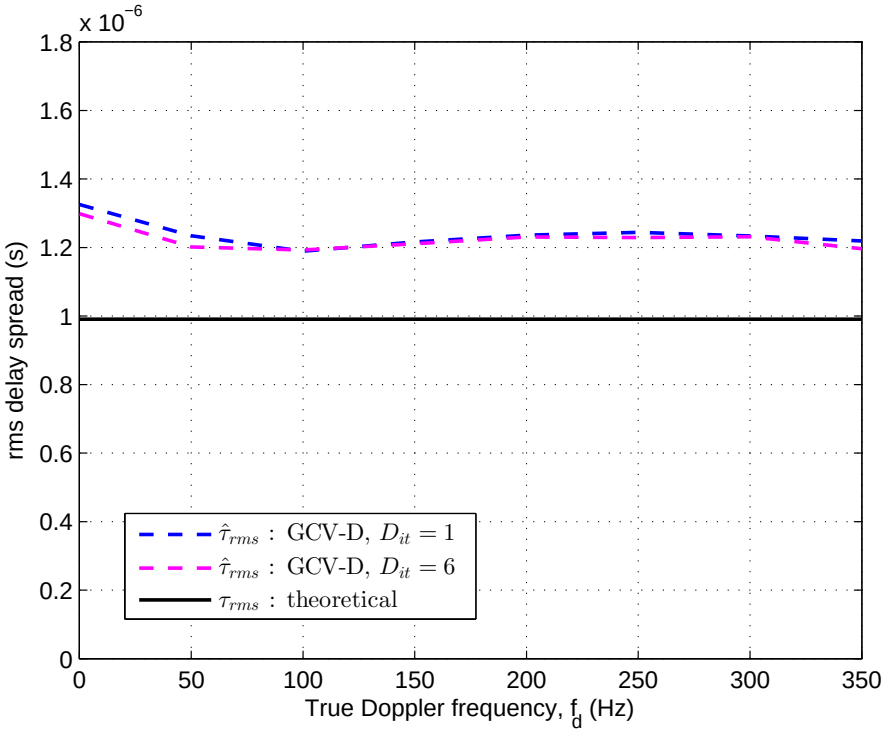

(a)

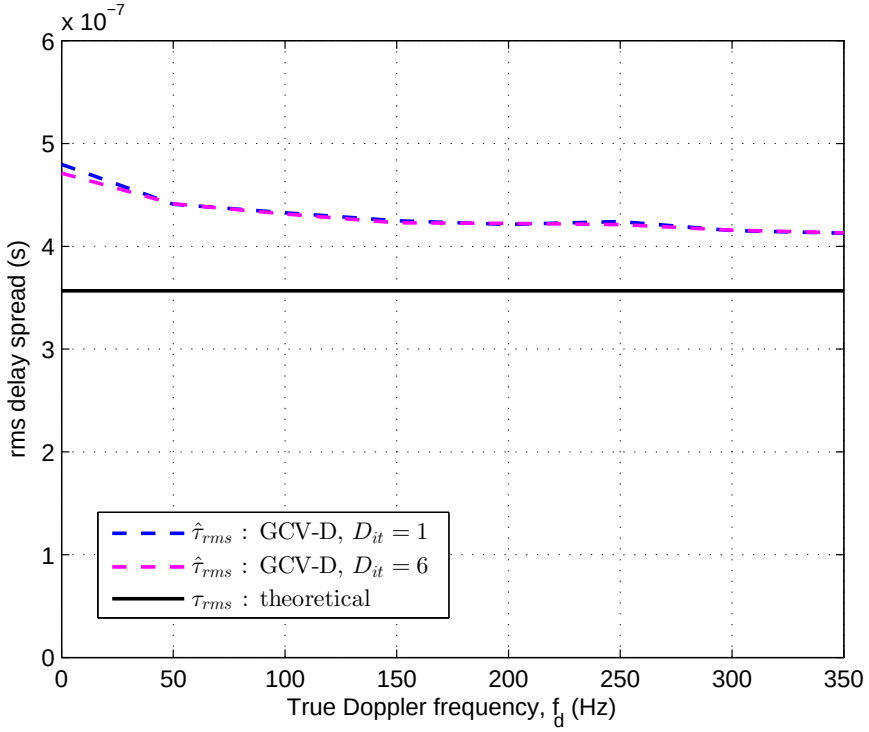

(b)

Figure 5.7: Performance of the proposed rms delay spread estimator in (a) ETU and (b) EVA channels at SNR=15 dB and $\alpha = 1.1$.

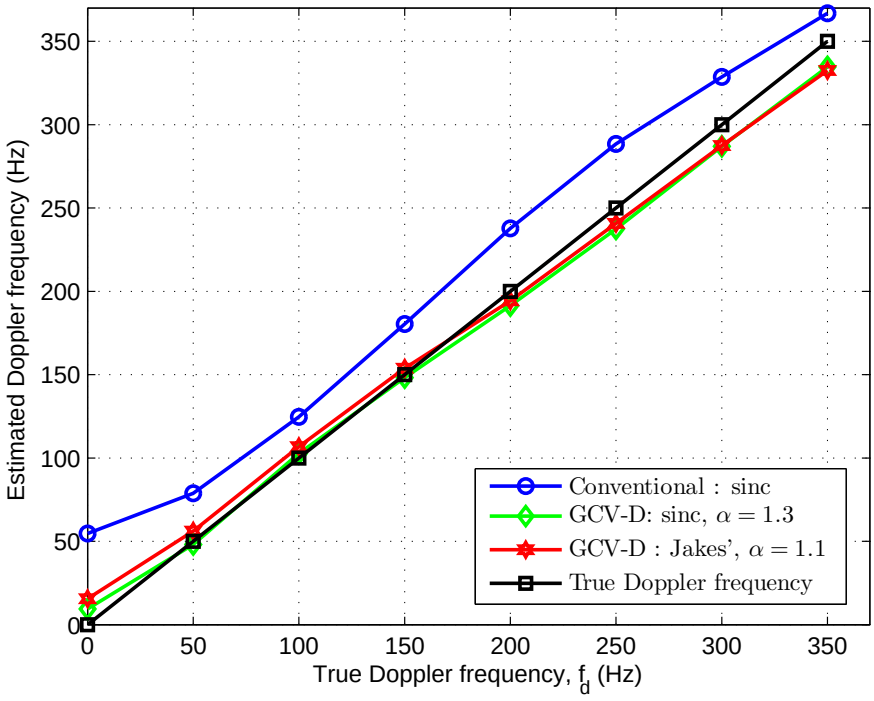

(a)

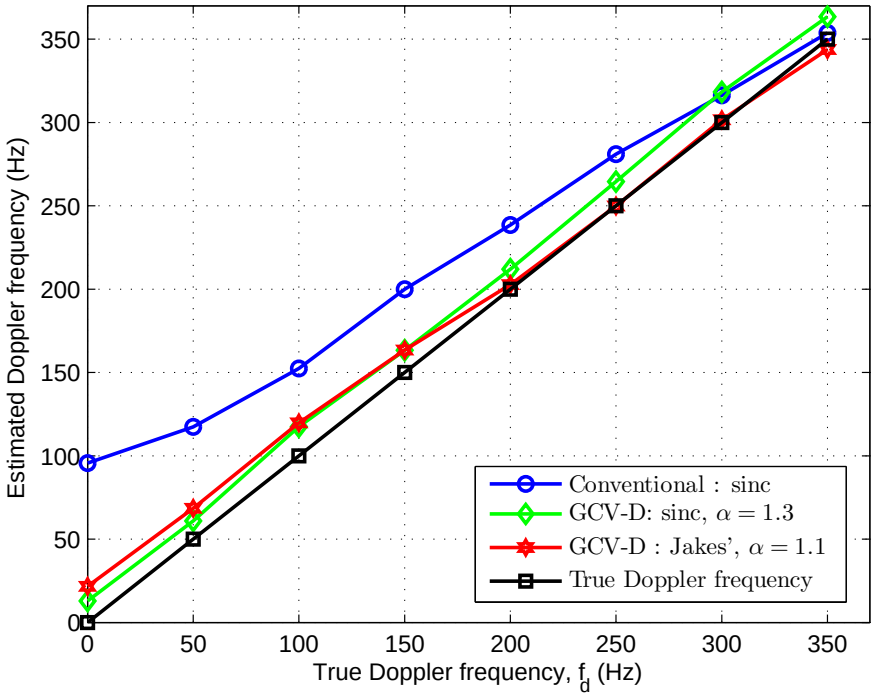

(b)

Figure 5.8: Performance of Doppler frequency estimators in the case of Doppler spectrum mismatch; (a) ETU channel; (b) EVA channel. SNR=15 dB.

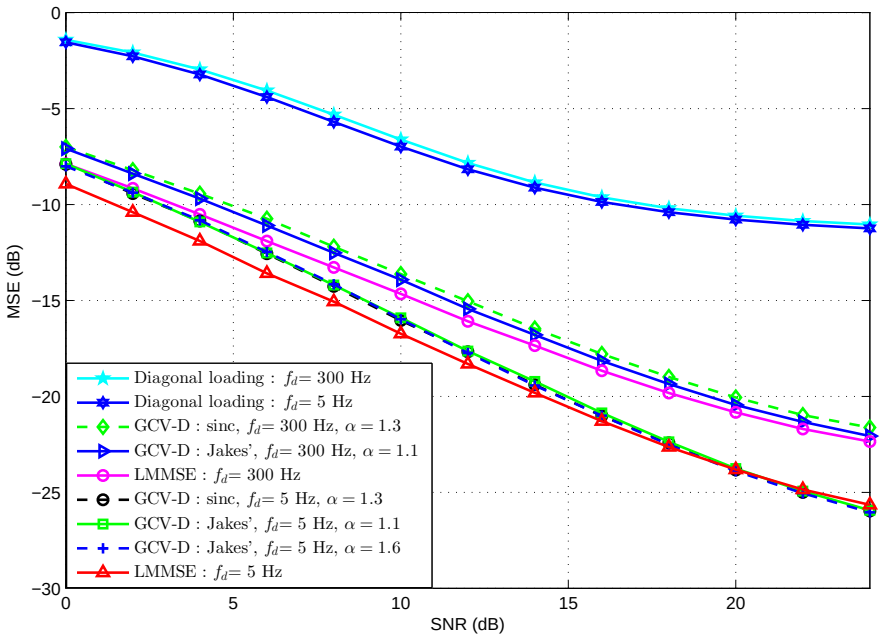

(a)

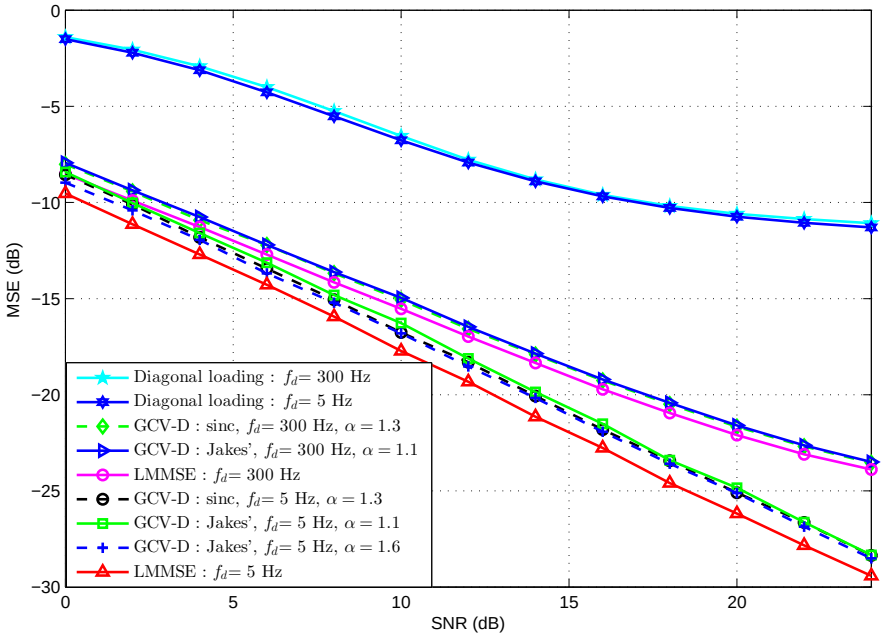

(b)

Figure 5.9: MSE performance of the proposed channel estimator using matched and mismatched Doppler spectrum; (a) ETU channel, (b) EVA channel.

computation of $\boldsymbol{\Upsilon}_t$, the difference in the estimation performance is very small, which again shows the robustness of the proposed estimator. In Figure 5.9 (b), in the EVA channel at 5 Hz Doppler frequency, the performance of the proposed estimator using Jakes' Doppler model (Jakes' auto-correlation function) at $\alpha = 1.1$ is about 1.2$\sim$1.5 dB away from that of the pilot-based LMMSE channel estimator. When $\alpha = 1.6$, the gap is reduced to about 0.7$\sim$1 dB. This shows that, in the EVA channel, more improvement at low Doppler frequencies can be achieved by re-adjusting α. It can be seen that the efficiency of the proposed estimator can be affected by the choice of α. Therefore, α should be re-adjusted for different scenarios in order to achieve an improved performance. The adjusted α the same over all Doppler frequencies has shown a good performance, especially at medium to high Doppler frequencies. However, a better performance can be achieved by varying α over Doppler frequencies.

Now, the simulations for the re-adjustable joint estimator that is described in Section 5.7 is considered. First, α is adjusted over different range of Doppler frequencies. From Figure 5.3, it can be seen that at $f_d \in [150, 350]$ Hz, the constant $\alpha = 1.1$ provides a better Doppler frequency estimation performance than other values of α. For Doppler frequencies lower than $f_d = 150$ Hz, a better performance is achieved by $\alpha > 1.1$. In Figure 5.10 (a), $\alpha = 1.2$ provides the better estimation performance for $f_d \in [10, 150]$ Hz, while $\alpha = 1.5$ provides the better performance for $f_d \in [0, 10)$ Hz. In Figure 5.10 (b), $\alpha = 1.3$ is the better for $f_d \in [10, 150]$ Hz, while $\alpha = 1.6$ is the better for $f_d \in [0, 10)$ Hz. The value of α is set to $\alpha = 1.1$ in the initial joint estimator. The Doppler frequency estimation error at $f_{d,thr2} = 10$ Hz is high and can effect the estimation performance of the re-adjustable estimator. Therefore, $f_{d,thr1}$ is set to $f_{d,thr1} = 150$ Hz and $f_{d,thr2}$ is set high enough to take into account the effect of the estimation error, and thus $f_{d,thr2}$ is set to $f_{d,thr2} = 25$ Hz. The values α_1 and α_2 are set to $\alpha_1 = 1.2$ and $\alpha_2 = 1.5$ as they can provide the best performance in the ETU channel with small degradation in the EVA channel.

Figure 5.11 compares the Doppler frequency estimation of the GCV-D using the adjusted $\alpha = 1.1$ and the proposed re-adjustable GCV-D. It can be seen that the re-adjustable estimator significantly improves the Doppler frequency estimation performance at low to medium Doppler frequencies in both the ETU and EVA channels. At high Doppler frequencies, the re-adjustable GCV-D has similar performance as that of the GCV-D.

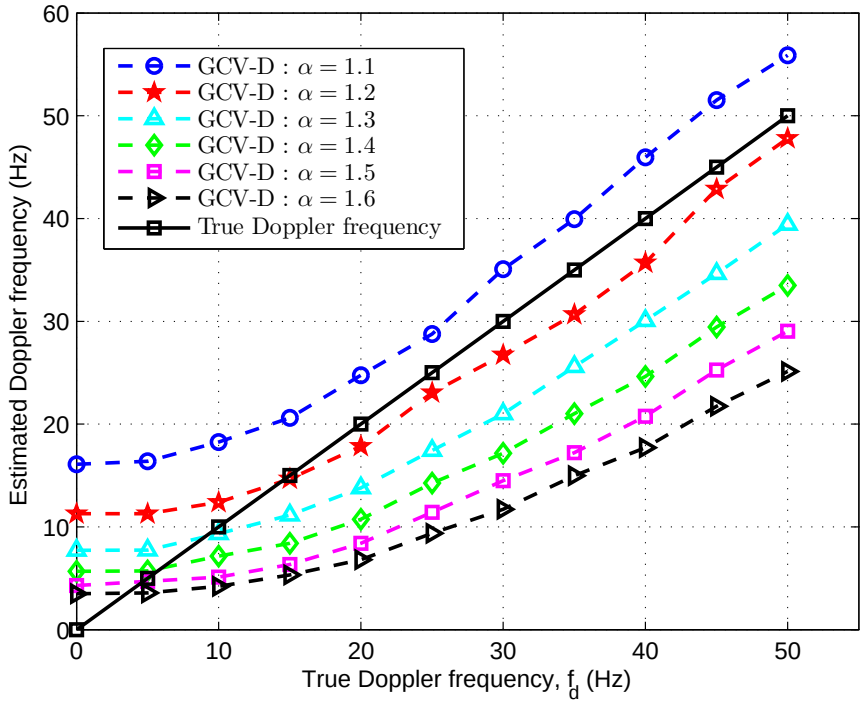

(a)

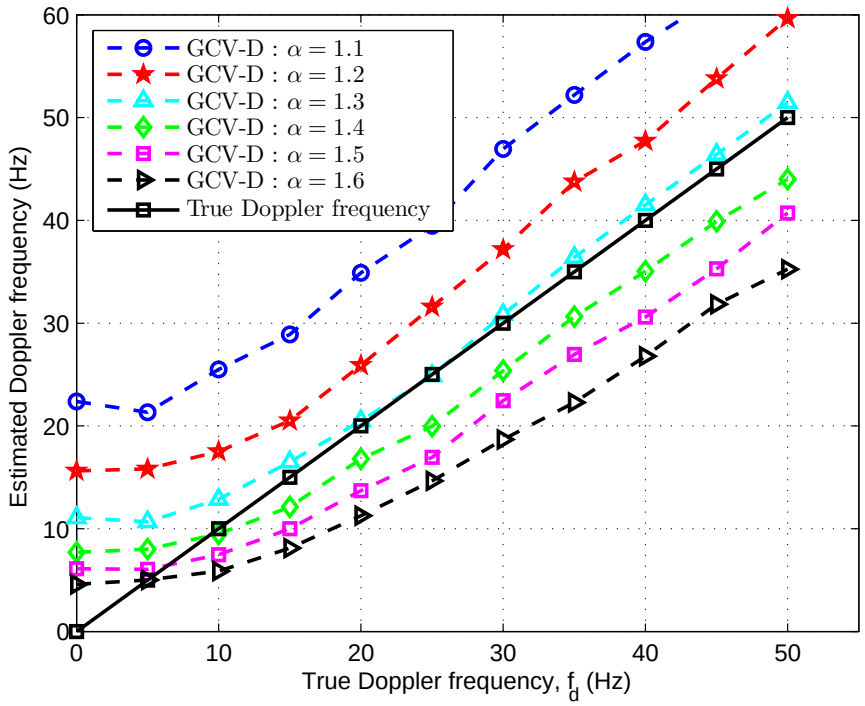

(b)

Figure 5.10: Performance of estimation of small to medium Doppler frequencies in (a) ETU and (b) EVA channels. SNR=15 dB.

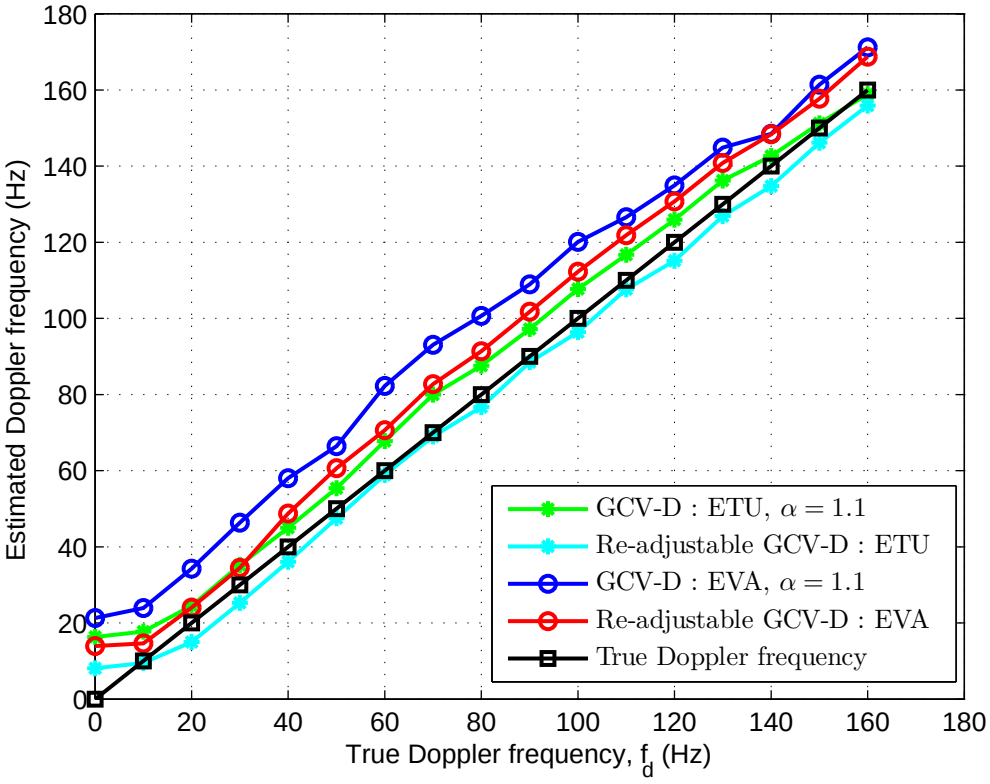

Figure 5.11: Performance of Doppler frequency estimation of the re-adjustable GCV-D estimator in the ETU and EVA channels at SNR=15 dB.

Figure 5.12 shows the performance of rms delay spread estimation by the re-adjustable GCV-D. In the ETU channel, in the range $f_d \in [0, 150]$ Hz, the re-adjustable GCV-D provides around $4 \sim 17\%$ improvement in the rms delay spread estimation performance over that of the original GCV-D. In the EVA channel, the improvement is in the range of $4 \sim 19\%$.

Figures 5.13 and 5.14 show the channel estimation performance of the re-adjustable channel estimator. Figure 5.13 (a) and Figure. 5.14 show that the improvement obtained by the re-adjustable GCV-D estimator over the GCV-D estimator is very small to almost negligible. In Figure 5.13 (b), at $f_d = 5$ Hz, the improvement achieved by the re-adjustable estimator over the GCV-D estimator is around 0.4 dB and the performance is almost 1 dB away from that of the LMMSE estimator. For Doppler frequencies greater than $f_d = 5$ Hz, in the EVA channel (see Figure 5.13 and Figure 5.14), the improvement is very small. When the channel estimation performance of the re-adjustable GCV-D estimator is compared with that of the GCV-D estimator. It can be concluded that the channel estimates obtained by the GCV-D estimator (with $\alpha = 1.1$) are already good enough. This shows that the GCV-D estimator

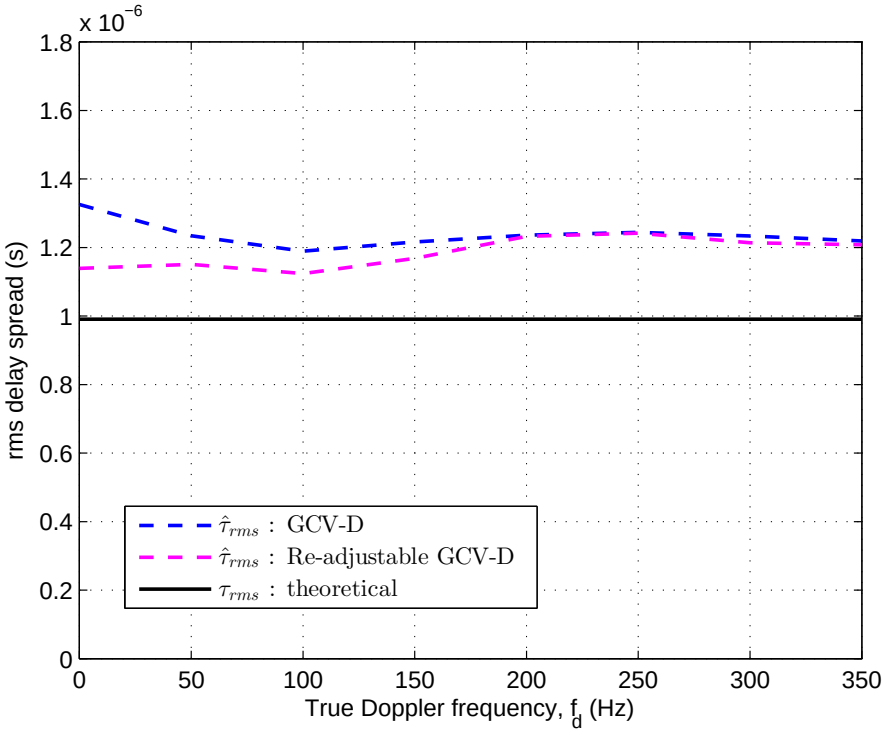

(a)

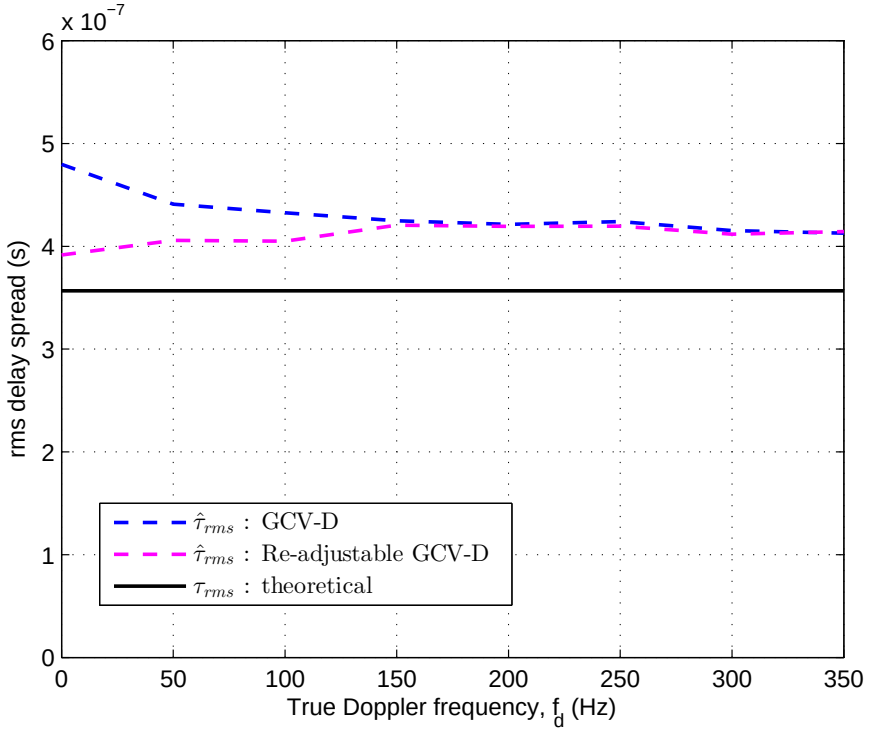

(b)

Figure 5.12: Performance of the re-adjustable delay spread estimator in (a) ETU and (b) EVA channels. SNR=15 dB.

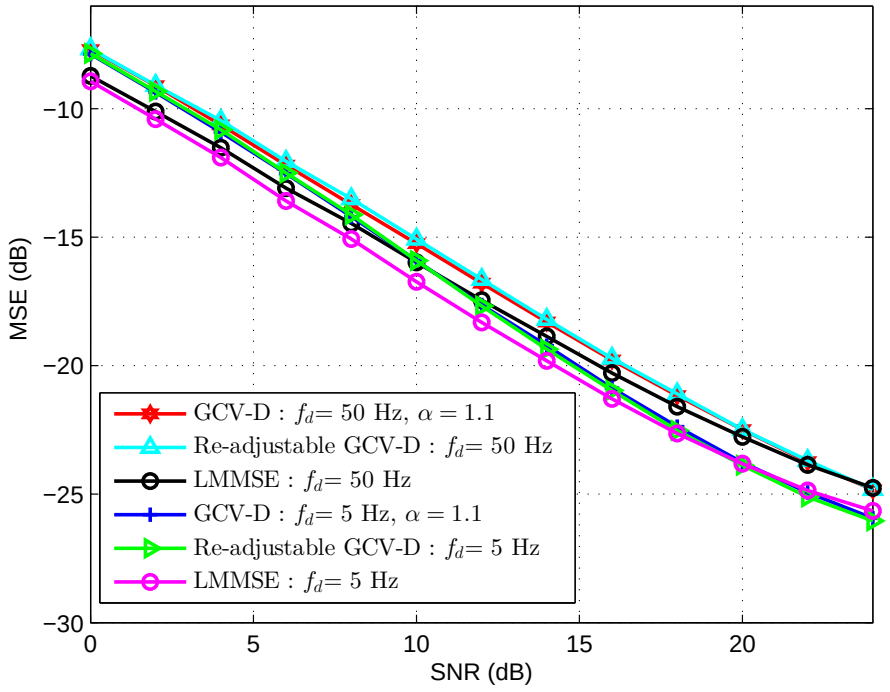

(a)

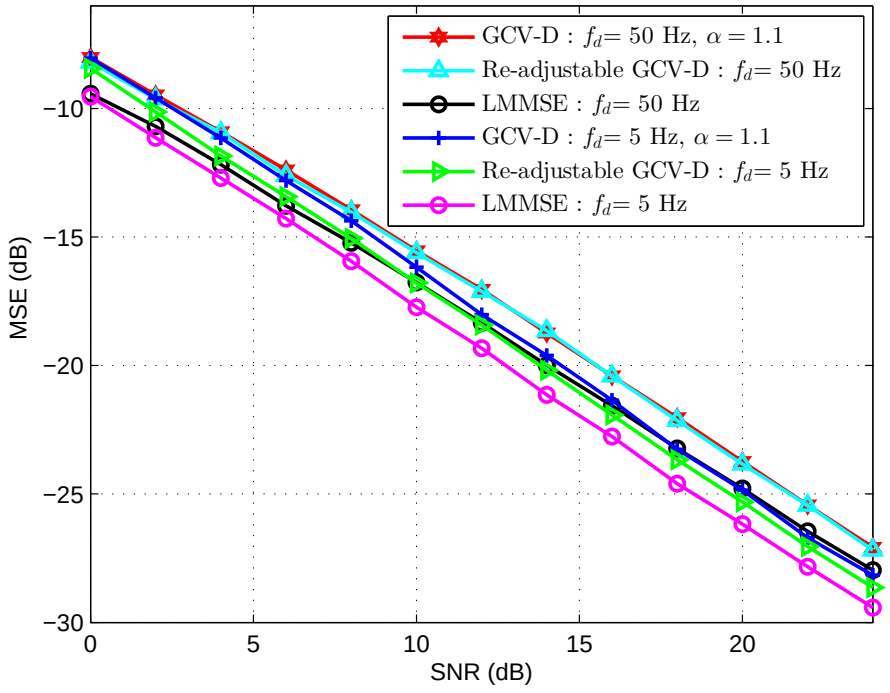

(b)

Figure 5.13: Channel estimation performance of the re-adjustable channel estimator in (a) ETU and (b) EVA channels at low Doppler frequencies.

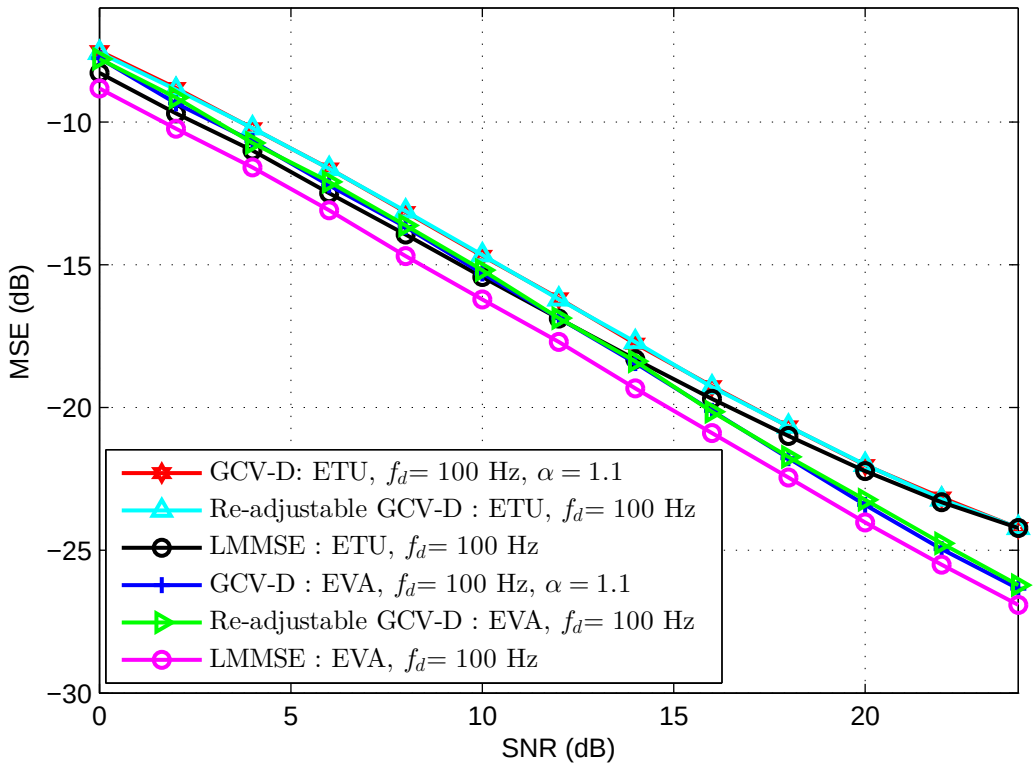

Figure 5.14: Channel estimation performance of the re-adjustable channel estimator in the ETU and EVA channels at a Doppler frequency of $f_d = 100$ Hz.

without the re-adjustment is robust to a certain degree to the inaccuracy of the Doppler frequency and delay spread estimation and still can provide channel estimates close to that obtained with perfect channel statistics. However, the re-adjustable estimator provides an extra improvement in the estimation performance for the Doppler frequency and the delay spread at low to medium Doppler frequencies.

It is important to note that the proposed re-adjustment of the constant α is considered for the case of Jakes' Doppler model. For other Doppler models, the values of $f_{d,thr1}$, $f_{d,thr2}$, and α may be different. Therefore, the re-adjustment has to be modified for Doppler spectrum models different from Jakes' model.

5.9 Summary

This chapter can be summarized as the following:

- A new joint Doppler frequency, delay spread and channel estimator using the GCV method is proposed.
- It is proposed to use the dichotomous search for the implementation of the GCV method. The complexity of the GCV method with the dichotomous search is significantly reduced compared to the exhaustive search.
- It has been shown that, in the LTE downlink scenarios, this estimator can provide a significantly better Doppler frequency estimation performance than the conventional Doppler frequency estimator. The channel estimation performance of the proposed estimator without knowledge of the channel statistics is close to that of the LMMSE channel estimator (with the perfect knowledge of channel statistics).
- The reduction of the memory load using the properties of the BEM matrix and channel covariance has been discussed for the proposed estimator.
- It has been shown that when the Doppler model used in the estimator differs from the true Doppler model, the proposed estimator shows robustness.
- A re-adjustable joint Doppler frequency, delay spread and channel estimator is proposed to further improve the estimation performance at low to medium Doppler frequencies.
- The improvement in the channel estimation performance achieved by the re-adjustable estimator is small at low to medium Doppler frequencies. However, at very low Doppler frequencies, the improvement is relatively good compared to the joint estimation with a single GCV constant.
- However, the re-adjustable estimator provides extra improvement in the estimation performance of the Doppler frequency and delay spread over that of the joint estimator with a single GCV constant.

Chapter 6

Conclusions and future work

Contents

6.1 Conclusions

The conclusions of this thesis can be summarized as the following:

- Chapter 1 provided an introduction to the research topic while Chapter 2 provided the literature review of previous work that we used throughout this thesis which includes: the principles of OFDM and MIMO setup, the LTE downlink and its design parameters, doubly-selective channels, channel modelling, the use of BEMs in channel estimation, mismatched detection and basics of turbo coding.

- In Chapter 3, the performance of the mismatched detection with the reweighted LMMSE BEM channel estimation was investigated in a doubly-selective channel under the downlink LTE scenarios. The reweighted LMMSE channel estimation performance was shown to outperform that of the traditional (unweighted) LMMSE channel estimation.

- In Chapter 4, a selective symbol-by-symbol optimal receiver with an adaptive channel estimator was proposed for MIMO OFDM systems in doubly-selective channels. The

proposed receiver allows significantly lower complexity with almost the same detection performance in comparison with the symbol-by-symbol optimal receiver applied to all received data symbols. The performance of the optimal and the selective optimal receivers with adaptive regularization was investigated. The performance of these receivers with the adaptive regularisation was found to be close to that of receivers with full knowledge of channel statistics.

- In Chapter 5, a joint Doppler frequency, delay spread and channel estimator was proposed, based on the adaptive regularization. The Doppler frequency and delay spread that correspond to the optimal regularization matrix are selected as their estimates. The performance of these estimates is very close to that of estimates obtained with the perfect knowledge of channel statistics. Re-adjustment of the optimization criterion was proposed to further improve the estimator performance. The re-adjustment was shown to provide extra improvement in the performance of the Doppler frequency and delay spread estimation at low to medium Doppler frequencies.

6.2 Future work

Based on the analysis and results obtained in this thesis, the following suggestions for future research are suggested:

- In Chapter 4, the sub-optimal and selective sub-optimal receivers were implemented using the adaptive regularization with perfect knowledge of the Doppler frequency. In Chapter 5, the adaptive regularization that estimates jointly the Doppler frequency and delay spread was presented. Also, this adaptive regularization provides improvement in the estimation performance by utilizing a better model for the PDP. Therefore, the investigation of the sub-optimal and selective sub-optimal receivers using the approach in Chapter 5 is suggested.

- In Chapter 5, the joint Doppler-delay spread and channel estimation was investigated using the uniform Doppler spectrum that is different from the true channel Doppler spectrum (Jakes' Doppler spectrum). The estimation performance of the proposed joint estimator with the mismatched Doppler model showed a good performance. However, for future work, the investigation of the proposed joint estimator performance is

suggested for different channel models, other than Jakes' model. For example, different Doppler models can be used to design the proposed estimator, which then will be investigated in environments with a direct line of sight (i.e, Rician fading) or environments with non-isotropic scattering models [131–133].

- In this thesis, an efficient complexity reduction technique was proposed in Chapter 4. In Chapter 5, a joint Doppler-delay spread and channel estimation technique was presented. The techniques in Chapters 4 and 5 were investigated for the case of a single user MIMO OFDM transmission. The investigation of theses techniques is suggested for other cases, where the channel estimation and/or receiver complexity reduction are crucial, such as multi-user MIMO OFDM transmission, the LTE uplink scenarios [29] (with single and multi-user transmissions).

Appendix A

In the appendix, extra results for the proposed GCV-D estimator in Chapter 5 are provided. Figure A.1 shows the performance of the Doppler frequency estimation of GCV-D using a mismatched Doppler model (*sinc* time auto-correlation function) against α. The constant $\alpha = 1.3$ provides a better Doppler frequency estimation performance in the ETU channel than other values of α, while $\alpha = 1.4$ provides the better performance in the EVA channel. It can be seen that $\alpha = 1.4$ significantly degrades the estimation performance in the ETU channel at medium to high Doppler frequencies. A trade-off with small degradation in the performance in the EVA channel can be obtained by selecting $\alpha = 1.3$ for both the channels, which is used in the simulations in Chapter 5.

Now, the effect of the choice of the PDP model, used in designing the proposed estimator, on the estimation performance is investigated. Figure A.2 compares the channel estimation performance of the proposed channel estimator for a frequency auto-correlation computed using the uniform or exponential PDP models. The frequency auto-correlation that corresponds to the uniform PDP model can be obtained from (5.24), by setting $\tau_{rms} \to \infty$ [128]:

$$[\boldsymbol{\Upsilon}_f]_{p,q} = \frac{1 - e^{-2\pi j T_d (p-q)\Delta f}}{2\pi j T_d (p-q)\Delta f}. \tag{A.1}$$

The frequency auto-correlation function in (A.1) is used in the simulation with replacing T_d by τ_{max}, which is defined by the set in (4.36). In Figure A.2 (a), in the ETU channel, the channel estimator using the exponential PDP model outperforms that of the uniform PDP model. In Figure A.2 (b), in the EVA channel, the channel estimator using the exponential PDP model outperforms that of the uniform PDP model, especially at low SNR. This shows that the exponential PDP model provides a better approximation of the PDPs of the ETU and EVA channels. Therefore, the exponential model is used in our simulations in Chapter 5.

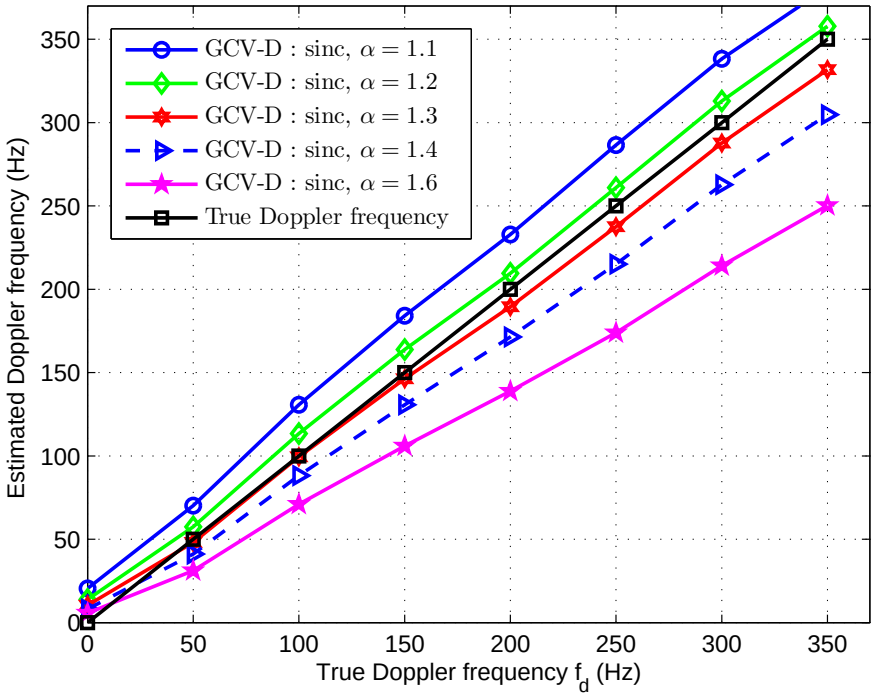

(a)

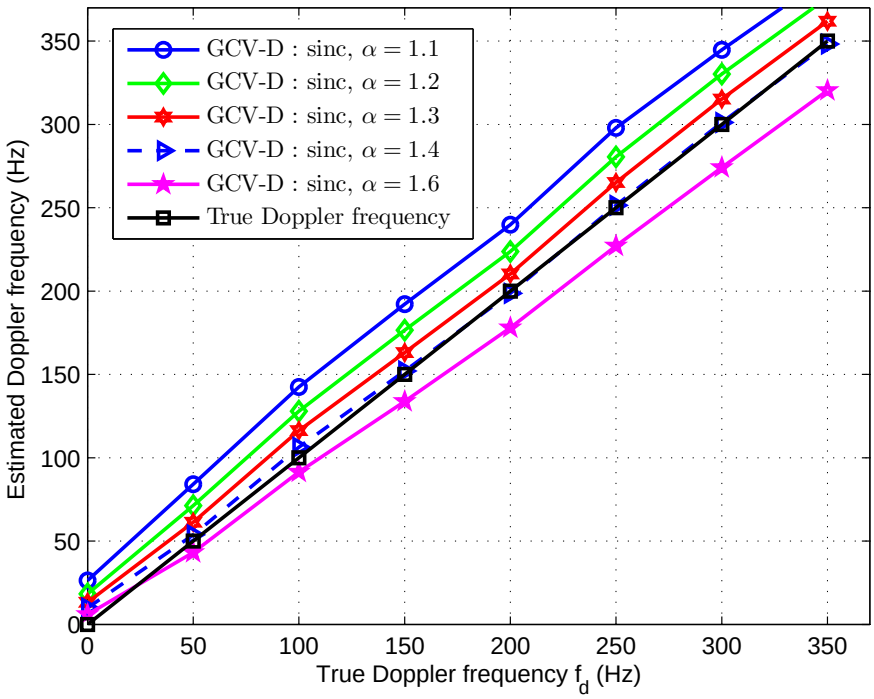

(b)

Figure A.1: Performance of Doppler frequency estimation of the proposed GCV-D estimator with different values of α using mismatched Doppler model (*sinc* time auto-correlation function) in (a) ETU and (b) EVA channels. SNR=15 dB.

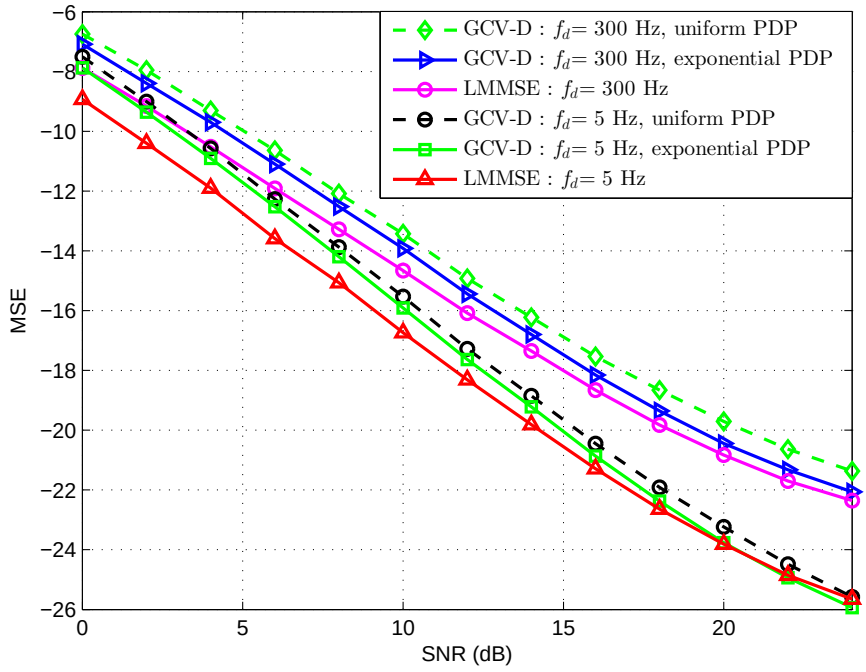

(a)

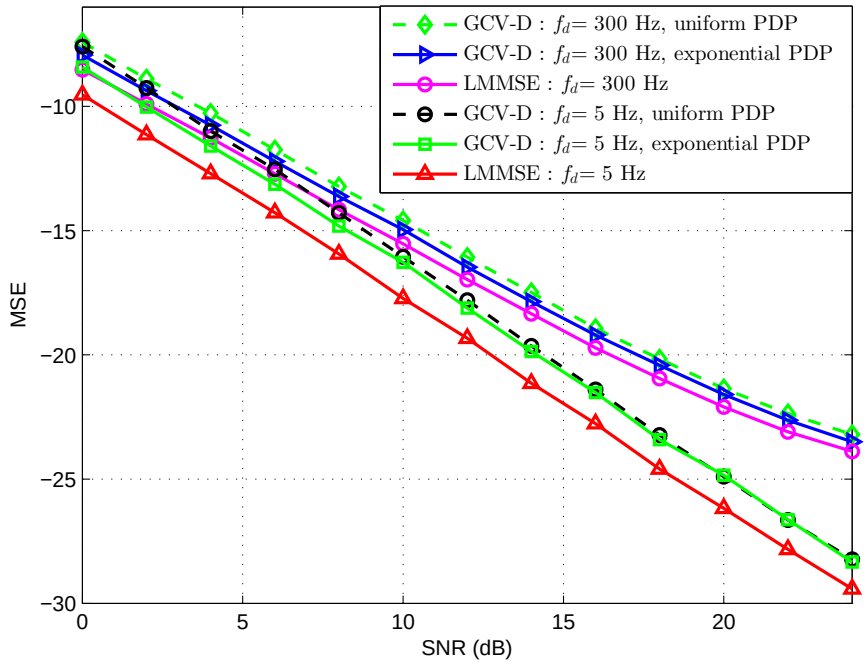

(b)

Figure A.2: Comparison of the channel estimation performance of the proposed GCV-D estimator in case of different PDP models in (a) ETU and (b) EVA channels. $\alpha = 1.1$.

Glossary

APP	**A** **P**osteriori **P**robability
BLAST	**B**ell **L**aboratories Layered **S**pace **T**ime
BEM	**B**asis **E**xpansion **M**odel
BLER	**B**lock **E**rror **R**ate
BPSK	**B**inary **P**hase **S**hift **K**eying
CE	**C**omplex **E**xponentials
CP	**C**yclic **P**refix
CRC	**C**yclic **R**edundancy **C**heck
CRS	**C**ell-**S**pecifc **R**eference
DFT	**D**iscrete **F**ourier **T**ransform
DPSS	**D**iscrete **P**rolate **S**pheroidal **S**equences
EPA	**E**xtended **P**edestrian **A** model
EVA	**E**xtended **V**ehicular **A** model
ETU	**E**xtended **T**ypical **U**rban model
FDD	**F**requency **D**ivision **D**uplexing
FEC	**F**orward **E**rror **C**orrection
FFT	**F**ast **F**ourier **T**ransform
GCV	**G**eneralized **C**ross-**V**alidation
ICI	**I**nter **C**arrier **I**nterference
IFFT	**I**nverse **F**ast **F**ourier **T**ransform
ISI	**I**nter **S**ymbol **I**nterference
KL	**K**arhunen **L**oeve
LLR	**L**og **L**ikelihood **R**atio
LMMSE	**L**inear **M**inimum **M**ean **S**quare **E**rror

LS	**L**east **S**quares
LTE	**L**ong **T**erm **E**volution
MAC	**M**edium **A**ccess **C**ontrol
MAP	**M**aximum **A** **P**osteriori
MIMO	**M**ulti **I**nput **M**ulti **O**utput
ML	**M**aximum **L**ikelihood
MMSE	**M**inimum **M**ean **S**quare **E**rror
MSE	**M**ean **S**quare **E**rror
OFDM	**O**rthogonal **F**requency **D**ivision **M**ultiplexing
OFDMA	**O**rthogonal **F**requency **D**ivision **M**ultiple **A**ccess
PAPR	**P**eak-to-**A**verage **P**ower
PCI	**P**erfect **C**hannel **I**nformation
PDF	**P**robability **D**ensity **F**unction
PDP	**P**ower **D**elay **P**rofile
PDSCH	**P**hysical **D**ownlink **S**hared **C**hannel
QAM	**Q**uadrature **A**mplitude **M**odulation
RE	**R**esource **E**lement
SbS	**S**ymbol-by-**S**ymbol
SC-FDMA	**S**ingle **C**arrier- **F**requency **D**ivision **M**ultiple **A**ccess
SISO	**S**ingle **I**nput **S**ingle **O**utput
SISO	**S**oft **I**nput **S**oft **O**utput
SNR	**S**ignal-to-**N**oise **R**atio
TDD	**T**ime **D**ivision **D**uplexing
UE	**U**ser **E**quipment
UE-RS	**UE**-specifc **R**eference **S**ignal
V-BLAST	**V**ertical-**B**ell **L**aboratories Layered **S**pace **T**ime
Wi-Fi	**Wi**reless-**Fi**delity
Wi-Max	**W**orldwide **I**nteroperability for **M**icrowave **A**ccess
WSS	**Wi**de **S**ense **S**tationary
WSSUS	**W**ide **S**ense **S**tationary **U**ncorrelated **S**cattering
ZF	**Z**ero **F**orcing

Bibliography

[1] S. Coleri, M. Ergen, A. Puri, and A. Bahai, "Channel estimation techniques based on pilot arrangement in OFDM systems," *IEEE Transactions on Broadcasting*, vol. 48, no. 3, pp. 223–229, Sep. 2002.

[2] D. Borah and B. Hart, "Frequency-selective fading channel estimation with a polynomial time-varying channel model," *IEEE Transactions on Communications*, vol. 47, no. 6, pp. 862–873, Jun. 1999.

[3] M. Chang and Y. Su, "Model-based channel estimation for OFDM signals in Rayleigh fading," *IEEE Transactions on Communications*, vol. 50, no. 4, pp. 540–544, Apr. 2002.

[4] M. Tsatsanis and G. Giannakis, "Modelling and equalization of rapidly fading channels," *International Journal of Adaptive Control and Signal Processing*, vol. 10, no. 2-3, pp. 159–176, 1996.

[5] M. Visintin, "Karhunen-Loeve expansion of a fast Rayleigh fading process," *Electronics Letters*, vol. 32, no. 18, pp. 1712–1713, Aug. 1996.

[6] P. Hammarberg, F. Rusek, and O. Edfors, "Iterative receivers with channel estimation for multi-user MIMO-OFDM: complexity and performance," *EURASIP Journal on Wireless Communications and Networking 2012*, no. 1, pp. 1–17, 2012.

[7] T. Zemen and C. Mecklenbrauker, "Time-variant channel estimation using discrete prolate spheroidal sequences," *IEEE Transactions on Signal Processing*, vol. 53, no. 9, pp. 3597–3607, Sep. 2005.

[8] Y. Zakharov, T. Tozer, and J. Adlard, "Polynomial spline-approximation of Clarke's model," *IEEE Transactions on Signal Processing*, vol. 52, no. 5, pp. 1198–1208, May 2004.

[9] N. Mai, Y. Zakharov, and A. Burr, "Iterative channel estimation based on B-splines for fast flat fading channels," *IEEE Transactions on Wireless Communications*, vol. 6, no. 4, pp. 1224–1229, Apr. 2007.

[10] M. Unser, A. Aldroubi, and M. Eden, "B-spline signal processing. I. Theory," *IEEE Transactions on Signal Processing*, vol. 41, no. 2, pp. 821–833, Feb. 1993.

[11] D. Kim, H. Kim, and G. Im, "Iterative channel estimation with frequency replacement for SC-FDMA systems," *IEEE Transactions on Communications*, vol. 60, no. 7, pp. 1877–1888, Jul. 2012.

[12] P. Salvo Rossi and R. Muller, "Joint twofold-iterative channel estimation and multiuser detection for MIMO-OFDM systems," *IEEE Transactions on Wireless Communications*, vol. 7, no. 11, pp. 4719–4729, Nov. 2008.

[13] X. Wang and H. V. Poor, "Iterative (turbo) soft interference cancellation and decoding for coded CDMA," *IEEE Transactions on Communications*, vol. 47, no. 7, pp. 1046–1061, Jul. 1999.

[14] M. Zhao, Z. Shi, and M. Reed, "Iterative turbo channel estimation for OFDM system over rapid dispersive fading channel," *IEEE Transactions on Wireless Communications*, vol. 7, no. 8, pp. 3174–3184, Aug. 2008.

[15] D. Yoon and J. Moon, "Low-complexity iterative channel estimation for turbo receivers," *IEEE Transactions on Communications*, vol. 60, no. 5, pp. 1182–1187, May 2012.

[16] C. Lam, D. Falconer, and F. Danilo-Lemoine, "Iterative frequency domain channel estimation for DFT-precoded OFDM systems using in-band pilots," *IEEE Journal on Selected Areas in Communications*, vol. 26, no. 2, pp. 348–358, 2008.

[17] N. Aboutorab, W. Hardjawana, and B. Vucetic, "A new iterative Doppler-assisted channel estimation joint with parallel ICI cancellation for high-mobility MIMO-OFDM systems," *IEEE Transactions on Vehicular Technology*, vol. 61, no. 4, pp. 1577–1589, 2012.

[18] Y. Zakharov and Z. Delai, "Weighted LS multiuser channel estimation for LTE," in *2015 IEEE 16th International Workshop on Signal Processing Advances in Wireless Communications (SPAWC), Stockholm, Sweden*, Jun. 2015, pp. 405–409.

[19] G. Taricco and E. Biglieri, "Space-time decoding with imperfect channel estimation," *IEEE Transactions on Wireless Communications*, vol. 4, no. 4, pp. 1874–1888, Jul. 2005.

[20] J. Zhang, V. Baronkin, and Y. Zakharov, "Optimal detection in MIMO OFDM systems with imperfect channel estimation," *IET Communications*, vol. 4, no. 4, pp. 384–394, Mar. 2009.

[21] Y. Zakharov and D. Zheng, "Adaptive regularization for BEM channel estimation in multicarrier systems," in *2016 IEEE International Conference on Acoustics, Speech and Signal Processing (ICASSP), Shanghai, China*, Mar. 2016, pp. 3676–3680.

[22] J. Lin and J. Proakis, "A parametric method for Doppler spectrum estimation in mobile radio channels," in *Proceedings of the 27th Conference on Information Systems and Sciences (CISS)*, 1993, pp. 875–880.

[23] M. Kashoob and Y. Zakharov, "Selective detection with adaptively regularized weighted channel estimation for MIMO OFDM," *submitted to IEEE Transactions on Wireless Communications*, 2016.

[24] M. Kashoob and Y. Zakharov, "Joint Doppler-delay spread and channel estimation in doubly-selective channels," *to be submitted to IEEE Transactions on Vehicular Technology*, 2016.

[25] M. Kashoob and Y. Zakharov, "Data-aided iterative reweighted LMMSE channel estimation for MIMO OFDM," in *2015 IEEE International Symposium onSignal Processing and Information Technology (ISSPIT), Abu, Dhabi, UAE*, Dec. 2015, pp. 663–667.

[26] M. Kashoob and Y. Zakharov, "Selective Optimal detection for MIMO OFDM systems," in *2016 IEEE Sensor Array and Multichannel Signal Processing Workshop (WCNC), Doha, Qatar*, Apr. 2016.

[27] M. Kashoob and Y. Zakharov, "Selective Detection with Adaptive Channel Estimation for MIMO OFDM," in *2016 IEEE Wireless Communications and Networking Conference (SAM), Rio de Janeiro, Brazil*, Jul. 2016.

[28] E. Biglieri, R. Calderbank, A. Constantinides, A. Goldsmith, A. Paulraj, and H. V. Poor, *MIMO Wireless Communications*, New York, NY, USA: Cambridge University Press, 2007.

[29] ETSI-TS-136-201, "3rd Generation Partnership Project; Technical specification group radio access network; Evolved Universal Terrestrial Radio Access (E-UTRA); Physical Channels and Modulation (3GPP TS 36.211, V12.3.0, Release 12)," Sep. 2014.

[30] "IEEE Standard for Air Interface for Broadband Wireless Access Systems," *IEEE Std 802.16-2012 (Revision of IEEE Std 802.16-2009)*, pp. 1–2542, Aug. 2012.

[31] "Information technology–Telecommunications and information exchange between systems Local and metropolitan area networks–Specific requirements Part 11: Wireless LAN Medium Access Control (MAC) and Physical Layer (PHY) Specifications," *ISO/IEC/IEEE 8802-11:2012(E) (Revison of ISO/IEC/IEEE 8802-11-2005 and Amendments)*, pp. 1–2798, Nov. 2012.

[32] E. Institute, "Digital Video Broadcasting (DVB); Framing structure, channel coding and modulation for digital terrestrial television (ETSI ETS 300 744, V1.6.1)," Jan. 2009.

[33] V. Bogachev and I. Kiselev, "Optimum combining of signals in space-diversity reception," *Telecommun. Radio Eng.*, vol. 34/35, pp. 83–85, Oct. 1980.

[34] J. Winters, "Optimum combining in digital mobile radio with cochannel interference," *IEEE Journal on Selected Areas in Communications*, vol. 2, no. 4, pp. 528–539, Jul. 1984.

[35] A. Paulraj and T. Kailath, "Increasing capacity in wireless broadcast systems using distributed transmission/directional reception (DTDR)," Sep. 1994, US Patent 5,345,599.

[36] I. Telatar, "Capacity of Multi-antenna Gaussian Channels," *European Transactions on Telecommunications*, vol. 10, pp. 585–595, 1999.

[37] G. Foschini, "Layered space-time architecture for wireless communication in a fading environment when using multi-element antennas," *Bell Labs Technical Journal*, vol. 1, no. 2, pp. 41–59, 1996.

[38] P. Wolniansky, G. Foschini, G. Golden, and R. Valenzuela, "V-BLAST: an architecture for realizing very high data rates over the rich-scattering wireless channel," in *1998 URSI International Symposium on Signals, Systems, and Electronics (ISSSE), Palazzo Dei Congressi, Pisa, Italy*, Sep. 1998, pp. 295–300.

[39] S. Alamouti, "A simple transmit diversity technique for wireless communications," *IEEE Journal on Selected Areas in Communications*, vol. 16, no. 8, pp. 1451–1458, 1998.

[40] Y. Zakharov, V. Baronkin, and J. Zhang, "Optimal and mismatched detection of QAM signals in fast fading channels with imperfect channel estimation," *IEEE Transactions on Wireless Communications*, vol. 8, no. 2, pp. 617–621, 2009.

[41] J. Zhang, Y. Zakharov, and V. Baronkin, "Optimal detection in MIMO Rayleigh fast fading channels with imperfect channel estimation," in *42nd Asilomar Conference on Signals, Systems and Computers , Pacific Grove, CA, US*, 2008, pp. 470–474.

[42] Y. Zakharov, V. Baronkin, and J. Zhang, "Optimal detection of QAM signals in fast fading channels with imperfect channel estimation," in *2008 IEEE International Conference on Acoustics, Speech and Signal Processing (ICASSP), Las Vegas, Nevada, US*, Mar. 2008, pp. 3205–3208.

[43] J. L. Bai, J. Choi and Q. Yu, *Low complexity MIMO receivers*, Springer Publishing Company, Incorporated, 2014.

[44] R. Chang, "Synthesis of Band-Limited Orthogonal Signals for Multichannel Data Transmission," *Bell System Technical Journal*, vol. 45, no. 10, pp. 1775–1796, 1966.

[45] S. Weinstein and P. Ebert, "Data transmission by frequency-division multiplexing using the discrete Fourier transform," *IEEE Transactions on Communication Technology*, vol. 19, no. 5, pp. 628–634, Oct. 1971.

[46] A. Peled and A. Ruiz, "Frequency domain data transmission using reduced computational complexity algorithms," in *IEEE International Conference on Acoustics, Speech, and Signal Processing (ICASSP), Denver, Colorado, US*, vol. 5, Apr. 1980, pp. 964–967.

[47] P. Xia, S. Zhou, and G. Giannakis, "Bandwidth- and power-efficient multicarrier multiple access," *IEEE Transactions on Communications*, vol. 51, no. 11, pp. 1828–1837, Nov. 2003.

[48] J. Proakis and M. Salehi, *Digital Communications*, 5th ed., ser. Electrical engineering series, McGraw-Hill, 2007.

[49] T. Chiueh and P. Tsai, *OFDM baseband receiver design for wireless communications*, Wiley Publishing, 2007.

[50] G. Giannakis, *Space-time coding for broadband wireless communications*, Hoboken, N.J. Wiley-Interscience, 2007.

[51] S. Han and J. Lee, "PAPR reduction of OFDM signals using a reduced complexity PTS technique," *IEEE Signal Processing Letters*, vol. 11, no. 11, pp. 887–890, Nov. 2004.

[52] K. Du and M. Swamy, *Wireless communication systems: from RF subsystems to 4G enabling technologies*, New York, NY, USA: Cambridge University Press, 2010.

[53] S. Eom, H. Nam, and Y. Ko, "Low-complexity PAPR reduction scheme without side information for OFDM systems," *IEEE Transactions on Signal Processing*, vol. 60, no. 7, pp. 3657–3669, Jul. 2012.

[54] T. Pollet, M. Bladel, and M. Moeneclaey, "BER sensitivity of OFDM systems to carrier frequency offset and Wiener phase noise," *IEEE Transactions on Communications*, vol. 43, no. 2/3/4, pp. 191–193, Feb. 1995.

[55] Y. Zhao and S. Haggman, "Sensitivity to Doppler shift and carrier frequency errors in OFDM systems-the consequences and solutions," in *46th Vehicular Technology Conference (VTC), Atlanta, Georgia, US*, vol. 3, Apr. 1996, pp. 1564–1568.

[56] H. Holma and A. Toskala, *LTE for UMTS: evolution to LTE-Advanced*, 2nd ed., Wiley Publishing, 2011.

[57] D. Chu, "Polyphase codes with good periodic correlation properties (Corresp.)," *IEEE Transactions on Information Theory*, vol. 18, no. 4, pp. 531–532, Jul. 1972.

[58] L. Zheng and D. Tse, "Diversity and multiplexing: a fundamental tradeoff in multiple-antenna channels," *IEEE Transactions on Information Theory*, vol. 49, no. 5, pp. 1073–1096, May 2003.

[59] X. Ma and G. Giannakis, "Maximum-diversity transmissions over doubly selective wireless channels," *IEEE Transactions on Information Theory*, vol. 49, no. 7, pp. 1832–1840, Jul. 2003.

[60] P. Schniter, "Low-complexity equalization of OFDM in doubly selective channels," *IEEE Transactions on Signal Processing*, vol. 52, no. 4, pp. 1002–1011, Apr. 2004.

[61] P. Bello, "Characterization of randomly time-variant linear channels," *IEEE Transactions on Communications Systems*, vol. 11, no. 4, pp. 360–393, Dec. 1963.

[62] P. Hoeher, "A statistical discrete-time model for the WSSUS multipath channel," *IEEE Transactions on Vehicular Technology*, vol. 41, no. 4, pp. 461–468, Nov. 1992.

[63] J. Sadowsky and V. Kafedziski, "On the correlation and scattering functions of the WSSUS channel for mobile communications," *IEEE Transactions on Vehicular Technology*, vol. 47, no. 1, pp. 270–282, Feb. 1998.

[64] R. Clarke, "A statistical theory of mobile-radio reception," *Bell System Technical Journal*, vol. 47, no. 6, pp. 957–1000, 1968.

[65] W. Jakes and D. Cox, Eds., *Microwave Mobile Communications*, Wiley-IEEE Press, 1994.

[66] M. Pop and N. Beaulieu, "Limitations of sum-of-sinusoids fading channel simulators," *IEEE Transactions on Communications*, vol. 49, no. 4, pp. 699–708, Apr. 2001.

[67] P. Dent, G. Bottomley, and T. Croft, "Jakes fading model revisited," *Electronics Letters*, vol. 29, no. 13, pp. 1162–1163, Jun. 1993.

[68] M. Patzold, U. Killat, F. Laue, and Y. Li, "On the statistical properties of deterministic simulation models for mobile fading channels," *IEEE Transactions on Vehicular Technology*, vol. 47, no. 1, pp. 254–269, Feb. 1998.

[69] Y. Zheng and C. Xiao, "Simulation models with correct statistical properties for Rayleigh fading channels," *IEEE Transactions on Communications*, vol. 51, no. 6, pp. 920–928, Jun. 2003.

[70] Y. Zheng and C. Xiao, "Improved models for the generation of multiple uncorrelated Rayleigh fading waveforms," *IEEE Communications Letters*, vol. 6, no. 6, pp. 256–258, Jun. 2002.

[71] C. Xiao, Y. Zheng, and N. Beaulieu, "Novel sum-of-sinusoids simulation models for Rayleigh and Rician fading channels," *IEEE Transactions on Wireless Communications*, vol. 5, no. 12, pp. 3667–3679, Dec. 2006.

[72] ETSI-TS-136-201, "3rd Generation Partnership Project; Technical specification group radio access network; Evolved Universal Terrestrial Radio Access (E-UTRA); Base Station (BS) radio transmission and reception (3GPP TS 36.104, V12.4.0, Release 12)," Jun. 2014.

[73] S. Zhou, B. Muquet, and G. Giannakis, "Subspace-based (semi-) blind channel estimation for block precoded space-time OFDM," *IEEE Transactions on Signal Processing*, vol. 50, no. 5, pp. 1215–1228, May 2002.

[74] E. Moulines, P. Duhamel, J. Cardoso, and S. Mayrargue, "Subspace methods for the blind identification of multichannel FIR filters," *IEEE Transactions on Signal Processing*, vol. 43, no. 2, pp. 516–525, Feb. 1995.

[75] M. Necker and G. Stuber, "Totally blind channel estimation for OFDM on fast varying mobile radio channels," *IEEE Transactions on Wireless Communications*, vol. 3, no. 5, pp. 1514–1525, Sep. 2004.

[76] C. Shin, R. Heath, and E. Powers, "Blind Channel Estimation for MIMO-OFDM Systems," *IEEE Transactions on Vehicular Technology*, vol. 56, no. 2, pp. 670–685, Mar. 2007.

[77] B. Muquet, M. de Courville, and P. Duhamel, "Subspace-based blind and semi-blind channel estimation for OFDM systems," *IEEE Transactions on Signal Processing*, vol. 50, no. 7, pp. 1699–1712, Jul. 2002.

[78] M. Baek, M. Kim, Y. You, and H. Song, "Semi-blind channel estimation and PAR reduction for MIMO-OFDM system with multiple antennas," *IEEE Transactions on Broadcasting*, vol. 50, no. 4, pp. 414–424, Dec. 2004.

[79] Y. Zeng and T. Ng, "A semi-blind channel estimation method for multiuser multi-antenna OFDM systems," *IEEE Transactions on Signal Processing*, vol. 52, no. 5, pp. 1419–1429, May 2004.

[80] M. Hsieh and C. Wei, "Channel estimation for OFDM systems based on comb-type pilot arrangement in frequency selective fading channels," *IEEE Transactions on Consumer Electronics*, vol. 44, no. 1, pp. 217–225, Feb. 1998.

[81] F. Dietrich and W. Utschick, "Pilot-assisted channel estimation based on second-order statistics," *IEEE Transactions on Signal Processing*, vol. 53, no. 3, pp. 1178–1193, Mar. 2005.

[82] K. Hung and D. Lin, "Pilot-based LMMSE channel estimation for OFDM systems with power-delay profile approximation," *IEEE Transactions on Vehicular Technology*, vol. 59, no. 1, pp. 150–159, Jan. 2010.

[83] X. Li and H. Fan, "Blind channel identification: subspace tracking method without rank estimation," *IEEE Transactions on Signal Processing*, vol. 49, no. 10, pp. 2372–2382, Oct. 2001.

[84] P. Hoeher, "TCM on frequency-selective land-mobile fading channels," in *In Proc. 5th Tirrenia International Workshop on Digital Communications, Tirrenia, Italy*, Sep. 1991, pp. 317–328.

[85] K. W. Yip and T. S. Ng, "Karhunen-Loeve expansion of the WSSUS channel output and its application to efficient simulation," *IEEE Journal on Selected Areas in Communications*, vol. 15, no. 4, pp. 640–646, May 1997.

[86] T. Hrycak, S. Das, G. Matz, and H. G. Feichtinger, "Practical estimation of rapidly varying channels for OFDM systems," *IEEE Transactions on Communications*, vol. 59, no. 11, pp. 3040–3048, Nov. 2011.

[87] J. Zhang, "Optimal detection with imperfect channel estimation for wireless communication," Ph.D. dissertation, The University of York, 2009.

[88] D. Slepian, "Prolate spheroidal wave functions, Fourier analysis and uncertainty x2014; IV: Extensions to many dimensions; generalized prolate spheroidal functions," *The Bell System Technical Journal*, vol. 43, no. 6, pp. 3009–3057, Nov. 1964.

[89] S. M. Kay, *Fundamentals of Statistical Signal Processing: Estimation Theory*, Upper Saddle River, NJ, USA: Prentice-Hall, Inc., 1993.

[90] L. Hanzo and B. Yeap, *Turbo coding, turbo equalisation and space-time coding*, John Wiley & Sons, 2002.

[91] C. Berrou, A. Glavieux, and P. Thitimajshima, "Near Shannon limit error-correcting coding and decoding: Turbo-codes. 1," in *IEEE International Conference on Communications (ICC), Geneva, Switerland*, vol. 2, May 1993, pp. 1064–1070.

[92] C. Berrou and A. Glavieux, "Near optimum error correcting coding and decoding: turbo-codes," *IEEE Transactions on Communications*, vol. 44, no. 10, pp. 1261–1271, 1996.

[93] G. White, "Optimised turbo codes for wireless Channels," Ph.D. dissertation, The University of York, 2001.

[94] L. Bahl, J. Cocke, F. Jelinek, and J. Raviv, "Optimal decoding of linear codes for minimizing symbol error rate (Corresp.)," *IEEE Transactions on Information Theory*, vol. 20, no. 2, pp. 284–287, Mar. 1974.

[95] A. Burr, *Modulation and coding for wireless communications*, 1st ed., Boston, MA, USA: Addison-Wesley Longman Publishing Co., Inc., 2001.

[96] P. Robertson and E. Villebrun, "Optimal and sub-optimal maximum a posteriori algorithms suitable for turbo decoding," *European Transactions on Telecommunications*, vol. 8, pp. 119–125, 1997.

[97] P. Wan, M. McGuire, and X. Dong, "Near-optimal channel estimation for OFDM in fast-fading channels," *IEEE Transactions on Vehicular Technology*, vol. 60, no. 8, pp. 3780–3791, Oct. 2011.

[98] ETSI-TS-136-201, "3rd Generation Partnership Project; Technical specification group radio access network; Evolved Universal Terrestrial Radio Access (E-UTRA); Base Station (BS) radio transmission and reception (3GPP TS 36.104, V12.4.0, Release 12)," Jun. 2014.

[99] ETSI-TS-136-201, "3rd Generation Partnership Project; Technical specification group radio access network; Evolved Universal Terrestrial Radio Access (E-UTRA); Multiplexing and channel coding (3GPP TS 36.212, V12.2.0, Release 12)," Sep. 2014.

[100] R. Nilsson, F. Sjoberg, O. Edfors, P. Odling, H. Eriksson, S. K. Wilson, and P. O. Borjesson, "A low complexity threshold detector making MLSD decisions in a multiuser environment," in *48th IEEE Vehicular Technology Conference (VTC), Ottawa, Canada*, vol. 1, May 1998, pp. 333–337.

[101] J. Li, K. Letaief, and Z. Cao, "A reduced-complexity maximum-likelihood method for multiuser detection," *IEEE Transactions on Communications*, vol. 52, no. 2, pp. 289–295, Feb. 2004.

[102] Y. Li, L. Cimini, and N. Sollenberger, "Robust channel estimation for OFDM systems with rapid dispersive fading channels," *IEEE Transactions on Communications*, vol. 46, no. 7, pp. 902–915, Jul. 1998.

[103] P. Craven and G. Wahba, "Smoothing noisy data with spline functions," *Numerische Mathematik*, vol. 31, no. 4, pp. 377–403, 1979.

[104] N. Nguyen, P. Milanfar, and G. Golub, "Efficient generalized cross-validation with applications to parametric image restoration and resolution enhancement," *IEEE Transactions on Image Processing*, vol. 10, no. 9, pp. 1299–1308, Sep. 2001.

[105] C. Tepedelenlioglu and G. Giannakis, "On velocity estimation and correlation properties of narrow-band mobile communication channels," *IEEE Transactions on Vehicular Technology*, vol. 50, no. 4, pp. 1039–1052, Jul. 2001.

[106] J. Cai, W. Song, and Z. Li, "Doppler spread estimation for mobile OFDM systems in Rayleigh fading channels," *IEEE Transactions on Consumer Electronics*, vol. 49, no. 4, pp. 973–977, Nov. 2003.

[107] Y. Tsai and K. Yang, "Approximate ML Doppler Spread Estimation Over Flat Rayleigh Fading Channels," *IEEE Signal Processing Letters*, vol. 16, no. 11, pp. 1007–1010, Nov. 2009.

[108] M. Souden, S. Affes, J. Benesty, and R. Bahroun, "Robust Doppler spread estimation in the presence of a residual carrier frequency offset," *IEEE Transactions on Signal Processing*, vol. 57, no. 10, pp. 4148–4153, Oct. 2009.

[109] N. Aboutorab, W. Hardjawana, and B. Vucetic, "A new iterative Doppler-assisted channel estimation joint with parallel ICI cancellation for high-mobility MIMO-OFDM systems," *IEEE Transactions on Vehicular Technology*, vol. 61, no. 4, pp. 1577–1589, May 2012.

[110] T. Miyamoto, K. Naito, K. Mori, and H. Kobayashi, "Proposal of Doppler estimation method of using frequency channel response for OFDM systems," in *7th International Conference on Signal Processing and Communication Systems (ICSPCS), Gold Coast, Australia*, Dec. 2013, pp. 1–7.

[111] M. Raju, R. Annavajjala, and A. Chockalingam, "BER analysis of QAM on fading channels with transmit diversity," *IEEE Transactions on Wireless Communications*, vol. 5, no. 3, pp. 481–486, Mar. 2006.

[112] J. Zhang, V. Baronkin, and Y. Zakharov, "Optimal detector of OFDM signals for imperfect channel estimation," in *16th European Signal Processing Conference, Lausanne, Switzerland*, Aug. 2008, pp. 1–5.

[113] T. Yucek, R. Tannious, and H. Arslan, "Doppler spread estimation for wireless OFDM systems," in *IEEE/Sarnoff Symposium on Advances in Wired and Wireless Communication 2005, Princton, NJ, US*, Apr. 2005, pp. 233–236.

[114] K. Witrisal, Y. Kim, and R. Prasad, "RMS delay spread estimation technique using non-coherent channel measurements," *Electronics Letters*, vol. 34, no. 20, pp. 1918–1919, Oct. 1998.

[115] T. Yucek and H. Arslan, "Time dispersion and delay spread estimation for adaptive OFDM systems," *IEEE Transactions on Vehicular Technology*, vol. 57, no. 3, pp. 1715–1722, May 2008.

[116] C. Athaudage and A. Jayalath, "Delay-spread estimation using cyclic-prefix in wireless OFDM systems," *IEE Proceedings - Communications*, vol. 151, no. 6, pp. 559–566, Dec. 2004.

[117] T. Hrycak, S. Das, G. Matz, and H. G. Feichtinger, "Low complexity equalization for doubly selective channels modeled by a basis expansion," *IEEE Transactions on Signal Processing*, vol. 58, no. 11, pp. 5706–5719, Nov. 2010.

[118] X. Zhao, T. Peng, M. Yang, and W. Wang, "Doppler spread estimation by tracking the delay-subspace for OFDM systems in doubly selective fading channels," *IEEE Signal Processing Letters*, vol. 16, no. 3, pp. 212–215, Mar. 2009.

[119] P. Schniter, "Low-complexity estimation of doubly-selective channels," in *4th IEEE Workshop on Signal Processing Advances in Wireless Communications (SPAWC), Rome, Italy*, Jun. 2003, pp. 200–204.

[120] R. Iltis, "Joint channel, doppler shift and time-delay estimation for spread-spectrum communications," in *Twenty-Third Asilomar Conference on Signals, Systems and Computers, Pacific Grove, CA, US*, vol. 1, Oct. 1989, pp. 206–210.

[121] Y. Kim and C. Gu, "Smoothing spline gaussian regression: more scalable computation via efficient approximation," *Journal of the Royal Statistical Society: Series B (Statistical Methodology)*, vol. 66, no. 2, pp. 337–356, 2004.

[122] Y. Zakharov and T. Tozer, "Frequency estimator with dichotomous search of periodogram peak," *Electronics Letters*, vol. 35, no. 19, pp. 1608–1609, Sep. 1999.

[123] S. Saunders and S. Simon, *Antennas and propagation for wireless communication systems*, 1st ed., New York, NY, USA: John Wiley & Sons, Inc., 1999.

[124] A. Molisch, *Wireless Communications*, Wiley-IEEE Press, 2005.

[125] B. Carlson, "Covariance matrix estimation errors and diagonal loading in adaptive arrays," *IEEE Transactions on Aerospace and Electronic Systems*, vol. 24, no. 4, pp. 397–401, Jul. 1988.

[126] S. Vorobyov, A. Gershman, and Z. Luo, "Robust adaptive beamforming using worst-case performance optimization: a solution to the signal mismatch problem," *IEEE Transactions on Signal Processing*, vol. 51, no. 2, pp. 313–324, Feb. 2003.

[127] R. Clarke and W. Khoo, "3-D mobile radio channel statistics," *IEEE Transactions on Vehicular Technology*, vol. 46, no. 3, pp. 798–799, Aug. 1997.

[128] O. Edfors, M. Sandell, J. van de Beek, S. Wilson, and P. Borjesson, "OFDM channel estimation by singular value decomposition," *IEEE Transactions on Communications*, vol. 46, no. 7, pp. 931–939, Jul. 1998.

[129] G. Golub and C. Loan, *Matrix computations*, 4th ed., The Johns Hopkins University Press, 2013.

[130] Y. Cho, J. Kim, W. Yang, and C. Kang, *MIMO-OFDM wireless communications with MATLAB*, Wiley Publishing, 2010.

[131] A. Sampath and J. Holtzman, "Estimation of maximum Doppler frequency for handoff decisions," in *43rd IEEE Vehicular Technology Conference, New Jersey, US*, May 1993, pp. 859–862.

[132] K. Anim-Appiah, "On generalized covariance-based velocity estimation," *IEEE Transactions on Vehicular Technology*, vol. 48, no. 5, pp. 1546–1557, Sep. 1999.

[133] K. Baddour and N. Beaulieu, "Robust Doppler spread estimation in nonisotropic fading channels," *IEEE Transactions on Wireless Communications*, vol. 4, no. 6, pp. 2677–2682, Nov. 2005.